

**Pannexin-1 In Silico Modeling Towards Physiological and
Pathological Functioning**

**By
Joel Subach**

**A Dissertation Submitted
In partial fulfillment of the Requirements for the Degree of
Doctor of Philosophy in Biomedical Informatics**

**Department of Health Informatics
Rutgers, The State University of New Jersey
School of Health Related Programs**

January, 2020



Final Dissertation Defense Approval Form

Pannexin-1 In Silico Modeling Towards Physiological and Pathological
Functioning

BY

Joel Subach

Dissertation Committee:

Masayuki Shibata, PhD

Frederic Coffman, PhD

Dinesh Mital, PhD

Approved by the Dissertation Committee:

_____	Date: _____
_____	Date: _____
_____	Date: _____

TABLE OF CONTENTS

ABSTRACT.....	viii
ACKNOWLEDGMENTS.....	ix
LIST OF TABLES.....	x
LIST OF FIGURES.....	xiv
LIST OF FORMULAS.....	xvi
CHAPTER 1: INTRODUCTION.....	1
1.1 Background of the Problem.....	1
1.2 Statement of the Problem (Purpose of the Study).....	1
1.3 Goals, Objectives and Research Questions of the Study.....	1
1.4 Significance of the Study (Need i.e. Theoretical and Practical).....	3
1.5 Hypothesis.....	5
CHAPTER 2: REVIEW OF LITERATURE.....	6
2.1 Pannexin-1 Structure and Function.....	6
2.1.1 Pannexin-1 Structural and Functional Experimental Evidence.....	8
2.1.2 Pannexin-1 Phylogeny.....	12
2.1.2.1 Pannexin-1 Residue Constraints.....	14
2.2 Purinergic Receptor Structure and Function.....	20
2.3 AR Receptor Structure and Function.....	21
2.4 Pannexin-1 Inhibitors.....	24
2.4.1 CBX.....	24
2.4.2 Probenicid.....	24
2.4.3 Food Dyes.....	25
2.4.4 ¹⁰ Panx1.....	25
2.5 Pannexin-1 Towards Physiology and Pathology.....	25
2.5.1 Ischemic Stroke	25
2.5.2 Apoptosis	26
2.5.3 Atherosclerosis	26
2.5.4 Blood Pressure Regulation	27
2.5.5 Neuropathic Pain	27
2.5.6 Synaptic Plasticity Towards Learning	28

2.5.7 Immune-Regulation	28
2.5.7.1 HIV and Pannexin-1 Modulation and Immunosuppression.....	28
2.6 Protein Modeling, an Overview.....	31
2.6.1 Membrane Protein Modeling.....	32
2.6.1.1 Orientation/Positioning Prediction.....	34
2.6.2 Template Selection.....	35
2.6.3 Target-Template Alignment Selection.....	36
2.6.4 Protein Molecular Modeling.....	39
2.6.4.1 MODELLER Molecular Modeling.....	40
2.6.4.1.1 Homology Modeling (Single-Template Approach).....	41
2.6.4.1.2 Multiple-Template Modeling.....	42
2.6.4.1.2.1 Multiple-Template Modeling, Single Template per Target.....	42
2.6.4.1.2.2 Multiple-Template Modeling, Multiple Templates per Target.....	44
2.6.4.2 GalaxyWeb Molecular Modeling.....	45
2.7 Ligand-Target Docking Dynamic Simulation.....	46
Conclusion.....	48
CHAPTER 3: RESEARCH METHOD AND DESIGN.....	49
3.1 Overview and Objectives.....	49
3.1.1 Research Overview.....	49
3.1.2 Research Objective.....	49
3.1.3 Future Research Objective.....	49
3.2 Pannexin-1 Modeling, an Overview.....	49
3.2.1 Pannexin-1 Template Selection.....	50
3.2.1.1 NCBI BLAST Assay.....	50
3.2.1.2 Phyre ² HHBlits Assay.....	51
3.2.2 Pannexin-1 Target-Template Alignment Selection.....	52
3.2.2.1 Clustal	52
3.2.2.2 Promals3D	53
3.2.2.3 Phyre ²	53
3.2.2.4 RaptorX/CNFpred	53
3.2.2.5 Consensus Pannexin-1 Structural Threading Alignment.....	53
3.2.3 Pannexin-1 Orientation and Positioning Selection.....	54

3.2.3.1 Modeling Topology.....	54
3.2.3.1.1 TMPred	54
3.2.3.1.2 TMHMM	55
3.2.3.1.3 SOUSI	55
3.2.3.1.4 RaptorX	56
3.2.3.1.5 Phyre ²	56
3.2.3.1.6 Consensus Topology Determination.....	57
3.2.3.1.7 Structural Threading and Topology Consensus.....	57
3.2.3.1.8 Innexin6 Topology	57
3.2.4 Pannexin-1 Target-Multiple Template Alignment Selection.....	58
3.2.4.1 Multiple Template/Target Approach.....	58
3.2.4.2 Single Template/Target Approach.....	60
3.3 Pannexin-1 Molecular Modeling Methodology.....	67
3.3.1 Multiple Template/Target MODELLER A-Chain.....	68
3.3.2 Single Template/Target MODELLER A-Chain.....	68
3.3.3 GalaxyWeb Monomer Input.....	69
3.3.4 GalaxyWeb Sequence Input.....	69
3.4 Ligand-Target Docking Dynamic Simulation Method.....	70
3.4.1 ¹⁰ Panx1-Pore Docking Method.....	70
3.4.2 Target-EL1 Docking Method.....	71
3.4.3 Target-EL2 Docking Method.....	71
CHAPTER 4: RESULTS.....	72
4.1 Pannexin-1 Templates Selected.....	72
4.2 Pannexin-1 Single Target-Template Alignments.....	73
4.2.1 Clustal.....	73
4.2.2 Promals3D	75
4.2.3 Phyre ²	75
4.2.4 CNFpred	76
4.2.5 Consensus Target-Template Structural Threading.	76
4.3 Pannexin-1 Topology.....	78
4.3.1 TMPred Topology Prediction.....	78
4.3.1.1 Pannexin-1	78
4.3.1.2 Connexin26	79

4.3.2 TMHMM Topology Prediction.....	80
4.3.2.1 Pannexin-1.....	80
4.3.2.2 Connexin26	82
4.3.3 SOUSI Topology Prediction.....	83
4.3.3.1 Pannexin-1.....	83
4.3.3.2 Connexin26.....	83
4.3.4 RaptorX Topology Prediction.....	84
4.3.4.1 Pannexin-1.....	84
4.3.4.2 Connexin26.....	85
4.3.5 Phyre ² Topology Prediction.....	87
4.3.5.1 Pannexin-1.....	87
4.3.5.2 Connexin26.....	87
4.3.6 Topology Consensus.....	88
4.3.7 Structural Threading Topology Consensus.....	90
4.3.8 Innexin6 Topology.....	92
4.4 Pannexin-1 Multiple Template Alignments.....	93
4.4.1 Multiple Template/Target Alignment File.....	93
4.4.2 Single Template/Target Alignment File.....	94
4.5 MODELLER A-Chain Models.....	95
4.5.1 Multiple Template/Target Monomer.....	96
4.5.2 Single Template/Target Monomer.....	96
4.5.3 Single/Multiple Template-Target Monomers.....	97
4.6 Galaxy Oligomer Models.....	97
4.6.1 GalaxyHomomer Hexamers.....	98
4.6.1.1 Galaxy Scores.....	98
4.6.1.2 Monomer vs. FASTA Hexamers.....	99
4.7 Ligand-Target Experimental and Docking Dynamic Simulation Results.....	103
4.7.1 Experimental Results.....	103
4.7.2 In Silico Results.....	104
4.7.2.1 Pore Docking Results.....	105
4.7.2.2 EL-1 Docking Results.....	106
4.7.2.3 EL-2 Docking Results.....	108

CHAPTER 5: DISCUSSION.....	109
5.1 Interpretation of Main Findings.....	109
CHAPTER 6: CONCLUSION.....	111
6.1 Final Statement.....	111
6.2 Limitations.....	111
6.3 Future Research.....	112
REFERENCES.....	113

ABSTRACT

The transmembrane pore protein Pannexin-1 (Pnx1) forms channels allowing the release of purine nucleotides and participates in processes related to purinergic signaling, including blood pressure regulation, apoptotic cell clearance, and neuropathic pain. Pnx1 has also been implicated in several pathological mechanisms, including facilitating HIV entry. While several naturally occurring inhibitors of Pnx1 activity have been discovered, elucidating structure-function relationships within the Pnx1 oligomer and the ability to design molecules to regulate Pnx1 activities has been limited due to the absence of a Pnx1 crystal structure. To address this limitation, an *in silico* model of Pnx1 was constructed, based on homologous protein channel structures, established physicochemical characteristics and binding properties of the Pnx1 channel.

Homologous template protein searches, transmembrane topologies and sequence alignments were subsequently used by MODELLER software to generate Pnx1 A-Chain monomer subunits via a multi-template stitching approach. These A-chain subunit models and a GalaxyWeb Pnx1 sequence generated A-chain subunit were subsequently used to construct four model homo-oligomers (pentamers, hexamers, heptamers, and octamers) using GalaxyWEB, all oligomeric structures were compared to established biophysical parameters of Pnx1 channels. Docking experiments using Medusa Guide were performed using four small molecules and the ¹⁰Pnx1 mimetic peptide known to block the Pannexin-1 channel. Docking simulation free energy results were used to assess the regional validity of the designed Pnx1 model.

The optimum Pannexin-1 model was a hexameric structure exhibiting compact helices and dynamic loops and tails which promoted both pore and oligomer diameters and an overall structure matching Pannexin-1 experimental data. Docking experiments overall exhibited moderate affinity free energy values for Pnx1 inhibitors inferring an overall fair modeling accuracy. A high affinity free energy value of -46.38 kcal mol⁻¹ was discovered for the mimetic ¹⁰Pnx1 which partially sterically blocks the Pannexin-1 pore region.^{2,8,66} EL-1/2 docking results demonstrated high (< -30 to -50 kcal mol⁻¹) to poor (> -20 kcal mol⁻¹) affinities. The model suggested these small molecules bound to the EL1/2 regions primarily through steric/hydrophobic and polar interactions. Overall, this model fits with established experimental results and is a reasonable tool for the initial design of compounds which modulate Pannexin-1 gating.

ACKNOWLEDGMENTS

I would like to give great thanks and appreciation to the entire Rutgers School of Health Related Programs for the opportunity to enroll and be enriched within Biomedical Informatics and nanomedicine, special thanks to Dr. Srinivasan for administrating me through this process. Special gratitude to my mentor Dr. Coffman for his great patience in educating and streaming me through this dissertation via his consistent and insightful feedback. Further thanks goes to Dr. Shibata and Dr. Mital for being part of my research committee, thank you both for your guidance and in particular Dr. Shibata for your great knowledge towards streaming my dissertation towards its best end results. A final thanks to the remaining Rutgers Faculty that encouraged, challenged and enriched me via their superb instruction, thank you Dr. Gohel for reading. I dedicate this dissertation to my Dad because of his consistent encouragement towards me completing a PhD.

LIST OF TABLES

Table 1.) Pannexin-1 and ViPR Biomedical Informatics Database.....	3
Table 2.) Pannexin-1 Channel an HIV Resource Fact.....	4
Table 3.) Biomedical Informatics Protein Database (PDB) Adding Pannexin 1.....	4
Table 4.) Pannexin-1 Experimental Data.....	8
Table 5.) Residue Constraints Pannexin-1, Connexin26 and Innexin6.....	14
Table 6.) NCBI BLAST Non-Redundant Search Near Homologs.....	19
Table 7.) PSI-Blast Multiple Sequence Alignment Search Distant Homologs.....	19
Table 8.) MODELLER Single-Template Input.....	41
Table 9.) MODELLER Output File Illustrated.....	41
Table 10.) MODELLER Multiple-Template Input.....	42
Table 11.) Automodel Class MODELLER Stitching.....	43
Table 12.) Alignment File MODELLER Stitching.....	43
Table 13.) Clustal Multiple Template Alignment, Multiple Residues.....	44
Table 14.) GalaxyWeb Results Summary Illustration.....	46
Table 15.) Multiple Template Alignment, Single Template/Target Alignment.....	61

Table 16.) NCBI PSI-BLAST 1NZP_A.....	66
Table 17.) NCBI PSI-BLAST 4UXF_A.....	67
Table 18.) NCBI PSI-BLAT 4Y2C_A.....	67
Table 19.) Phyre ² HH 5H5P.....	67
Table 20.) MODELLER Script, Clustal Multiple Template Alignment.....	68
Table 21.) MODELLER Script, Single Template/Target Alignment Filename.....	69
Table 22.) GalaxyWeb Loop or Termini Refinement.....	69
Table 23.) NCBI blastp Results.....	72
Table 24.) PSI-BLAST Results.....	72
Table 25.) Phyre ² HH Results.....	73
Table 26.) Clustal Innexin6-Pannexin-1 Alignment Results.....	74
Table 27.) Phyre ² Innexin6-Pannexin-1 Alignment Results.....	75
Table 28.) Consensus Threading.....	76
Table 29.) TMPred Pannexin-1 Topology Prediction.....	78
Table 30.) TMPred Pannexin-1 Topology Prediction.....	79
Table 31.) UniProtKB Pannexin-1 Topology Prediction.....	79
Table 32.) TMPred Connexin26 Topology Prediction.....	80

Table 33.) UniProtKB Connexin26 Topology Prediction.....	80
Table 34.) TMHMM Pannexin-1 Topological and Transmembrane Probabilities.....	81
Table 35.) TMHMM Connexin26 Topological and Transmembrane Domain Results.....	82
Table 36.) SOSUI Pannexin-1 Hydrophobicity Prediction.....	83
Table 37.) SOSUI Connexin26 Transmembrane Results.....	83
Table 38.) RaptorX Pannexin-1 Prediction, Disorder.....	84
Table 39.) RaptorX Pannexin-1 Prediction, Solvent Exposure.....	84
Table 40.) RaptorX Pannexin-1 Prediction, ss.....	85
Table 41.) RaptorX Connexin26 Prediction, Disordered.....	85
Table 42.) RaptorX Connexin26 Prediction, Solvent Exposure.....	86
Table 43.) RaptorX Connexin26 Prediction, ss.....	86
Table 44.) Pannexin-1, Connexin26 Topology Consensus, Orientation.....	88
Table 45.) Pannexin1, Connexin26 Topology Consensus, Positions.....	90
Table 46.) Pannexin-1-Connexin26 Manual Alignment, Positions.....	91
Table 47.) UniProtKB Innexin6 Positions.....	93
Table 48.) Clustal 6-Template align3.ali File.....	93
Table 49.) 5-Template align2.ali File.....	94

Table 50.) MODELLER A-Chain Results.....	96
Table 51.) GalaxyHomomer Hexamer Monomer Input Scores.....	98
Table 52.) GalaxyHomomer Hexamer Sequence Input Scores.....	99

LIST OF FIGURES

Figure 1.) Experimentally Deduced Pannexin 1 with Homozygous Mutant Histidine.....	6
Figure 2.) Experimentally Deduced Pannexin-1 (uHC) Oligomer with Pore-Channel.....	7
Figure 3.) Pannexin Paralogs.....	13
Figure 4.) Panx1 Pore and Oligomer Diameters.....	13
Figure 5.) 3-D Image of Adenosine A2A Receptor:Antagonist, Pie-Stacking Displayed.....	22
Figure 6.) Human Adenosine A2A Receptor Bound to Antagonist ZM241385.....	23
Figure 7.) Pannexin-1 Channel Opening Towards Apoptosis via Caspase Cleavage.....	26
Figure 8.) Pannexin-1 Hemichannel and Purinergic Receptors During HIV Infection.....	29
Figure 9.) Pathological HIV Life Cycle via a Tyrosine Kinase.....	30
Figure 10.) Pannexin-1 and ATP Hydrolyses.....	31
Figure 11.) Transmembrane Topology Orientation.....	32
Figure 12.) Transmembrane Residue Positioning.....	33
Figure 13.) Alignment Score.....	36
Figure 14.) Multiple Sequence Alignment.....	37
Figure 15.) Clustal Alignment Illustration.....	37

Figure 16.) Alignment Mismatch, Insertion and Deletion Illustration.....	38
Figure 17.) ss Promals3D Alignment Illustrated.....	38
Figure 18.) Phyre ² Pannexin-1 Topology Prediction.....	87
Figure 19.) Phyre ² Connexin26 Topology Prediction.....	87
Figure 20.) Phyre ² Innexin6 Topology Prediction.....	92
Figure 21.) Pymol Innexin6, MODELLER Pannexin-1, Connexin26 A-Chain Comparison.....	97
Figure 22.) Pymol Visual Extracellular View of Modeled Hexamers.....	99
Figure 23.) Pymol Visual Side-View of Modeled Hexamers.....	100
Figure 24.) Pymol Visual Cytoplasmic View of Modeled Hexamers.....	100
Figure 25.) Pymol Visual Side-View of Modeled Hexamers, TM1-EL1 Illustrated.....	101
Figure 26.) Pymol Visual of Modeled Hexamers Superimposed.....	101
Figure 27.) Pymol GalaxyHomomer FASTA Input Visualization Side View.....	102
Figure 28.) Pymol GalaxyHomomer FASTA Input Visualization Areal View.....	102
Figure 29.) Pymol GalaxyHomomer FASTA Input Visualization Ribbon Areal View.....	103
Figure 30.) Pannexin-1 Extracellular Loop Region 1 (EL1).....	104
Figure 31.) Pymol Visualization of Mimetic ¹⁰ Panx1 Bound to Pannexin-1 Pore region.....	105
Figure 32.) Pymol Visualization of CBX Nonbonding Steric Effect on Pannexin-1 EL-1.....	106

Figure 33.) Pannexin-1-CBX Inflated.....	107
--	-----

LIST OF FORMULAS

Formula 1.) $\Delta G_{\text{bind}} = \Delta G_{\text{solvent}} + \Delta G_{\text{conf}} + \Delta G_{\text{int}} + \Delta g_{\text{motion}}$	47
--	----

Chapter 1

Introduction

1.1 Background of the Problem

Ubiquitously expressed channel transmembrane protein Pannexin-1 controls a multitude of connected homeostatic functions that are interlaced and carried over via a conduit of purinergic receptors ultimately catapulting physiological responses. A deep understanding of these mechanisms is obscure and the Pannexin-1 has not yet been crystallized, moreover current Pannexin-1 pore experimental gating is limited via undiscovered promoters and discovered inhibitors only inferring pore closure via steric block or conformational closure via an elusive Pannexin-1 regional-blocker electro-steric interaction.

1.2 Statement of the Problem (Purpose of the Study)

Therapeutically controlling Pannexin-1 gating will ameliorate a number of health issues, this gating control requires a characterization of pivotal Pannexin-1 uncrystallized regions. The purpose of this study is to complete an in silico reasonable beginning design of these Pannexin-1 pivotal domains that promote channel closure.

1.3 Goals, Objectives and Research Questions of the Study

The overall goal of this research project is to accurately design in silico the uncrystallized Pannexin-1. The objective of this study is to prove this model's accuracy via designing a Pannexin-1 transmembrane protein exhibiting an overall structure matching experimental data and objectified regional accuracy via Dynamic Docking Simulations of known pore blocking partners that bind particular Panx1 electro-steric areas of interest with minimum affinities.

Future goals will include further elucidation of the pivotal residues within Pannexin-1 binding area(s) of interest and development of a preliminary conjugated smart nanoparticle that allows preferential accumulation and conjugation to Pannexin-1 channels (targeted delivery). This smart nanoparticle will promote an enhanced blocking and opening therapeutic efficacy while maintaining a reduced cytotoxicity.⁹⁸

Proposed Future Study Objectives:

- 1.) Identify conformational changes and host cell membrane depolarization in time during Pannexin-1 protein/channel opening and closing via Molecular Dynamic Simulations.
- 2.) Generate by computer learning a program predicting binding and functioning of the transmembrane channel as a measure of therapeutic efficiency.
- 3.) Further characterize the extracellular, intracellular and membrane associated areas of uncrystallized Pannexin-1 and discover the pivotal residues essential for channel opening/closing and trigger mechanisms.
- 4.) The nano-engineering design of a stealth nanoparticle exhibiting promoter and inhibitor conjugates promoting Pannexin-1 channel opening and closing respectively.
- 5.) In vitro and in vivo experiments to confirm Molecular Dynamic Simulation in silico results of a designed AuNP and its tuned AuNP-tag allowing the activation of the Pannexin-1 Channel into a closed/open position, (nanoparticle subsequent fragmentation will be accommodated).⁹⁹

Pivotal questions toward this study:

- 1.) How compact is the modeled pore region and how similar is the overall structural design compared to experimental data i.e. pore and oligomer diameters/oligomerization?
- 2.) How regionally precise and characterized was the uncrystallized Pannexin-1 transmembrane protein?
- 3.) What are the inhibitor chemical/protein binding affinities?

Pivotal questions toward future study:

- 1.) What is the potency and efficacy of the nanoparticle in silico, in vitro and in vivo?
- 2.) Which residues within the key-domains are responsible for Panx1 closure and opening?
- 3.) What are the AuNP conjugate Panx1 binding affinities and specificities in silico, in vitro and in vivo?
- 4.) What will be the nanoparticles, bioavailability, stability, solubility, circulation time/clearance and non-specific toxicity in vivo?⁹⁸
- 5.) What homeostatic mechanisms may adversely be effected via a blocked or opened Panx1 Channel i.e. immunoregulation etc.?

1.4 Significance of the Study (Need i.e. Theoretical and Practical)

The in silico methodology towards this Pannexin-1 modeling and its energy dockings will contribute theoretical knowledge towards parallel works. Moreover this preliminary design will be a staple to subsequent Molecular Dynamic Simulations towards Pannexin-1 regional refinement and therapeutic Pannexin-1 gating.

The design of an uncrystallized Pannexin-1 to treat disease will practically contribute to Biomedical Informatics Databases characterizing new Pannexin-1 treatment regimens and Pannexin-1 structure and function. For example, Biomedical Informatics databases ViPR (Virus Pathogen Resource), Viral Zone and PDB will fruitfully add Pannexin-1 resource facts.

ViPR Home » Reoviridae Home » Antiviral Drug Search

Antiviral Drug Search

From this interface find and retrieve information on antiviral drugs, their targets, and specific interaction sites in viral proteins. Information for [ATC defined 'Direct Acting Antivirals'](#) can be accessed from this interface.

Descriptive, taxonomic, and pharmacologic information for antiviral drugs, and drug targets were imported from the [Drugbank Drug and Target Database](#).

Specific drug interaction site data was imported [Protein Data Bank](#).

Viral mutations affecting drug sensitivity were collected from public databases and through manual curation of available literature.

Results matching your criteria: 0

SELECT VIRUS(ES) TO INCLUDE IN SEARCH

Family	Subfamily	Genus	Species
All	===Herpesviridae===	===Flaviviridae===	Human Parainfluenza Virus 2
Flaviviridae	Alphaherpesvirinae	Hepacivirus	===Pneumovirus===
Hepadnaviridae	Betaherpesvirinae	===Hepadnaviridae===	Respiratory Syncytial Virus
Herpesviridae	Gammaherpesvirinae	Orthohepadnavirus	===Enterovirus===
Orthomyxoviridae	===Paramyxoviridae===	===Alphaherpesvirinae===	Enterovirus D
Paramyxoviridae	Paramyxovirinae	Simplexvirus	Enterovirus J
Picornaviridae	Pneumovirinae	Varicellovirus	Rhinovirus A
Poxviridae	===Poxviridae===	===Betaherpesvirinae===	Rhinovirus B
Retroviridae	Chordopoxvirinae	Cytomegalovirus	===Orthopoxvirus===
	===Retroviridae===	Roseolovirus	Variola Virus
	Orthoretrovirinae	===Gammaherpesvirinae===	===Deltaretrovirus===
		Lymphocryptovirus	Human T-Lymphotropic Virus 1
		===Orthomyxoviridae===	===Lentivirus===
		Influenzavirus A	Human Immunodeficiency Virus 1
		Influenzavirus B	Human Immunodeficiency Virus 2

DRUG CLASS

Amines
Benzene and substituted derivatives
Benzoxazines
Carbohydrates and carbohydrate conjugates
Carboxylic Acids and Derivatives
Carboxylic acids and derivatives

PROTEIN TARGET

Nonstructural protein 5A
Nuclear receptor subfamily 1 group I member 2
Polyprotein
Protease

FDA STATUS

Abandoned
Approved
Experimental
Investigational

SEARCH SPECIFIC ANTIVIRAL DRUG

Drug Name:

Drugbank ID:

Table 1.) Pannexin-1 as a new target protein towards HIV prevention will be added to ViPR Biomedical Informatics Database's Antiviral Drug Search.¹⁰²

1.5 Hypothesis

The main hypothesis of this proposal is to demonstrate the accurate in silico design of the uncrystallized Pannexin-1 transmembrane protein via the exhibition of a software visualized best overall structure matching experimental published structural and functional data. Moreover docking simulation free energy results will assess the regional validity of the designed Panx1 model that controls homeostatic gating. This design will be a beginning towards Pannexin-1 therapy via a controlled gating mechanism.

Chapter 2

Literature Review

2.1 Pannexin-1 Structure and Function

Pannexins are a highly conserved transmembrane oligomer protein family encoded via three genes in humans (Panx1, Panx2, Panx3).^{2, 8, 21} Pannexin-1 is expressed in at least five inter-species and is ubiquitously plasma membrane expressed (brain, spinal cord, heart, skeletal muscle, skin, testis, ovary, placenta, thymus, prostate, lung, liver, small intestine, pancreas, spleen, colon, blood endothelium, erythrocytes) being highly expressed in the Nervous System and Human Primary Macrophages and CD4⁺ T-Lymphocytes controlling a multitude of bodily functions.^{21, 170} Pannexin-1 may moreover be intracellularly expressed contributing to Ca²⁺ leak signaling mechanisms.¹⁷⁷

One subunit protein Pannexin-1 gene product has been experimentally inferred to exhibit four ordered compact conserved helical transmembrane domains, three disordered dynamic loops (two extracellular (ELs) and one intracellular (IL)) and two disordered dynamic coils (C-N terminals).²

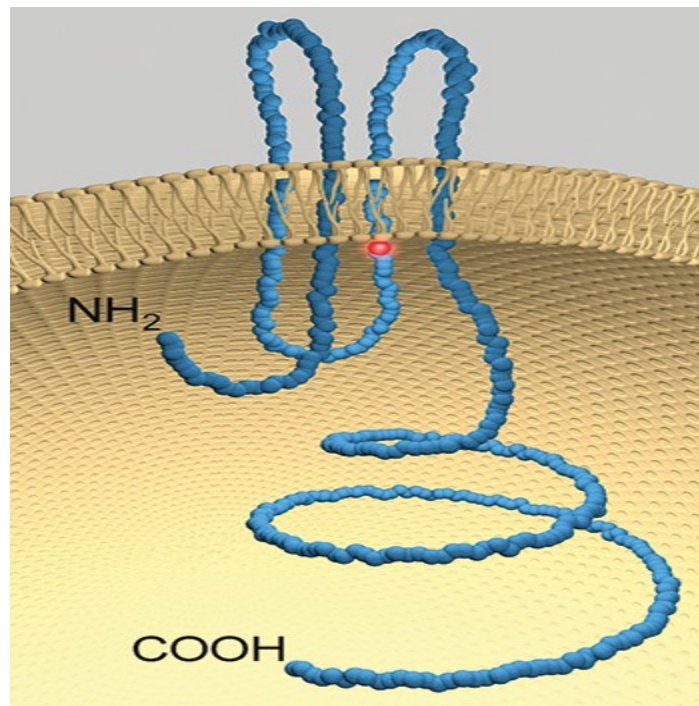


Figure 1.) Experimentally inferred Pannexin 1 with indicated red loop tucked homozygous mutant histidine replacing arginine blocking ATP passage.⁶ Ubiquitous Pannexin-1 controls a multitude of bodily functions accordingly blocked ATP-passage may affect a multitude of bodily functions.⁵

Pannexin-1 uHC has been experimentally inferred to be an un-apposed hemichannel homo-oligomer composed of six-glycosylated homologous Pannexin-1 subunit proteins (A-F) forming a hexamer arranged into a large pore exhibiting oligomer and pore cytoplasmic diameters of ~14 nm and ~1.9 nm respectively.^{2,8,14,166} Pannexin-1 hemichannels are plasma membrane located and can be opened at the un-apposed cell surface forming non-discriminatory but highly regulated aqueous conduits permeable to ions and small molecules <1 kDa (i.e. ATP, UTP, glutamate, NAD^+ , PGE_2). The large size of the Pannexin-1 channel coupled to its lack of selectivity should allow an unhindered efflux of ATP down its concentration and voltage gradients.^{8,173,188} This flexibility allows the diffusional exchange between the intra- and extracellular compartments constituting a route towards an autocrine/paracrine cellular communication, i.e. Pannexin-1 ATP release and its subsequent hydrolysis triggers an adjacent Purinergic/Adenosine Receptor autocrine conduit towards homeostasis/physiology.^{8,173}

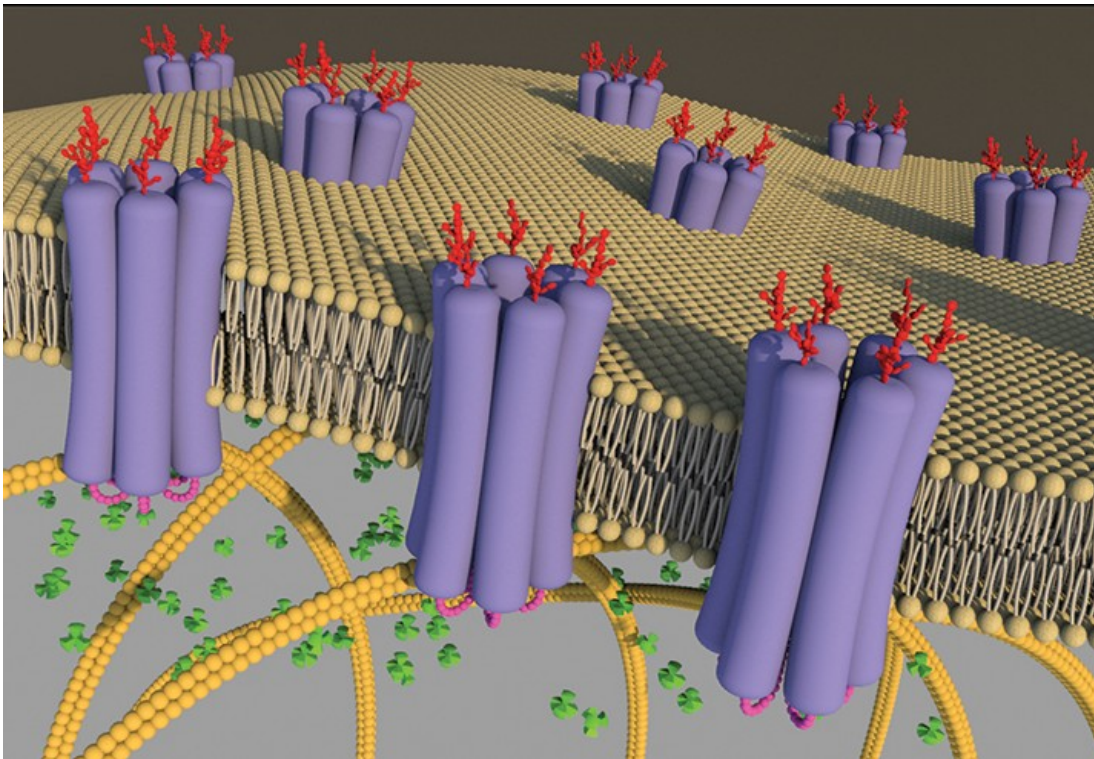


Figure 2.) Experimentally deduced oligomer illustration of six-glycosylated Pannexin-1/homologous subunit proteins arrange into large pore-channels ~1.9 nm in diameter (unopposed hemichannels (uHC)) suitable for 2nd messenger ATP (green-clovers) or other ions and intracellular messengers up to ~1 kDa in molecular mass.⁷

Various pathological and physiological stimuli have been experimentally inferred to open and activate Pannexin-1 channels; i.e. mechanical stimulation, ATP membrane depolarization, activation via different membrane receptors (i.e. HIV gp120/40-CD4 receptor-chemoreceptor complex), hypoxemia, caspase activation C-terminal cleavage, a high concentration of extracellular potassium or intracellular Ca^{2+} , voltage stimulation and pathological membrane to host membrane (i.e. HIV-Host cell membrane) induced stress.^{2, 10, 15, 90, 101} Carbon dioxide-mediated acidification, negative ATP feedback and channel blockers probenecid, carbenoxolone (CBX), food dyes Brilliant Blue FCF [BB FCF] and FD&C Green No. 3 (Fast Green FCF) and flufenamic acid close Pannexin-1 channels.¹⁰¹ How Pannexin-1 senses and integrates such diverse stimuli to form an open and closed channel is yet elusive.

2.1.1 Pannexin-1 Structural and Functional Experimental Evidence

Protein Structure	Panx1 Deduced Structure	Laboratory Evidence
Channel	Mobile Large-Pore Single-Membrane Hemmi-Channels In Vivo, not Double Membrane Gap Intercellular Channels (possible gap junction formation in vitro).	<p>Synthetic rat Panx1 RNA injection results in voltage-activated currents in a non-junctional plasma membrane.¹⁰⁷</p> <p>Panx1 open gating macroscopic currents via extracellular ligand activator ATP coincide with single plasma membrane channel currents.</p> <p>EM does not exhibit canonical gap junction views in Panx1 cell appositional regions; Panx1 intercellular spacings are 20-50 nm, Cx43 gap junction spacings are 2-5 nm.^{108, 172}</p> <p>Immunocytochemistry, detection via light and EM exhibit rodent Panx1 localization within hippocampal and cortical principal neurons to a single plasma membrane not opposing membranes.</p> <p>Residing/operating single blood and airway epithelial cells exhibit Panx1 intracellular and plasma membrane localizations.</p> <p>Whole-cell patch-clamp intercellular conductance recordings upon Panx1 exhibit no significance towards electrical coupling.¹⁰⁹</p>

		<p>Fluorescence recovery subsequent to photobleaching exhibits a highly mobile Panx1 at the cell surface in contrast to significantly less mobile gap junction channels.¹⁶⁵</p> <p>Panx1 exhibited surface glycoproteins repel adjacent plasma membranes via steric hindrance precluding Panx1 dockings and gap junction formation.¹⁰⁸</p> <p>Immuno-labeling via specific primary antibodies and secondary gold conjugated antibodies exhibit gold labels on just one side of Panx1.¹⁶⁶</p> <p>Injected synthetic rat Panx1 RNA precipitates nonselective, voltage-activated currents in a non-junctional plasma membrane.</p> <p>Panx1 channels are small molecule permeable and blocked via gap-junction blockers indicating hemichannel formation.¹⁰⁷</p> <p>Chemical cross-linking and sedimentation studies indicate Panx1 to exhibit a single membrane channel.¹⁶⁹</p> <p>Panx1 Polarity reversal experimentation indicates dependent hemichannel activity.¹⁰⁸</p> <p>Panx1 homomeric pannexons form functional hemichannels in tissues and functional gap-junctions in <i>Xenopus</i> oocytes.¹⁶⁶</p>
Topology Orientation	Tetra-Spanning, 1-Intracellular Loop (IL1), 2-Extracellular Loops (EL1/2), In Terminals	<p>Sequence analysis (eg. positive inside rule) indicates a tetra-spanning Panx1 exhibiting an In Topology with 1IL and 2ELs.^{169, 210}</p> <p>Directed primary antibody 4512 fluorescent conjugate specific to the peptide sequence in the putative first extracellular loop indicates EL1 topology.</p> <p>Directed primary antibody 4515 fluorescent conjugate specific to the peptide sequence in the putative carboxyl-terminal portion indicates a C-tail cytosol topology via sole reactions in cryo-sectioned cells.¹⁶⁷</p> <p>Rabbit polyclonal antibodies similarly characterized a Panx1 second extracellular loop (EL2-247) topology.¹⁶⁸</p> <p>Toppred algorithms predicted a Panx1 with four transmembrane domains.¹⁰⁹</p> <p>Membrane topology studies, hydrophobicity plots and secondary structural predictions portend Panx1 to have four transmembrane domains, In Topology and two extracellular loops containing disulfide bonds.</p>

		<p>* EM images exhibit Panx1 overall topology to match Connexin26.¹⁶⁶</p> <p>Site-directed mutagenesis of the sole Panx1 surface N-linked glycosylation Asn254 site indicates an EL2 topology via a defunct cell-surface trafficking.^{168, 169}</p> <p>Cryo-electron microscopy studies infer a preserved gap junction family cytoplasmic domain cooperating with N and C-terminals during pore-funnel conformation inferring a conserved Pannexin-1 In Topology.¹⁸³</p>
Oligomeric State	Multimer Homomeric Hexamer	<p>Extrapolated data from hemichannel experiments, i.e. ionic selectivity, permeability, voltage gating behavior, indicate Panx1 to exhibit homomeric channel functioning via a large unitary conductance of ~500 pS and a minimum of four substates (5%, 25%, 30% and 90%).¹⁰⁷</p> <p>Chemical cross-linking and sedimentation studies indicate Panx1 to exhibit a homomeric hexameric structure.¹⁶⁹</p> <p>DSP cross-linking experiments and N254Q glycosylation-deficient rPanx1 mutants exhibited monomer, dimer, trimer intermediates and an assembled oligomeric primary channel state hexamer rPanx1 respectively.¹⁷²</p> <p>Via a C-terminal truncation mutant Panx1 is predicted to oligomerize to six subunits.¹⁷⁰</p> <p>Biochemical, co-immunoprecipitation and electrophysiological evidence indicates Panx1/Panx2 heteromeric channels, these heteromers are unstable over time due to a Panx2 symmetric octomeric mismatch (tissue-heteromeric evidence does not exist).^{107,166}</p> <p>Current analysis within <i>Xenopus</i> oocyte system using rPanx1, rPanx2 and heteromers 3:1, 1:1, 1:3 indicate significant channel activity only within Panx1.²¹⁵</p>
TM Positions	4-TM Domains, 8-Positions	<p>Tmmpred, TMHMM and DNA Star softwares based upon hydrophobicity predicted the following TM segment boundaries for Panx1:</p> <p>TM1, M37-I60</p> <p>TM2, F108-W127</p> <p>TM3, L218-S236</p> <p>TM4, L275-F296¹⁷¹</p>
Channel Diameter	Oligomer and Pore Diameters	EM rPanx1 oligomer and pore diameters of ~140 Å and ~19 Å. ¹⁶⁶
Channel Passage	Chemical Flux/Efflux	Panx1 channel ATP efflux determined via luminometry. ¹⁷³

		<p>Negative and positive dye uptake indicates a Panx1 channel permeable to both cations and anions.¹⁸⁸</p> <p>Over-expression systems infer an intracellular Panx1 ER Ca²⁺ leak and Panx1 intercellular Ca²⁺ diffusion.¹⁶⁹</p>
Channel States; Open/Closed	Channel Deactivation/Activation	<p>Voltage-activated Panx1 channel currents are inhibited via food dyes Brilliant Blue FCF [BB FCF] and FD&C Green No. 3 (Fast Green FCF) and Probenecid. Luciferase assays exhibit Panx1 attenuations of ATP release in K⁺ induced Oocytes via the addition of these same blockers.^{69, 70}</p> <p>ATP application exhibits attenuated Panx1 currents indicating an ATP negative feedback loop. (Panx1 EL1 R75 mutant analysis exhibits attenuated ATP inhibitions of Panx1 currents.)¹⁷⁶</p> <p>Mutational deletions of the C-terminal region distal to the caspase cleavage site indicate a Panx1 C terminus auto-inhibition via current analysis.¹⁷⁴</p> <p>Experimentally stimulated Glial-like type II cells expressing functional ketanserin-sensitive 5-HT₂ receptors increase cytoplasmic Ca²⁺ activating a ketanserin-sensitive inward current thats blocked via CBX indicating high concentration intracellular Ca²⁺ Panx1 activation and CBX inactivation.¹⁷⁵</p> <p>Fluorescent tracer molecule uptake in erythrocytes indicates Panx1 activated ATP efflux via shear stress, low oxygen content and a high potassium depolarization. CBX addition blocks dye uptake indicating Panx1 inhibition.¹⁶⁷</p> <p>Ethidium (Etd) dye-up take and subsequent intracellular fluorescence experiments indicate Panx1 hemichannel openings via a membrane- receptor activation (i.e. HIV gp120/40-CD4 receptor-chemoreceptor complex). siRNA of Panx1 or host cell chemoreceptor blockers preclude dye-intake indicating an HIV Panx1 hemichannel activation conduit.⁸</p> <p>Single channel patch clamp tests indicate Panx1 membrane channels to be mechanosensitive ATP conduits.¹⁷³</p>
Channel Structural Analysis	Outer-Pore TM1/EL1, Inner-Pore C-Tail.	<p>Substituted Cysteine Accessibility Method (SCAM) inferred a TM1 and EL1 Panx1 outer pore channel lining and carboxy-terminal inner pore lining.¹⁷¹</p>
Protein Localization	Ubiquitously Expressed, Plasma Membrane and ER	<p>Panx1 is expressed in at least five inter-species. Northern Blot Analysis indicates plasma membrane Panx1 expression in the human brain, heart, skeletal muscle, skin, testis, ovary placenta, thymus, prostate, lung, liver, small intestine, pancreas, spleen, colon, blood endothelium and erythrocytes.¹⁷⁰</p>

		Overexpression of Panx1 indicates intracellular ER Panx1 permeable expression contributing to Ca ²⁺ leak. ¹⁷⁷
--	--	---

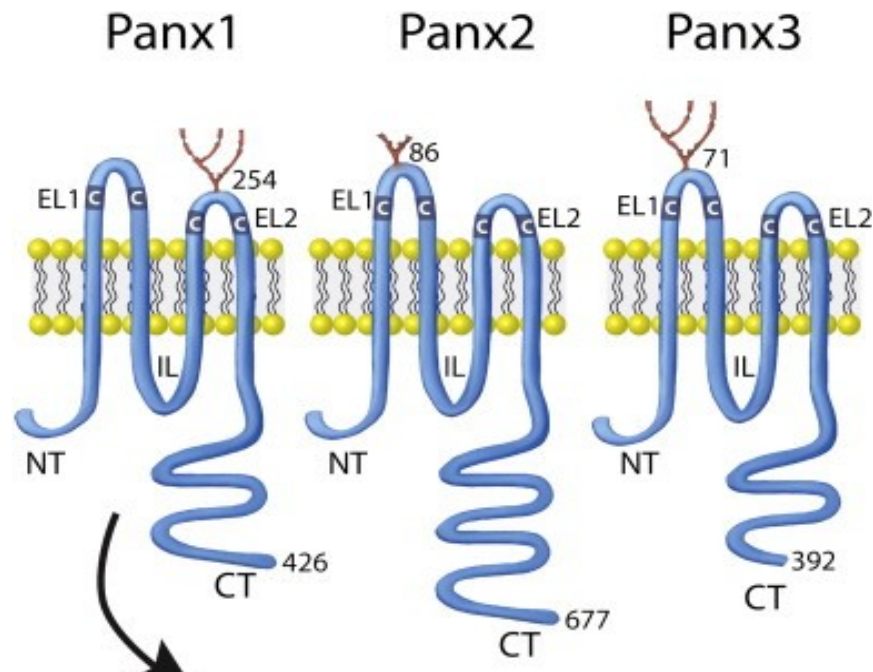
Table 4.) Pannexin-1 Structural/Functional Experimental Evidence

2.1.2 Pannexin-1 Phylogeny

Phylogenic and bioinformatics analyses suggests that Pannexin-1, 2 and 3 are paralogs diverged via gene duplication a priori to vertebrate species differentiation sharing their superfamily with the ortholog invertebrate gap junction innexin found in insects and nematodes (gap junctions are membrane proteins connecting the cytoplasm of cells towards communication via permeable ions and small molecules). Vertebrate connexins are similarly functioning gap junctions exhibiting a same tetra-membrane-spanning structure and hexamer channel, however, are not homologous to innexins nor pannexins. Connexins may have diverged first from pannexins and innexins from a distant protein ancestor.^{163, 164}

Pannexin sequence homology is closer amongst interspecies than paralogs, i.e. human to mouse Pannexin-1 exhibits a very high sequence homology of 86/94 identical(%) / conserved(%) whereas the most closely related human Pannexin-1 and Pannexin-2 family members exhibit just 41/59 sequence homology.¹⁶⁸ Pannexin-1 has evolved ubiquitous expression whereas Pannexin-2 and 3 are more limited to the brain and skin respectively, this variable expression may be mostly contributed to glycosylation and Pannexin-tail diversity. Pannexin-1 exhibits Gly-O, Gly-1 and Gly-2 variability promoting a more diverse tissue trafficking whereas Pannexin-2 only exhibits Gly-O limiting its distribution to mostly the ER.^{168, 169} The Pannexin N-tails are highly conserved contrarily their C-tails exhibit a great diversity linked to cell localization, function and interactions, i.e. Pannexin-1 and 3 exhibit a shorter C-tail exhibiting a higher LRR HCS consensus sequence than Pannexin-2 resulting in a greater tissue distribution.¹⁹² Pannexin trafficking is moreover connected to oligomerization and embryonic development; Pannexin-2 exhibits heptameric and or octameric states and Pannexin1 and 2 spatio-temporal neural distribution are inversely regulated during development.^{169, 107}

Figure 3.) Paralog Pannexin monomers exhibiting similar tetra-spanning transmembranes with In-Tail topology and cysteine homology. C-tail and glycosylation states effect tissue distribution.¹⁵⁹



Connexin26 and Innexin6 resemble Pannexin-1 most via topology and sequence respectively.^{166,}

¹¹¹ Pannexin-1 and Innexin6 exhibit similar weights and topology diameters.

	Pore Diameter	Oligomer Diameter	Weight
Panx1	1.7-2.1 nm	16.0-12.0nm	48.05 kDa
INX-6	1.9 nm	11 nm	45.13 kDa
Cx26	1.25 nm	8.1 nm	26.22 kDa ^{179, 166, 207, 208.}

209

Protein	Molecular Weight kDa ~	Single Particle Reconstruction Averages			Diameter Å ~	Pore size Å ~
		Ptcls	Class Avg	Rotational Avg		
Panx1	50	50			120	21
					160	17

Figure 4.) EM images of two grid orientations and two resolutions of clear pore rat Pannexin1 (rPanx1) oligomers, respective diameters exhibited.¹⁶

2.1.2.1 Pannexin-1 Residue Constraints

Structural and functional constraints restrain residue substitutions that occur during evolution maintaining a properly functioning folded protein (mutations may be compensated via a double-mutational compensation).¹³⁵

Protein Structure	Hemichannel Panx1 Pivotal Residues	Gap Junction Cx26 Pivotal Residues	Gap Junction INX-6 Pivotal Residues	Function
Membrane Juxtaposition	N-linked glycosylated at asparagine 255 in EL2 (mPanx1, site directed mutagenesis, N-glycosidase F treatment) ¹⁷⁰	Non-glycosylated (cryo-electron microscopy) ¹⁷⁸	Non-glycosylated ²⁰¹	Glycosylation promotes channel-channel steric hindrance precluding gap junction formation. ¹⁷⁰ Glycosylation effects protein structure function and stability. ²²⁷
Extracellular Loop Cysteine-Disulfide Bridges	Two-conserved cysteines in each EL; 1 EL1(66, 84), EL2 (246, 265) ¹⁸⁷	Three-conserved cysteines in each EL; EL1(53)-EL2(180), EL1(60)-EL2(174), EL1(64)-EL2(169) ¹⁷⁸ (RatCx26 expressed exogenously in <i>Xenopus laevis</i> , reduced conductance, site directed mutagenesis) ²⁰²	Two-conserved cysteines in each EL; EL1(58)-EL2(265), EL1 (76)-EL2(248) ¹⁷⁹	Gap junction cysteine-cysteine intramolecular disulfide bonding is a prerequisite towards channel formation. ^{178, 179} Panx1 cysteine disulfide bonding may modulate channel activity. ¹⁸⁷
Channel Positioning	Mutagenesis substitutions C347S and C40S (<i>Xenopus laevis</i> and N2A cells expressing	Mutagenesis G45E Syndromic Deafness, (mutant human Cx26G45E transgenic 14	Point mutagenesis precipitated leakage undiscovered ²⁰¹	WT native state closed, Ca ²⁺ leak via mutant residue. ^{182, 184, 187}

	mPax1 exogenously, increased conductance, dye uptake, site directed mutagenesis) ^{182, 187}	mouse expression, increased dye uptake) ¹⁸⁴		
N-Terminal Positioning	N-Terminal Insertion M-GS (HEK293 and CHO cells expressing hPax1 and mPax1 exogenously, GS insertion, increased conductance) ¹⁹⁸	Mutagenesis M34A Non-Syndromic Deafness and M34A ^{del2-7} (DWGTLQ) (mutant human Cx26M34A exogenously expressed in <i>xenopus</i> oocytes, cryo-electron crystallography, reduced dye uptake, zero conductance, X-ray model analysis) ¹⁹⁹	Similar N-terminal blocking channel activity (cryo-EM, modeling via COOT and PHENIX) ¹⁷⁹	Channel Regulation WT Pax1 native state closed via Pax1 N-terminal, N-terminal indirectly pore-blocks via ion selectivity or conductance. ¹⁹⁸ WT Cx26 native state open while N-terminus backed into pore, N-terminus mutant channel modulates a pore-closure. ¹⁹⁹
ATP-Channel Flux	EL1 R75 (oocytes expressing mPax1 exogenously, ATP application, attenuated current and dye uptake, site-directed mutagenesis) ¹⁷⁶	Undiscovered ²⁰⁰	Undiscovered ²⁰¹	Extracellular ATP inhibits an open Pax1 channel via the EL1 R75 residue regulating ATP efflux, a negative feedback loop. ¹⁷⁶
P2XR/NMDA/ Caveolin-Channel Complex-Interaction, Lipid Rafts	P2XR-Pax1 Complex, sites of interaction misunderstood. (Coimmunoprecipitation in endogenous and exogenous expression systems)	Cx26-P2XR/NMDA Complex undiscovered. ²⁰⁰ 15	Undiscovered ²⁰¹	A P2XR/NMDA-channel coupling promotes a sustained channel chemical flux. ^{189, 190} Lipid Raft Caveolin membrane transports/traffics. ²⁰⁴ Highly concentrated

	<p>NMDA-Src/Caveolin Complex-Panx1 unelucidated.^{189, 190, 203}</p> <p>Lipid Rafts-Lens Panx1 58/120 kDa Isoforms. (Detergent extraction, methyl-B-cyclodextrin)²¹⁷</p>	<p>Cx26 binds Caveolin-1 Complex, binding sites undiscovered. (293 T cells exogenously expressing Rabbit WT Cx26, immunoprecipitation, immunofluorescence, confocal microscopy)²⁰⁴</p>		<p>cholesterol lipid rafts regulate cell signaling.²¹⁶</p>
<p>Caspase Cleavage Site: Motif: DXXD-A/G/S/T/V¹⁹⁴</p>	<p>376DVVD379 Caspase 3 and 7 at cleavage site D379.</p> <p>Caspase cleavage regulatory region residues K381, T382, A386. (serial deletion, hPanx1 Jurkat cells, caspase dependent current increase)</p> <p>Panx1 mutagenesis TM1 F54C, C-terminal C426S. (hPanx1 exogenously expressed in HEK293T cells, Reversible cysteine cross-linking studies, current increase)¹⁷⁴</p>	<p>Nonexhibited²⁰⁰</p>	<p>Nonexhibited²⁰¹</p>	<p>Caspase cysteine promotes substrate cleavage at ending aspartic acid, integral to apoptosis.^{193, 30}</p> <p>Caspase cleavage releases pore-associated C-terminal auto-inhibition, TM1 F54 and C426 binding.¹⁷⁴</p>
<p>Protein Phosphorylation Src Family Kinase (SFK)</p>	<p>Y10, Y150, Y345 predicted phosphorylation sites, Y199,</p>	<p>Tail phosphorylation undetected.¹⁹⁶ 16</p>	<p>Seven C-tail putative phosphorylation sites</p>	<p>Post-translational phosphorylation of substrate residues S, T, Y is integral towards a</p>

	Y309 verified phosphorylation sites. (phosphosite GPS 3.0 predictive software, rPanx1 exogenously expressed in rat N2a cells, site-directed mutagenesis, TAT-Panx ₃₀₈ blocker and current reduction) ^{195, 205}		unverified. ¹⁹⁷	highly regulated/sophisticated gating. SFK modifies residue tyrosine. Panx1 phosphorylation may regulate channel opening directly or indirectly via modulation. ¹⁹⁵
C-Terminus Leucine-Rich repeat (LRR)	Carboxy-Tail (CT) R300-D379 exhibits 5-Highly Conserved Segments (HCS) Solenoidal LRRs. S329-H349 LRR HCS2 (mPanx1 exogenously expressed in HEK293t cells, complementary cell surface oligomerization/ glycosylation state analysis, motif deletion mutants, biotinylation confocal microscopy, EGFP fluorescence, ScanProsite LRR search) ¹⁹²	Nonexhibited ²⁰⁰	Nonexhibited ²⁰¹	C-terminus LRR motifs promote cell surface localizations. LRR HCS2 required for cell-surface localization. ¹⁹²
Panx1 Blocker: Carbenoxolone (CBX)-Channel	EL1 W74 pivotal residue towards CBX	Gap-Junction 17	Gap-Junction 1	CBX modulates WT Panx1 stimulated open state attenuating channel

Interaction	hemichannel block, EL1 Conserved Region residues 67-86 mediate CBX binding. (hPanx1 exogenously expressed in HEK293T cells, mutagenesis CBX current analysis) ¹⁵			activity. W74 acts as a polarity switch. ¹⁵ Gap junction cell to cell adhesion precludes extracellular ligand block.
Panx1 Blockers: Probenecid, BB FCF, Fast Green FCF-Channel Interaction	EL1-74, EL2-237, 240, 247, 266 pivotal residues towards chemical hemichannel block. (mPanx1 exogenously expressed in Xenopus oocytes, alanine replacement mutants, mutant current enhancement) ⁶⁹	Gap-Junction-1	Gap-Junction	Blockers modulate WT Panx1 stimulated open state attenuating channel activity. ¹⁵ Gap junction cell to cell adhesion precludes extracellular ligand block.
Panx1 Blocker: Mimetic ¹⁰ Panx1-Channel Interaction	Hexamer pore-region pivotal residues towards mimetic peptide hemichannel block. A possible cryptic binding site(s). (mPanx1 exogenously expressed in Xenopus oocytes, dye and current attenuation) ⁶⁶	Gap-Junction	Gap-Junction	¹⁰ Panx1 sequence specific block unlikely, WT Panx1 stimulated open state steric block attenuating channel activity. A possible cryptic mimetic peptide Panx1 binding site may exist inducing conformational pore closure. ⁶⁶ Gap junction cell to cell adhesion precludes extracellular ligand block.

Table 5.) Potential functional and structural residue constraints via experimental evidence.

Non-experimental Pannexin-1 comparative protein sequence analysis amongst uncrystallized homologs further exhibit residue structural and functional constraints.

✓ NP_056183.2	376	DVVDGKTPMSA-EMR-EE-QGNQTAE---LQGMNIDSETKANNGEKNARQL	LDS	SC	426
✓ AAH16931.1	376	DVVDGKTPMSA-EMR-EE-QGNQTAE---LQGMNIDSETKANNGEKNARQL	LDS	SC	426
✓ XP_003813837.1	376	DVVDGKTPMSA-EMR-EE-QGNQTAE---LQGMNIDSETKANNGEKNARQL	LDS	SC	426
✓ CAR31475.1	376	DV-DGKTPMSA-EMR-EE-QGNQTAE---LQGMNIDSETKANNGEKNARQL	LDS	SC	425
✓ XP_004052028.1	376	DVVDGKTPVSA-EMR-EE-QGNQTAE---LQGMNIDSETKANNGEKNARQL	LDS	SC	426
✓ PNJ86390.1	376	DVVDGKTAMSA-ETR-EE-HGNQTAE---LQGMNIDSETKANNGEKNARQL	LNS	SC	426
✓ AAK91713.1	376	DVVDGKTPMSA-EMR-EE-QGNQTAE---LQ----DSETKANNGEKNARQL	LDS	SC	422
✓ AAC61779.1	376	DVVDGKTPMSA-EMR-EE-QGNQTAE---LQ----DSETKANNGEKNARQL	LDS	SC	422
✓ NP_001124868.1	376	DVVDGKTAMSA-ETR-EE-HGNQTAE---LQGMNIDSETKANNGEKNARQL	LNS	SC	426
✓ XP_025213190.1	376	DIVDGKTPMSA-ETR-EE-QGNQTAE---LKDMNIDSEIKANNGKKNARQL	LDS	SC	426
✓ EHH23343.1	376	DIVDGKTPMSA-ETR-EE-QGNQTAE---LKDMNIDSEIKANNGKKNARQL	LDS	SC	426
✓ XP_011781952.1	376	DIVDGKTPMST-ETR-EE-QGNQTAE---LKDMNIDSEIKANNGKKNARQL	LDS	SC	426
✓ XP_017729206.1	376	DIVDGKTPMSA-ETR-EE-QGNQTAE---LKDMNIDSEIKANNGKKNARQL	LDS	SC	426
✓ XP_011850409.1	376	DIVDGKTPMSA-ETR-EE-QGNQTAE---LKDMNIDSEIKANNGKKNARQL	LDS	SC	426
✓ XP_011744164.1	376	DIVDGKTPMSA-ETR-EE-QGNRTAE---LKDMNIDSEIKANNGKKNARQL	LDS	SC	426
✓ XP_005579427.1	376	DIVDGKTPVSA-ETR-EE-QGNQTAE---LKDMNIDSEIKANNGKKNARQL	LDS	SC	426
✓ PNJ86391.1	376	DVVDGKTAMSA-ETR-EE-HGNQTAE---LQ----DGETKANNGEKNARQL	LNS	SC	422
✓ XP_003253050.1	376	DVVDGKTPVSA-ETR-EE-PGNQTAK---LQGMNIDSETKANNGEKNARQL	LDS	SC	426
✓ XP_003910603.1	376	DIVDGKTPMST-ETR-EE-QGNQTAE---LKDMNIDSEIKANNGKKNARQL	LDS	SC	426
✓ XP_010353147.1	376	DIVDGKTPMSA-ETR-EE-QGNQMAE---LKDMNIDSEIKANNGKKNARQL	LDS	SC	426
✓ XP_001088479.1	376	DIVDGKTPVSA-ETR-ED-QGNQTAE---LKDMNIDSEIKANNGKKNARQL	LDS	SC	426
✓ XP_023081403.1	376	DIVDGKTPMST-ETR-EE-QGNQTAE---LKDMNIDSEIKANNGKKNARQL	LDS	SC	426
✓ XP_00801745.1	376	DIVDGKTPMSA-ETR-EE-QGNQTAE---LKDMNIDSEIKANNGKKNARQL	LDS	SC	426
✓ AOY63021.1	376	CASHLKTMSA-EMR-EE-QGNQTAE---LQGMNIDSETKANNGEKNARQL	LNS	SC	426
✓ XP_011933207.1	385	DIVDGKTPMSA-ETR-EE-QGNQTAE---LKDMNIDSEIKANNGKKNARQL	LDS	SC	435
✓ XP_025213191.1	376	DIVDGKTPMSA-ETR-EE-QGNQTAE---LKD----SEIKANNGKKNARQL	LDS	SC	422
✓ XP_011781953.1	376	DIVDGKTPMST-ETR-EE-QGNQTAE---LKD----SEIKANNGKKNARQL	LDS	SC	422

Table 6.) National Center for Biotechnology Information (NCBI) BLAST Non-Redundant Protein Sequence (nr) Database search exhibiting uncrystallized Pannexin-1 query homologs with comparatively high sequence identities (> ~80%) exhibiting micro-evolutionary constraints, i.e. non-red highlighted residues exhibiting Pannexin-1 functional constraints of the caspase cleavage site DVVD and its downstream associated regulatory regional residues highlighted in light blue.¹³³

Reference sequence (query): Pannexin-1
Identities normalised by aligned length.
Colored by: property

HSP processing: ranked
Search cycle: 3

Pannexin-1	bits	E-value	N	100.0%	1:426
1 UniRef50_Q292M7	Pannexin 4 n=4 Tax=Opisthob...	324	5e-87	12.54	11409 61411
2 UniRef50_Q4V7M6	Pannexin 2 n=4 Tax=Opisthob...	322	1e-86	14.38	12410 31412
3 UniRef50_Q216N1	Innexin3 n=5 Tax=Platyhelmi...	322	2e-86	14.64	61417 37471
4 UniRef50_Q96807	Pannexin-1 n=22 Tax=Buteleo...	319	1e-85	19.88	1426 1426
5 UniRef50_Q61966	Innexin protein 4 n=4 Tax=C...	308	2e-82	13.08	51425 29470
6 UniRef50_Q03412	Innexin unc-7 n=7 Tax=Chrom...	308	2e-82	11.64	13391 120157
7 UniRef50_Q81601	Innexin 2 n=2 Tax=Hirudo me...	305	2e-81	14.14	12386 1384
8 UniRef50_Q8M059	Innexin protein 18, isoform...	304	5e-81	11.04	19419 12413
9 UniRef50_Q17394	Innexin protein 1, isoform...	303	9e-81	11.74	14398 1379
10 UniRef50_A8PSM6	Innexin family protein n=1...	300	6e-80	13.78	9410 12413
11 UniRef50_A8W2H1	C. briggsae CBR-UNC-9 prote...	296	9e-79	13.88	12395 14448
12 UniRef50_Q87393	Innexin n=1 Tax=Chaetopteru...	291	3e-77	15.94	12389 1386
13 UniRef50_Q23157	Innexin-11 n=3 Tax=Caenorha...	289	2e-76	12.98	11421 2418
14 UniRef50_Q38H87	Innexin 4 n=1 Tax=Hirudo me...	285	1e-75	13.94	12385 1386
15 UniRef50_Q81602	Innexin 1 n=1 Tax=Hirudo me...	282	1e-74	13.78	12398 1395
16 UniRef50_Q216N2	Innexin n=1 Tax=Dugesia ja...	282	2e-74	15.28	61400 33442
17 UniRef50_Q2V7F0	Pannexin 5 n=1 Tax=Aplysia...	282	2e-74	12.78	11405 11400
18 UniRef50_Q46887	Innexin protein 13 n=2 Tax=...	281	4e-74	16.38	22402 81385
19 UniRef50_Q19746	Innexin-3 n=3 Tax=Chromador...	278	2e-73	16.18	24390 14376
20 UniRef50_Q216N0	Innexin4 n=1 Tax=Dugesia ja...	276	1e-72	12.14	81397 1407
21 UniRef50_Q22549	Innexin-10 n=4 Tax=Chromado...	275	2e-72	12.68	14403 1400
22 UniRef50_A8P215	Innexin protein 1, isoform...	274	4e-72	11.58	14395 1347
23 UniRef50_A8M0M6	C. briggsae CBR-INK-20 prot...	272	2e-71	15.94	14423 13421
24 UniRef50_Q4Q011	Innexin, putative n=1 Tax=S...	270	9e-71	16.08	14389 51394
25 UniRef50_Q216M6	Innexin9 n=2 Tax=Dugesia ja...	268	3e-70	11.98	11415 1422
26 UniRef50_A8NM61	Innexin family protein n=1...	267	6e-70	13.38	12394 1394
27 UniRef50_Q9V427	Innexin lnx2 n=34 Tax=Arthr...	266	1e-69	12.48	12381 1349
28 UniRef50_Q61715	Innexin-19 n=4 Tax=Caenorha...	266	1e-69	13.88	20409 25441
29 UniRef50_Q38H86	Innexin 5 n=1 Tax=Hirudo me...	263	1e-68	15.48	8416 1413
30 UniRef50_Q23027	Innexin-5 n=2 Tax=Caenorhab...	262	2e-68	13.58	12395 1389
31 UniRef50_Q4QFC5	Innexin, putative n=1 Tax=S...	258	2e-67	12.98	13414 4424
32 UniRef50_Q2V7E9	Pannexin 6 n=1 Tax=Aplysia...	258	3e-67	12.98	11405 4401
33 UniRef50_Q38H80	Innexin 11 n=2 Tax=Hirudo m...	257	9e-67	14.48	13417 1412
34 UniRef50_Q216N5	Innexin10 n=2 Tax=Dugesia j...	256	1e-66	13.98	12407 1411
35 UniRef50_A8PTT8	Innexin family protein n=1...	255	2e-66	13.68	57416 46402
36 UniRef50_Q01612	Innexin-12 n=2 Tax=root Rep...	255	1e-66	13.18	19385 4177
37 UniRef50_Q4QD21	Innexin, putative n=1 Tax=S...	254	4e-66	12.28	24425 19469
38 UniRef50_C5J901	Innexin, putative n=2 Tax=S...	253	1e-65	12.98	12405 6123
39 UniRef50_Q21123	Innexin-7 n=2 Tax=Caenorhab...	250	5e-65	12.28	13423 1448
40 UniRef50_Q61787	Innexin-16 n=3 Tax=root Rep...	245	2e-63	10.78	12384 33451
41 UniRef50_UF1000051A76F	PREDICTED: similar to Innex...	245	3e-63	11.98	61407 24046
42 UniRef50_Q216N6	Innexin7 n=2 Tax=Bukaryota...	244	4e-63	12.68	84143 1401
43 UniRef50_C5J944	Innexin, putative n=1 Tax=S...	241	4e-62	10.48	15408 107552

Table 7.) Phyre²²'s sequence profiling HHblits' View PSI-Blast Multiple Sequence Alignment tool gathering mostly non-crystallized Panx1 query homologs exhibiting a low (<20%) mutual sequence identity, i.e. yellow highlighted C-residues trace macro-evolutionary homologous EL channel structural constraints.^{136, 132}

2.2 Purinergic Receptor Structure and Function

Ubiquitously expressed Purinergic (P2) Receptors have affinities for Pannnexin-1 effluxed ATP and its hydrolyzed ADP. P2 is subdivided into Ionotropic P2X and Metabotropic P2Y Purinergic Receptors. P2X exhibits a trimeric structure using seven individual P2X subunits (P2X1-P2X7) and is a ligand gated cation channel/pore promoting Ca⁺ influx and K⁺ efflux when ATP bound. P2Y exhibits eight P2Y subtypes (P2Y1, P2Y2, P2Y4, P2Y6, P2Y11, P2Y12, P2Y13, and P2Y14) and is coupled to intracellular signaling pathways through heterotrimeric G-proteins.^{2, 10} Purinergic signaling is fundamental to many cellular processes (i.e. exocrine/endocrine secretion, neuromodulation) including inflammation and alternatively immunosuppression eg. Chlamydia infected macrophages are protected from apoptosis via a pathogenic hijacking of extracellular ATP purinergic receptors (HIV similarly promotes itself via purinergic modulation).^{1, 2, 8, 10, 14}

Purinergic receptor P2X is activated via extracellular ATP resulting in an increase in intracellular calcium.⁹ Mammalian ATP-gated cation channel (P2XR) subunits each contain a large ectodomain, two transmembrane domains and an intracellular N and C termini. Functioning P2XRs are homomeric or heteromeric trimers and contain binding sites involved in activation (orthosteric) and regulation (allosteric). Ectodomains contain three ATP orthosteric agonist binding sites promoting the conformational changes allowing gating, they are located between neighboring subunits and are composed of highly conserved residues. ATP agonist potency is determined via positively charged amino acids lysines coordinating binding of the negatively charged phosphate tail of ATP and aromatic phenylalanine residues coordinating the binding of the ATP adenine ring. Transmembrane domains account for the channel pore and the allosteric regulatory region. The N- and C- domain structures determine the kinetics of receptor desensitization and or pore dilation, critical towards the receptor regulation of ATP (N and C termini may also modulate allosterically).⁹¹

Purinergic receptor P2Y is activated via extracellular ATP byproducts ADP and UTP.⁹ P2Y receptors include an extracellular N-terminus containing several potential N-linked glycosylation

sites, seven transmembrane spanning domains assisting in forming the ligand binding pocket, three extracellular loops, three intracellular loops that participate in G protein coupling and an intracellular C-terminus containing several consensus binding phosphorylation sites for protein kinases.⁹² P2Y receptors are G protein-coupled receptors (GPCRs) coupling to heterotrimeric G-Proteins consisting of a $G\alpha$ subunit that is tightly associated with $G\beta\gamma$ subunits. P2Ys act as guanine nucleotide exchange factors (GEFs) for heterotrimeric G proteins causing dissociation of the G protein from the activated receptor and from its other $\beta\gamma$ subunits.⁹² Once released the separated G protein subunits may interact with a variety of effector proteins leading to activation or deactivation of the effector protein ultimately effecting homeostatic/physiological processes.³

9, 10, 12, 92

2.3 AR Receptor Structure and Function

AR Receptors have affinities for Pannnexin-1 effluxed ATP hydrolyzed adenosine. A1, A2A, A2B and A3 are the heterotrimeric guanine nucleotide-binding protein (G protein) coupled metabotropic receptors, each subtype has a unique binding profile, activation profile, subcellular localization and G protein binding preference. The primary sequence variation within GPCR family A is large and the A2A receptor characteristically displays seven-transmembrane α -helices (7TM, helices 1-7), one short membrane associated helix (helix 8), an extracellular amino-terminus (N-terminus), a cytosolic carboxy terminus (C-terminus), three extracellular loops (ECL1-3) and three intracellular loops (ICL1-3).

All subtypes have N-linked glycosylation sites and A1, A2B and A3 subtypes have potential palmitoylation sites at the end of helix-8, the former does not alter ligand binding properties but may target receptors to the plasma membrane, the later does not effect G-protein binding nor receptor down-regulation but does effect receptor degradation subsequent to synthesis. (The depalmitoylation of adenosine A3 receptor increases phosphorylation of the receptor causing a rapid desensitization of the receptor.)

The extramembrane domains display significant structural diversity between subtypes. The extracellular domain of A2A is a funnel-like ligand binding cavity displaying a negatively charged randomly coiled binding cleft primarily formed from ECL2 (extracellular loop 2). ECL2 contains a very short alpha helical segment forming a critical aromatic pie-stacking

interaction between phe168 and bound ligand and is held together via four disulfide bridges. Subtype receptors display affinities towards different agonists and antagonists due to very small sequence variations in the residues of their binding cavities. Only a few residues in the transmembrane domains are highly conserved indicating relevance and importance in conformational changes during activation. As well conserved towards the activation process are hydrogen bonds to internal water molecules connecting the extracellular cavity to the intracellular space, these waters are pivotal towards receptor activation via ligand.

A

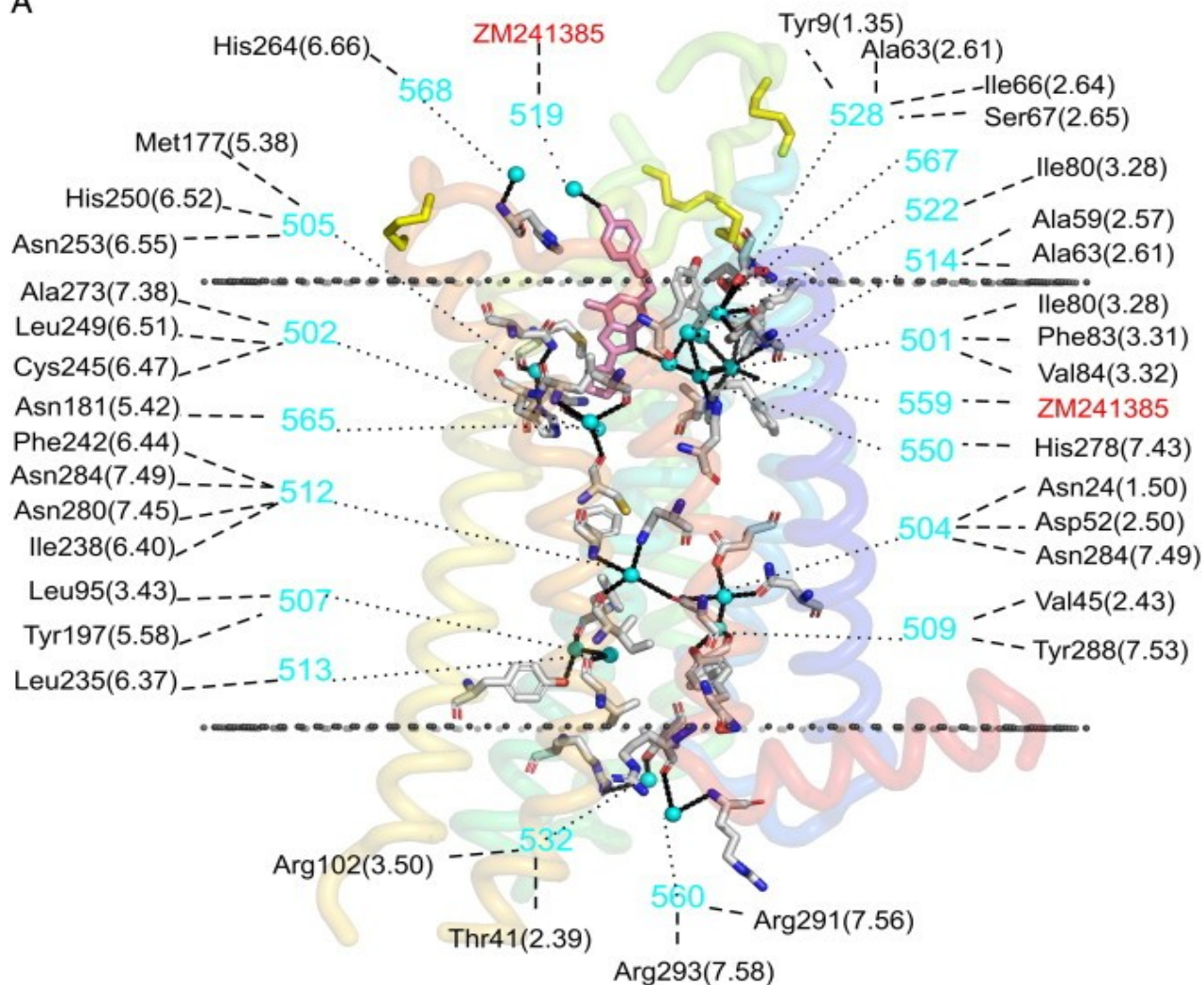


Figure 5.) Three-Dimensional image of human adenosine A2A receptor:antagonist ZM241385. Waters are blue-dots, interacting side-chains are white sticks and bound ZM241385 is a pink stick model.⁹⁵

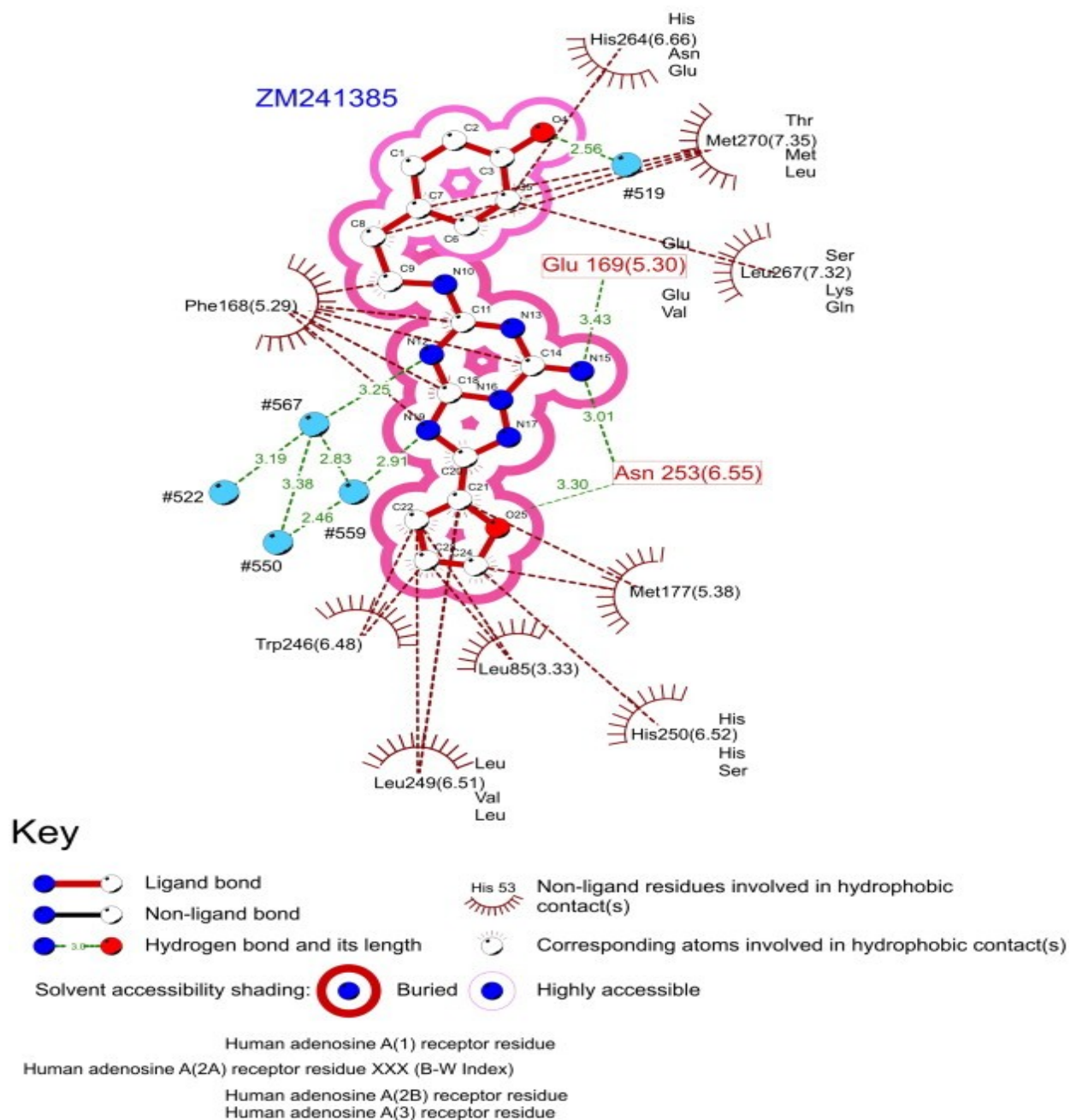


Figure 6.) Human adenosine A2A receptor bound to antagonist ZM241385 in pink. Water molecules #519, #559 and #567 directly interact with antagonist ZM241385. Image displays ECL2's critically flexible non-covalent aromatic pie-stacking interaction between phe168 and bound ligand.⁹⁶

The intracellular domain and carboxy terminus in A2A mediate G-protein binding and signaling. There are several predicted phosphorylation sites within the cytoplasmic and carboxy terminal domains of all four adenosine receptor subtypes.⁹⁴ Activation via extracellular adenosine results in an increase in intracellular calcium effecting homeostatic/physiological processes.

Future studies may aim to block the Pannexin-1 channel via a similar antagonistic mechanism exploiting flexible non-covalent bonding connected to a specific water molecule arrangement ultimately reducing negative AR signaling towards homeostatic/physiological processes.^{2, 93, 94}

2.4 Pannexin-1 Inhibitors

Pannexin-1 blockers are being used to therapeutically treat disease (eg. CBX is prescribed towards digestive ulcer and inflammation) and study the physiology of Pannexin-1 (eg. Food dyes Brilliant Blue FCF [BB FCF] and FD&C Green No. 3).^{69, 20} Although elusive, blocker experimental evidence has pointed to Pannexin-1 pivotal regional areas connected to pore gating, residues EL1 67-86 (FSPSSF*WRQAAFVDSYCWA) and EL2 (237 (L), 240 (L), 247 (S), 266 (K)).^{15, 69, 70} The following four small chemicals and one small mimetic peptide block open Pannexin-1 channels.

2.4.1 CBX

Chimeric Panx1/3 has proven the Pannexin-1 first extracellular loop (EL1) to be of pivotal importance towards chemical Carbenoxolone (CBX)-mediated inhibition. Moreover within EL1, mutant analysis has uncovered variable single aromatic residue position W74 to act as a polarity switch, i.e. CBX enhances currents in a Panx1 W74A point mutant proving CBX to function as a gating modulator of Pannexin-1. Additional cysteine mutagenesis experiments has proven residues 67-86 in Pannexin-1 EL1 to similarly compromise or reverse CBX effects, many of these proven conserved residues are hydrophobic and may therefore mediate a CBX hydrophobic to hydrophobic binding supporting its function.¹⁵

2.4.2 Probenecid

Chemical Probenecid, used to treat gouty arthritis, is specific to Pannexin-1 channels, however, its inhibitory effects are obscure.² Probenecid is hydrophobic and satisfactorily water-soluble and may therefore affect the Pannexin-1 transmembrane regions in addition to the EL1/2 Regions.⁷⁰

2.4.3 Food Dyes

Food dyes Brilliant Blue FCF [BB FCF] and FD&C Green No. 3 exhibit dose selective Pannexin-1 channel inhibition. Alanine mutant studies confirm Pannexin-1 EL1/2 areas to be food dye binding and or gating structures.⁶⁹

2.4.4 ¹⁰Panx1

Pannexin Mimetic Peptide ¹⁰Panx1, a Peptide-Based Inhibitor exhibiting Pannexin-1 EL1 10-residue regional sequence WRQAAFVDSY, most likely blocks Pannexin-1 partially (30% inhibition) via steric channel block not sequence specificity; high inhibiting peptide concentrations, small ion flux and Connexin-mimetic peptide block prove this.⁶⁶ Although elusive, ¹⁰Panx-1 may activate a docking gate via a cryptic binding site keeping the hemichannel closed, this has been demonstrated successfully in HIV CD4⁺ T lymphocytes and may therefore function towards the treatment of HIV.^{2, 8, 66}

2.5 Pannexin-1 Towards Physiology and Pathology

Pannexin-1 transmembrane protein, ATP and its byproducts and its conduit purinergic receptors effect an array of physiological functions towards homeostasis and pathology eg. blood pressure regulation, infectious disease. Accordingly a comprehension of an array of these conduits towards physiology/pathology will assist in determining nanoparticle gating viability and effects in vivo. For example blocking Pannexin-1 to treat HIV or Neuropathic Pain may deleteriously effect Blood Pressure, apoptosis and inflammatory homeostatic regulation.^{2, 35}

2.5.1 Ischemic Stroke

Ischemic Stroke is a dire disease effecting 15 million people worldwide annually resulting in devastating ~33% mortality and disability rates. Neural cell functioning requires an abundance of glucose and oxygen supplied via apropos blood flow. Thrombosis or cerebral artery obstruction precludes the former resulting in severe brain tissue damage via excitotoxicity, peri-infarct depolarizations, inflammation and apoptosis. Pannexin-1 and its conduit Purinergic Receptors are connected to these cell-damaging biochemical cascades.²

Anoxia over-activates the NMDA receptor which, via a Src kinase intermediate, opens the Pannexin-1 Channel releasing ATP which activates purinergic receptor opening and irregular intracellular Ca²⁺ influx.^{2, 34} This dis-regulated cationic pool subsequently mis-regulates enzymes

which damage neural cell membranes, DNA and structural cytoskeleton.^{34,33} Ischemic Peri-infarct depolarizations and inflammation are furthermore connected to Pannexin-1 channel openings via the NMDA pathway.^{33,32}

2.5.2 Apoptosis

Apoptosis is a natural programmed cell death integral to development and homeostasis, accordingly its mis-regulation can be deleterious. Apoptotic cells releasing ATP attract monocytes towards apoptosis, Pannexin-1 hemichannel is directly responsible for this release via Pannexin-1 intracellular carboxy terminal region caspase cleavage (the Pannexin-1 C-terminus is a dissociable channel blocker).^{2,31,30}

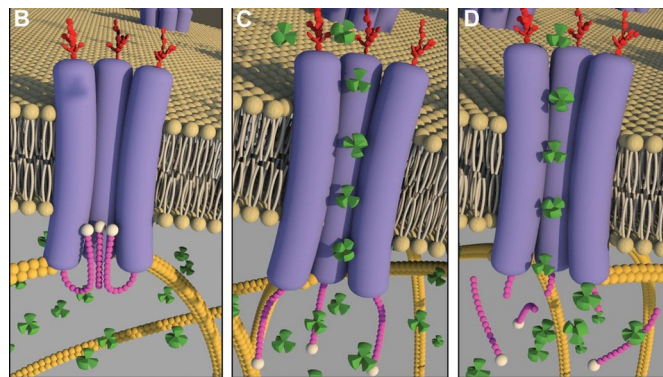


Figure 7.) Pannexin-1 channel opening towards immune cell apoptosis via caspase cleavage.⁷

Pannexin-1 hemichannel Ca^{2+} release located within the ER membranes further control apoptosis via an upgraded Ca^{2+} release out of the ER lumen triggering a Mitochondrial apoptotic conduit.^{2,}

31

2.5.3 Atherosclerosis

Chronic Inflammatory Disease Advanced Atherosclerosis develops via a cascade of events involving arterial plaque formation, fatty streaks, arterial wall thickness, oxygen supply reduction; together these may cause vascular disease, ischemic stroke and myocardial infarction. During the progression of Atherosclerosis there is a monocyte recruitment to the arterial inflamed region, Pannexin-1, its ATP byproduct and purinergic receptor conduit are intimately linked to this inflammatory migration event. HIF-1 α (Hypoxia-Inducible Factor-1) and its expressed VEGF (Vascular Endothelial Growth Factor) are linked to atherogenesis when exposed to atherogenic conditions, adenosine and its receptors precipitate each of these factors. Accordingly

a Pannexin-1 hemichannel opening and ATP extracellular release and subsequent hydrolysis to adenosine may play an existing role in this adenosine-mediated atherosclerosis mechanism. Contrastingly and importantly if considering Pannexin-1 blockage towards Artherosclerosis or other Pannexin-1 related illnesses, functioning adenosine and its receptors are integral to anti-atherosclerosis mechanisms in the liver.

Atherosclerotic plaques are composed of dysregulated SMC (Smooth Muscle Cell) expressions. ATP purinergic receptor binding stimulates these SMC irregularities, however as in the liver, adenosine byproducts act as endogenous modulators integral to anti-atherosclerosis. Accordingly Pannexin-1 closure to prevent Atherosclerosis may contrastingly aid in the development of atherosclerosis.

ATP purinergic receptor activation yields fibroblast proliferation integral to vascular adventitia and therefore possibly a conduit to atherosclerotic lesion and rupture causing ischemic stroke and myocardial infarction. Accordingly Pannexin-1 may as well be intimately involved in plaque destabilization and fatality.²

2.5.4 Blood Pressure Regulation

Blood pressure is highly regulated via an interwoven neural, vascular and renal mechanic network evolved to maintain a proper activity/time dependent blood pressure within physiological limits.²⁹ Pannexin-1 is an integral vascular source of ATP release within this BP regulating cellular response network heavily relying on purinergic autocrine/paracrine signaling, i.e. vasoconstriction regulation via the Pannexin-1 intracellular loop activated via an $\alpha 1$ adrenoreceptor ($\alpha 1AR$) signal.^{29, 28} Accordingly, similar to apoptosis and inflammation homeostatic regulation, functioning Pannexin-1 is nontrivial.

2.5.5 Neuropathic Pain

Physicochemical neural insult triggers inflammation and sensor-neural remodeling precipitating neuropathic pain. This neuropathic pain conduit may be ameliorated via Pannexin-1 inhibition. Neuropathic pain exhibits homeostatic inflammation and apoptosis amongst neural and immune cells via a Pannexin-1 produced ATP intermediate. Accordingly, blocking Pannexin-1 signaling can be a viable therapeutic treatment towards neuropathic pain prevention.²⁷

2.5.6 Synaptic Plasticity Towards Learning

Synaptic plasticity is based on the brain's ability to develop memories and learn via micro-scale changes amongst neural dendrites formed via regulated electrical synaptic activity.²⁶ Open Pannexin-1 ATP channels maintain an extracellular pool of hydrolyzed byproduct adenosine, a critical nucleotide towards precluding glutamate and methyl-D-aspartate receptor (NMDAR) over-activation and persistent Long-term Potentiation (LTP). Hyper/persistent synaptic activity results in anxiety, sensor-motor gating disabilities and impaired learning and memory. Accordingly Pannexin-1 and its byproduct adenosine are needed to stabilize synaptic plasticity towards memory and learning and may ameliorate CNS Disorders.²⁵

2.5.7 Immune-Regulation

Inflammation is a self-defense mechanism to repair, i.e. cytoskeleton rearrangements towards repair. Pannexin-1s' form an ATP, small RNA, SL1, NAD⁺ and Ca²⁺ release channel integral towards immune-regulation, eg. Pannexin-1 intracellular ATP efflux promotes a 'Find Me Signal' towards macrophage apoptotic clearance and immune activation and self-deactivation (ATP closing Pannexin-1).² Pannexin-1 and its connected Purinergic/AR Receptors are intimately connected to this immune-regulation as well as its deregulation via a pathogenic hijacking, HIV host cell entry and immunosuppression is an example of the later.

2.5.7.1 HIV and Pannexin-1 Modulation and Immunosuppression

HIV has an innate ability to modulate the host-cell receptor/co-receptor-Pannexin-1-purinergic pathway promoting host-cell entry and later stages of the HIV life-cycle. HIV mediates adjacent Pannexin-1 hemichannel opening in CD4⁺ T cells and macrophages via the bound complex HIV surface glycoprotein gp120-CD4 receptor and HIV transmembrane glycoprotein gp41-CD4 chemoreceptor.⁸ Research cell lines indicate that gp120 signals through chemoreceptor CCR5 activating/opening Pannexin-1 channels resulting in intra to extracellular ATP passage (the molecular model of how HIV opens this channel is elusive and may involve membrane stress). Subsequent extracellular ATP and its hydrolyses promote autocrine activation of adjacent purinergic/AR receptors ultimately promoting HIV entry and its replication via a bi-phasic cascade of intra/extracellular events.^{2, 8, 9, 10} Purinergic P2X1 and P2Y2 receptors cause host-cell membrane depolarization and HIV-host-cell membrane fusion and are of pivotal importance towards the early entry stage of HIV infection in immune cells. P2X7 and P2Y1 receptors similarly create a membrane depolarization and participate in late stages of the HIV-life cycle

(P2Y1 may also participate in entry).^{2,9} Ca^{2+} signaling is pivotal to both early and late stage HIV infection, the exact mechanism of the former remains to be elucidated, the later involves a diversity of functions i.e. the promotion of HIV-1 Gag trafficking and viral particle release via Ca^{2+} -Gag-PI(4,5)P2 plasma membrane stabilization.^{17, 19}

Purinergic Receptors are HIV indirectly modulated via an open Pannexin-1 ATP efflux. Extracellular ATP released through open Pannexin-1 hemichannels binds to and initially activates P2X1 receptors causing calcium influx (P2X1 is highly sensitive to ATP being activated by low nano-molar concentrations, intracellular calcium pools precipitate via openings in nonselective cation channels, Ca^{2+} -activated K^{+} channels, as well) facilitating HIV entry.¹⁰ ATP antagonizes P2X7 poorly and therefore requires an accumulation, accordingly P2X7 is ATP activated subsequent to ATP-sensitive P2X1 activation. P2X7 then subsequently is ATP-activated causing further calcium influx downstream signaling facilitating later stages of the HIV life-cycle.^{3, 9, 10} ATP does not antagonize P2Y1 and must be converted to P2Y1's antagonist ADP via extracellular ecto-nucleoside triphosphate diphosphydrolase (E-NTDPase). Once activated via ADP, P2Y1's G-protein conduits a secondary IP3 signal promoting intracellular calcium storage release facilitating HIV later-replication stages (P2Y1 may also promote HIV entry).^{3, 8, 9, 10}

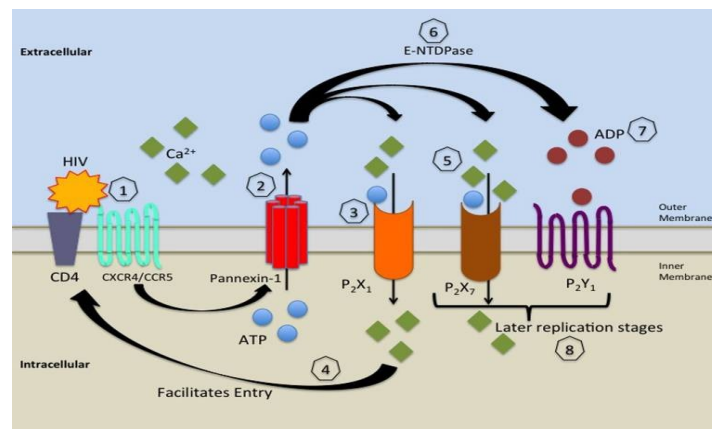
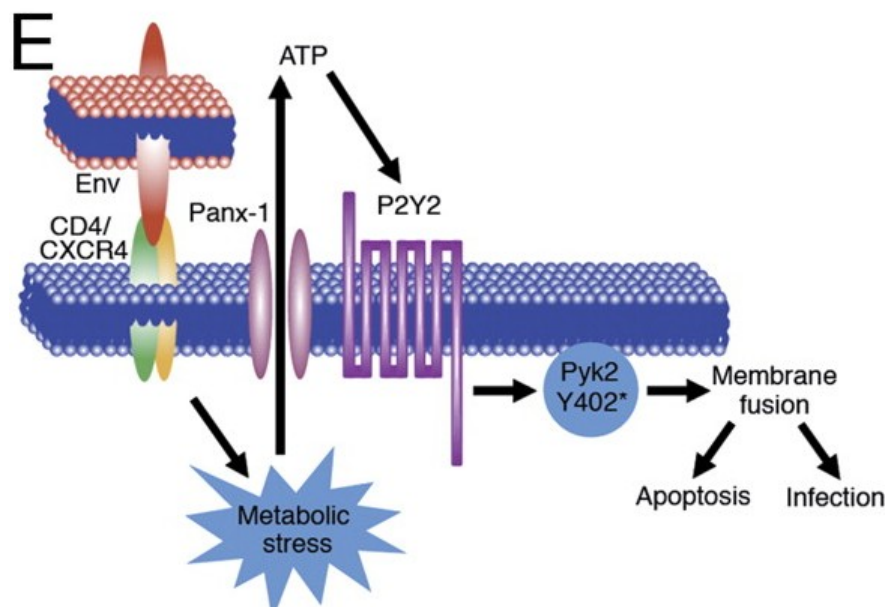


Figure 8.) Proposed model for the role of Pannexin-1 hemichannel and purinergic receptors during HIV infection; open Pannexin-1 channels precipitate HIV infection.³

In the case of P2Y2, effector protein proline/tyrosine kinase Pyk2 is activated/phosphorylated (Pyk2Y402*) (P2Y2's Src homology domain 3 (SH3) binding (PxxP) site controls the phosphorylation of tyrosine 402 of Pyk2 (pyk2 may autophosphorylate)) via P2Y2's G-protein

activating mechanism ultimately promoting plasma membrane depolarization, hemifusion and fusion, required for early HIV-1 infection. Pyk2 is a critical effector of HIV-1 infection operating downstream of P2Y2.¹⁰

Figure 9.) Involvement of Pannexin-1, ATP release, P2Y2 activation, and Pyk2Y402* phosphorylation in early stages of HIV-1 infection (the pathological HIV life cycle via a tyrosine kinase in the hypothetical cascade (pannexin-1 → ATP → P2Y2 → Pyk2)). Binding of HIV-1 envelope to cellular receptors leads to rapid ATP release from host cells through Pannexin-1 channels. ATP then activates P2Y2 receptors, leading to activation (phosphorylation) of Pyk2 (Pyk2Y402*). P2Y2 and Pyk2 control plasma membrane depolarization, hemifusion, and fusion, which are required for HIV-1 entry-infection.¹²

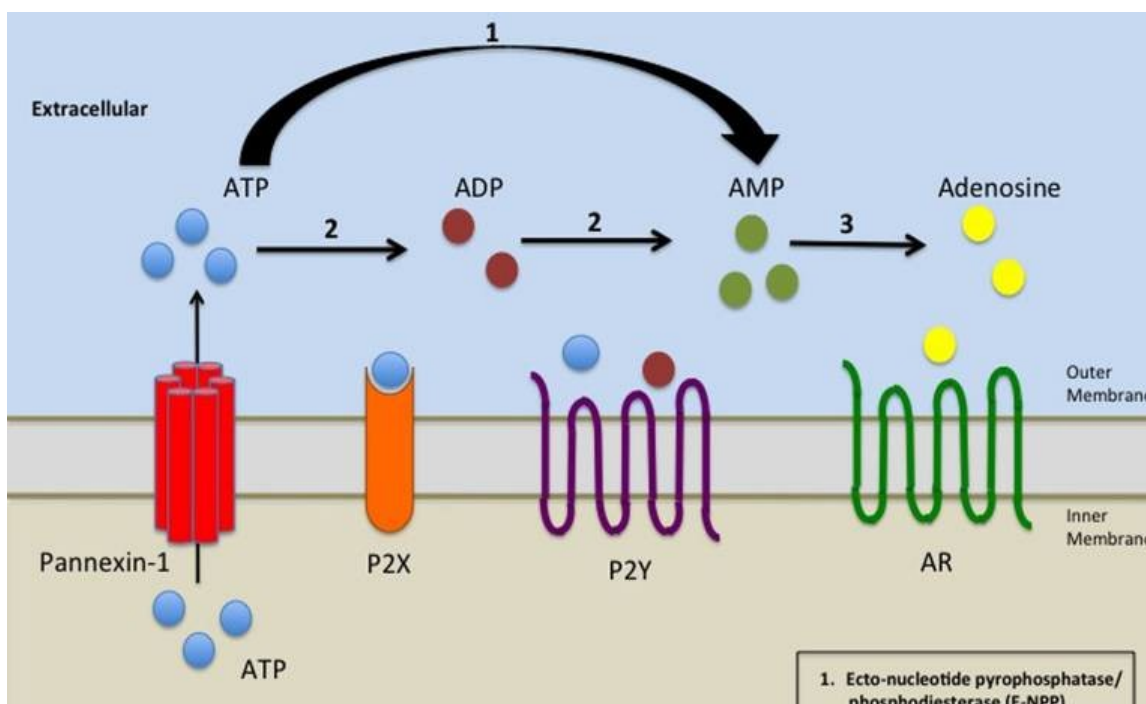


(P2Y2 activation is known to modulate Ca^{2+} influx after nucleotide binding and this may regulate Pyk2 activities and or promote its recruitment into a poly-protein complex that also contains the phosphorylating tyrosine kinase Src. Pyk2 regulates multiple signaling events that may modulate the formation of a signaling complex that contains Src family kinases and actin interacting proteins that reorganize the actin cytoskeleton controlling HIV-1 Env-mediated fusion (P2Y2 itself once activated directly interacts with filamin A, a modulator of the actin cytoskeleton). Although P2Y2 activation induces Pyk2Y402*, the precise mechanisms linking P2Y2 activation and polarization/phosphorylation of Pyk2 remains elusive.^{9, 10})

AR is a G protein coupled receptor that is activated via extracellular adenosine causing an increase in intracellular calcium and activity towards possibly both stages of the HIV life cycle.²

9, 10

Figure 10.) Ecto-nucleoside triphosphate diphosphohydrolase (E-NTDPase) including ecto-ATPase and ATP-diphospho-hydrolase promotes the hydrolysis of ATP to ADP or ADP to AMP (2). Ecto-nucleotide pyrophosphatase/phosphodiesterase (E-NPP) promotes the hydrolysis of ATP to AMP (1). AMP is further hydrolyzed by Ecto-5'-nucleotidase/ CD73 (3) to adenosine which activates adenosine receptors (AR).⁴



Accordingly elucidating the mechanisms of the uncrystallized Pannexin-1 hemichannel will lead to a therapeutic development towards a highly site-specific inhibitor against Pannexin-1 ultimately combatting HIV infection and replication in immune cells via modal entry attack preventing the spread of HIV.

2.6 Protein Modeling, an Overview

Many proteins' 3-D crystallographic structures are yet to be determined, their elucidation is pivotal towards protein-medicine interactions. In silico molecular modeling may elucidate pivotal misunderstood areas within a protein's 3-D atomic structure, these then determined

elusive regions may be experimented upon in silico and subsequently in vitro and in vivo leading to prescriptive medicines and cures.

In silico algorithmic methodology based upon prediction methods, use libraries of already crystallized functional, structural and evolutionarily conserved regional protein sequences and secondary structures to discover best/accurate protein models most resembling their 3-D crystallographic structures. In silico modeling methodologies vary from Homology Modeling, when a query protein exhibits a close evolutionary relationship to one selected library template-protein ($\sim >30\%$) (single target-template alignment approach), to a multiple-template approach when more distant relationships are exhibited and more than one template protein is selected towards modeling. Both methods align the target sequence(s) to the template(s) sequence(s) and use the template(s) 3-D coordinate files towards final protein model production via information from the template structure(s).⁸⁵

2.6.1 Membrane Protein Modeling

Membrane proteins (MP) control a multitude of biological functions ((MP) Pannexin-1 channel opening being a conduit towards fighting infection as well as precipitating HIV infection) and many drugs specifically target these highly functioning membrane proteins controlling their many biological functions.¹²¹ Pannexin-1 channels open and close via diverse stimuli, how it senses and integrates this gating mechanism is illusive and can not be determined solely by its sequence and secondary structure.¹⁵ A whole atomic-level model of Pannexin-1 is necessary exhibiting its precise topological orientation and regional positioning of transmembrane domains (i.e. orientation/positioning and function are connected eg. topology determined Cytoplasmic G-Protein-Coupled-Receptors, intra-membrane conserved hydrophobic proline pore-gating regulation respectively).^{121, 156, 157}

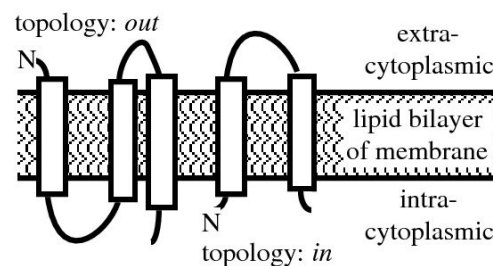


Figure 11.) Transmembrane Topology quasi-rigid cylindrical helices exhibiting 'Out and In Orientations' via N-terminal extra-cytoplasmic or intra-cytoplasmic distribution respectively.¹⁵²

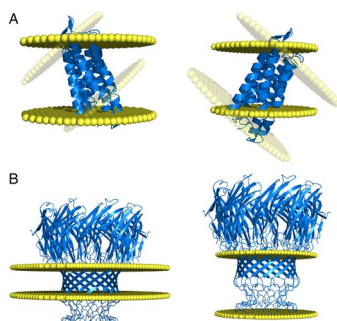


Figure 12.) Residue positioning within membranes is pivotal but difficult to model because of membrane compressibility and protein inclination limited data via experimental determination challenges, crystallized transmembrane proteins lack residue positioning.¹⁵³

Membrane protein determination identifies membrane spanning regions, hydrophobicity predicts this i.e. TM alpha helix stretches with high hydrophobicity have been predicted to be in the membrane sitting in a hydrophobic environment disfavoring any unsatisfied polar atom therefore adopting helical energetically favored compact conformations, this process balances entropy and is overall ordered.^{121, 61, 62, 59} Particular amino acids within transmembrane regions are highly conserved and pivotal towards proper biological functioning. Contrarily disordered proteins are highly flexible lacking a single well-defined structure via the containment of mostly electrostatic polar and charged amino acids promoting amino acid repulsion.^{54, 55} Disordered proteins play pivotal roles in cell signaling and regulation and are often extra-membranous dynamic/difficult to align/model hydrophilic coils and loops; in the case of transmembrane proteins, these are found in the cytosol and extracellular space as C/N-termini and loop domains. Moreover positive residues are thermodynamically favored to reside in the cytoplasm, a determinant towards topology.^{56, 210} Lipid-water interface regions exhibit positively charged residues and the aromatic residues tyrosine and tryptophan. Highly conserved specific-functioning energetically favorable polar residues reside within alpha-helical inner-membrane cores, further determinants towards membrane residue positioning.^{156, 100, 211}

Algorithms based upon hydrophobicity, disorder and existing crystallized transmembrane proteins may be used towards identifying query-template transmembrane and topological domain positioning and orientation, pivotal towards a most accurate transmembrane protein design via distinguishing membrane-bound functioning residues from solvent-bound and cytoplasmic from extracellular loops and coils respectively. Membrane protein channel templates are limited,

however, remotely related proteins may share tertiary features via shared critically conserved residues within membranes assisting positioning and orientational analysis.²²¹ Via additionally incorporating phylogeny, evolutionary analysis and experimentally determined evidence a best membrane protein query-template topological alignment may be determined.

2.6.1.1 Orientation/Positioning Prediction

Several algorithmic softwares may be cross referenced towards a best predicted orientation and re-entrant helix positioning via topology alignment consensus exhibiting agreement on the orientation of secondary structures and regional positioning of transmembrane domains.

TMPred is a computational algorithm using several weight-matrices towards scoring and is based on the statistical analysis of a database of naturally occurring transmembrane proteins predicting membrane-spanning regions (usually ~21-residues) and their orientation.⁶⁰

TMHMM is a protein transmembrane helices prediction method via a Hidden Markov Model (HMM) predicting unknowns via inference from knowns.^{58, 220}

SOSUI predicts transmembrane regions via a Hydrophobicity Analysis for Topology and Probe Helix Method for Tertial Structure; an index of amino acids and amphiphilicity plots of known 3-D structures enable the finding of end-regions of transmembrane helices.^{57, 58}

Phyre²'s transmembrane helix and topology prediction use a powerful Support Vector Machine (SVM) called memsat-svm predicting TM protein topology via integrating both signal peptide and re-entrant helix prediction, these are combined with Phyre²'s integral ability to discriminate between TM and disordered globular proteins.⁵²

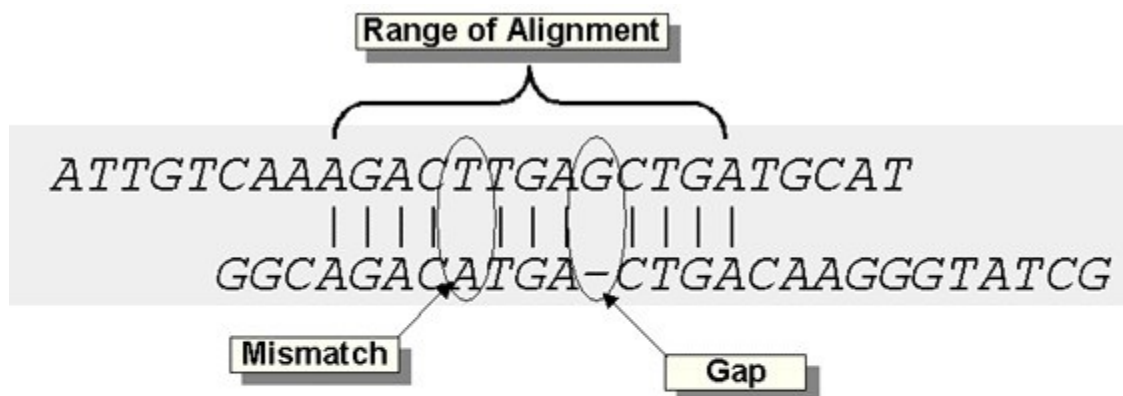
Solvent exposure algorithms may predict a best re-entrant helix prediction elucidation via loop/coil solvent exposure predictions, i.e. RaptorX's algorithm predicts the disorder of proteins via the machine learning model DeepCNF (Deep Convolutional Neural Fields), CNF captures the interdependency of order/disorder amongst adjacent residues and exploits disordered coils and loops existence in solvent.⁵³

2.6.2 Template Selection

BLAST (Basic Local Alignment Search Tool) and HHBlits are algorithmic tools used to selectively discover best template proteins via the comparison of regional similarities amongst already crystallized protein sequences within a sequence database. HHBlits discovers best fit homologs via mutational positional propensities amongst a query and homologs. NCBI BLAST hosts a family of algorithms; protein-protein BLAST (blastp) returning most similar crystallized proteins and Position-Specific Iterated BLAST (PSI-BLAST) is an expanded search of more distant crystallized relatives via a position-specific scoring matrix iterative approach involving multiple alignments, profile construction and arbitrary iteration or convergence.^{161, 185} Via calculating statistical significances BLAST and HHBlits output resulting crystallized template proteins, a ~>25% similarity is ideal.¹¹¹

A best NCBI BLAST template is best selected via analyzing resulting BLAST scores, Gaps, Positives, E-Values, Identities and Query-Coverage areas.

Score(S): the score of the alignment (S) is inversely proportional to the amount of substitutions (mismatched nonidentical amino acid template to query substitutes) and gaps (a space introduced into an alignment) within target-template alignments, accordingly a higher score exhibits a greater alignment integrity (scores are BLOSUM generated).⁴¹



$$S = \sum(\text{identities, mismatches}) - \sum(\text{gap penalties})$$

$$\text{Score} = \text{Max}(S)$$

Figure 13.) BLAST library search example exhibiting a template-target algorithmic alignment, mismatched residues and gaps dilute alignment integrity.^{40, 41}

Gap Score: represents the proportionality (gap/query residue number) and accordingly is inversely proportional to alignment integrity.⁴⁰

Positives: exhibit the number of residues that are identical or have similar chemical properties and represent the proportionality (positives/query residue number), accordingly these scores are proportional to alignment integrity.³⁹

E-Value: exhibits search chance template hits via size, accordingly E-Value is inversely proportional to match significance, best E-Values are $1e^{-4}$ or below.^{40, 39, 155}

Identity Value: exhibits what percent identical the query and template residues are at the same position and represent the proportionality (identical/query residue number), accordingly these scores are proportional to alignment integrity (identities are relative towards query covered i.e. at very low coverage areas an inverse proportionality may be exhibited).^{40, 39}

Query Coverage: exhibits the percent the query is aligned, low coverage areas may be significant towards multiple template alignments.⁴⁰

Confidence: query-template homology probability (Phyre² HMM-HMM matching).^{220, 230}

2.6.3 Target-Template Alignment Selection

Target proteins and more so transmembrane proteins (because of their partially hydrophobic surfaces, flexibility and lack of stability) lack solved protein structures within the Protein Data Bank (PDB), accordingly a single template alignment may be just a beginning approach towards 3D protein model building. Multiple templates threaded on a query sequence increases alignment coverage and better targets domain similarities circumnavigating the dearth of the crystallized protein library. Moreover a multi-template approach allows a better alignment of conserved ordered domains when homology is less than 25% and increases pivotal functional and structural residue alignments.^{24, 160} Multiple template approaches may be best aligned via slight manual adjustments to avoid gaps in ordered conserved transmembrane regions and pivotal residues.


```

                                * * * * *
PROTEIN_A|SEQUENCE      -----WAVQQKNSKAMIAE-----
TARGET_PROTEIN|SEQUENCE FRIYILLWAVLQSKNKAAYERTKNSS
PROTEIN_B|SEQUENCE      FRLNIKN-----ITMSNN
                                * * * * *

```

Figure 14.) Fictitious multiple sequence alignment conserving the target transmembrane region (yellow) and pivotal-residues (lime).¹⁵¹

Piecewise pairwise sequence alignment tools are best when query-template sequences exhibit high homology $\sim >30\%$.¹²³ Multi-Sequence Alignment tool Basic Clustal algorithm aligns via identifying template regions exhibiting functional, structural and evolutionary relationships matching the query.²³ Clustal may similarly be used when more distant homologies $<30\%$ are present via exploiting the limited number of protein folds (~ 5000) amongst several million existing proteins (~ 1 -10 billion). Multiple templates, in this case, from various species exhibiting high sequence similarities to query sequence targets may be used regardless of e-values above the threshold.¹³⁷

```

pannexin-1      LLYLPPLFWRFAAAPHICSDLKFIME-----E-----LDK
2ZW3:A|PDBID|CHAIN|SEQUENCE  LVVAAKEVWGDEQADFVCNTLQPGCKNVCYDHYFPISHIRLWALQLIFVSTPALLVAMHV
*:      .*      *  .:.*. *:      :      .      :.

```

Figure 15.) Panx1-2ZW3 respective query-template residue pairwise alignment via software Clustal exhibiting pairwise alignment amongst residues, * represents conserved residues, : represents residues with strongly similar chemical properties and . represents residues with weakly similar chemical properties.¹²⁰

Alignment methods perform best alignments via the introduction of gaps i.e. template insertions and query deletions. When aligning target-template(s), template insertions insert amino acid mutations into the molecular model while query deletions delete amino acids from the molecular model (final modeling patches up these defects via PDB library structural local sequence/geometry matching and tweaking).¹²² Regardless of these final modeling repairs, insertions and deletions throughout a protein may dilute the integrity of the model with a greater malignancy within ordered/conserved membraneous regions and pivotal residues. Incorporating more rigorous secondary structural algorithms slightly improves gap results and overall alignment in comparison to basic piecewise pairwise sequence alignment tools.

Figure 16.) Insertions in the template insert mutations into the model whereas deletions in the query delete amino acids from the model.

Promals3D new and improved alignment uses data from sequence database searches, secondary structural prediction, available homologs with 3D structures and user-defined constraints ultimately predicting more reliable alignments for more distantly related templates.¹¹⁷

Figure 17.) Panx1-2ZW3 respective query-template secondary structural alignment via software Promals3D, Consensus_ss Conserved Helix h Prediction exhibited.¹¹⁵

CNFPred is another powerful protein threading structural prediction program specializing in template discovery (via CNFPred) and template-query alignment with sparse sequence profile, ideal for remote template discovery. Similar to Phyre², this alignment algorithm discovers multiple templates to a single target.⁶⁵

A best final alignment may incorporate experimental evidence and constraints, hand-pairwise sequence alignment via multiple templates and topology/structural threading consensus amongst different algorithms.

2.6.4 Protein Molecular Modeling

Highly symmetric homo-oligomers are ubiquitous specifying distinct biochemical and biophysical properties via pivotally reactive sites within oligomeric interfaces, experimental evidence indicates Pannexin-1 to be a symmetric homo-hexamer transmembrane selective gating protein channel highly regulating multiple homeostatic mechanisms i.e. immune reactivity.¹³⁰ An accurately modeled Pannexin-1 protein structure is needed towards the optimization of a best *in silico* nanoparticle drug-design whose contents bind to the precisely designed functional alterable Pannexin-1 interface, ultimately altering opening or closure.¹²²

Final full 3-D best-molecular protein models may be completed via servers Pymol, MODELLER and GalaxyWeb. The former Pymol is an excellent visualization software tool enabling orientational manipulation, pore and oligomer diameter evaluation and optimization assessment. MODELLER software may generate a new model's 3-D atomic-coordinates when a query-template expresses high or remote homology via a coordinate randomization and repeated minimum score search outputting best molecular 3-D protein models.⁸⁵ The later software GalaxyWeb server is an excellent homo-oligomer protein prediction and refinement server specializing in polymer multimerization and orientation via an input monomer. GalaxyHomomer models sequences as well as structural files via homo-oligomer templates from the Protein Database and or the ab initio docking of an experimentally determined or computationally predicted monomer.

Coils and loops lack secondary structure and reside in solvent exposed areas precipitating great conformational flexibility challenging molecular modeling, the later two methods exhibit a final structural refinement towards this highly dynamic nature via ab initio re-modeling and energy minimization.¹³⁰ Ab Initio modeling may be physics and or knowledge based using minimization and protein library angle restraint data.¹⁶² Ab Initio modeling exhibits best results in unaligned areas containing less than seven-residues since the geometrical possible number of defined conformations within the known protein structure database past seven-residues becomes inconceivably.^{143, 162}

2.6.4.1 MODELLER Molecular Modeling

MODELLER in silico models a query uncrystallized protein via a comparative modeling technique ultimately predicting a target's 3-D structure via a selected best most similar crystallized template protein(s)'s distance-constraint information and input target-template alignment(s), predicted model errors evaluate the final model.¹⁵⁴ (3D model constructive methodology aside from modeling via a satisfaction of spatial restraints, may model via a 'rigid body modeling' of known atomic subunits or via a 'segment modeling' of conserved atoms within segments, accuracies amongst these three techniques are ultimately similar.)¹⁶⁰

Constraints and restraints are homology derived and precipitated via a library of proteins induced upon the target within the target-template alignment, additional stereochemical restraints via CHARMM22 force field promote an apropos stereochemistry (examples of restraints are C^α-C^α distances, main-chain and side-chain dihedral angles and hydrogen bonds). Within MODELLER, probability density functions expressing the spatial restraints are smoothly optimized towards a final energy minimization in Cartesian space deriving the final model.

MODELLER models unpredictable loops via multiple methods including an initial two-stem regional library search, molecular mechanics force fields, distance spatial and dihedral angle restraints via library proteins, ab initio modeling and energy minimization.^{160, 161} Side-chains are modeled similarly i.e via similar structures and steric and energetic modeling.¹⁶¹

Errors towards modeling increase as template-homology decreases; errors may be linked to pivotal side-chain packing, distortions and shifts within correctly aligned regions via structural evolution, regions with no template i.e. insertions, errors due to misalignments, and incorrect templates effecting pivotal residues. Errors may be tolerated if exhibited outside of model pivotal residue docking domains.

Model evaluation follows model building, the model-single.log output file assists in determining which model is best selected via its minimal DOPE potential energy score used to inspect the folds of the model and its runtime errors and restraint violations. MODELLER exhibits different techniques that may be combined to design a most accurate protein model.¹⁶⁰

2.6.4.1.1 Homology Modeling (Single-Template Approach)

Homology Modeling uses a single-selected template exhibiting homology >30% and is best aligned to the target and input together with the templates known 3-D atomic coordinate file.

```
from modeller import *
from modeller.automodel import *
#from modeller import soap_protein_od

env = environ()
a = automodel(env, alnfile='TvLDH-1bdmA.ali',
              knowns='1bdmA', sequence='TvLDH',
              assess_methods=(assess.DOPE,
                             #soap_protein_od.Scorer(),
                             assess.GA341))

a.starting_model = 1
a.ending_model = 5
a.make()
```

Table 8.) MODELLER software single template input demonstrated via automodel class, automodel object 'a' and set parameters to model-build. Sequence alignment input file 'TvLDH-1bdmA.ali' is the target-template alignment and known '1bdmA' is the template structural file. The above script file, model-single.py, will generate five-models, 'make' method calculates models.¹⁴⁸

Via a MODELLER input single-alignment and template structural file, similar best molecular 3-D protein models may be calculated and output via a coordinate randomization and repeated minimum score search, one best-fit model may be selected via energy profiling.⁸⁵

>> Summary of successfully produced models:

Filename	molpdf	DOPE score	GA341 score
Pannexin-1.B99990001.pdb	22649.97656	-241146.95312	0.15862
Pannexin-1.B99990002.pdb	22239.50000	-240925.09375	0.06260
Pannexin-1.B99990003.pdb	22451.53125	-243152.73438	0.16993
Pannexin-1.B99990004.pdb	22131.63477	-240422.79688	0.07378
Pannexin-1.B99990005.pdb	21885.76562	-243731.93750	0.04391

Table 9.) MODELLER's 'model-single.log' output file exhibits warnings, errors, input restraints used towards modeling that remain violated in the final model, the last few lines display a summary of five similar models built, here 'Pannexin-1.B99990005.pdb' exhibits a best selection via its best/lowest energy conformational DOPE and molpdf scores.^{139, 142}

- Filename: contains the coordinates of the model in the PDB format.¹³⁹
- molpdf: objective function score containing the sum of all restraints, lowest value selects the best model. Moldpdf scores are secondary to DOPE scores and are sole scores when MODELLER stitched.^{139, 140}

- iii.) DOPE score: assesses the quality of the selected atoms in the model via DOPE (Discrete Optimized Protein Energy) method, a statistical potential optimized towards model assessment. DOPE scores are based upon energy functions only (not interactions, restraints etc.), selection of the lowest DOPE score selects the best model structure.¹³⁸
- iv.) GA341 score: assesses the quality of the model via the GA341 method, a method using a percentage sequence identity between the template and the model as a parameter.¹⁴¹ Scores range from 0.0 (worst) to 1.0 (native-like) and are secondary to DOPE or SOAP scores in distinguishing ‘good’ models from ‘bad’ models.¹³⁹

2.6.4.1.2 Multiple-Template Modeling

When a more remote homology is exhibited a multiple-template approach works best via input multiple atomic coordinate files serving as templates towards a user input query-template multiple-sequence alignment. A multiple template alignment may align a single template to a query target or may align multiple templates to a query target (Clustal). A Multiple Template Method heightens model quality via simply comparing greater amounts of data, this multi-template approach may subtract data from single-template highly exhibited inserted areas ultimately promoting a stitching together of multiple-templates/models.

```
from modeller import *
from modeller.automodel import *

env = environ()
a = automodel(env, alnfile='TvLDH-mult.ali',
               knowns=('1bdmA', '2mdhA', '1b8pA'), sequence='TvLDH')
a.starting_model = 1
a.ending_model = 5
a.make()
```

Table 10.) MODELLER software multiple-template input demonstrated via automodel class, in this case the alignment input single file ‘TvLDH-mult.ali’ is the multiple template-query sequence alignment, the knowns input the three template PDB coordinate structural files (‘1bdmA’, ‘2mdhA’, ‘1b8pA’) towards modeling. Sequence remains the query ‘TvLDH’, 5-models to be generated.¹⁵¹

2.6.4.1.2.1 Multiple-Template Modeling, Single Template per Target

In this multiple template approach via MODELLER a single template is aligned per target resulting in multiple 3-D coordinate parts being stitched together to generate one final complete

protein model, i.e. C_Tail + TM + N_Tail → C_Tail-TM-N_Tail.

```
a = automodel(env,
               alnfile = 'align.ali', # alignment filename
               knowns   = ('1', '2', '3'), # codes of the templates
               sequence = 'C_TM_N')      # code of the target
```

Table 11.) Via automodel class, input alnfile residue sequence corresponds to input known 3-D coordinate files (knowns), sequence remains the target.

The extracted alignment file (align.ali) format for the above stitched modeling example exhibits three-lines per model.

```
>P1;1
structureX:1:  1 :10 ::::
CTVMKDVALE-----*
```

(this first line exhibits the protein code after >P1;1),
(the second line exhibits 'fields' separated by colons ':'),
(the third line exhibits the residue sequence to be modeled **CTVMKDVALE**)¹⁴⁶

```
>P1:2
structureX:2:  1 :15 ::::
-----WFLPPLYLLIAFLLL-----*
```

(Field-1 exhibits the specification, (**structureX**: (X-ray))¹⁴⁶

```
>P1;3
structureX:3:  1 :20 ::::
-----GQGSSKINELVKLCKYSINE*
```

(Field-2 exhibits the code to get the structural data, (**:3:**) atomic coordinates to be extracted),
(Fields 3-6 indicate starting (fields 3-4) and ending residues (fields 5-6) of the sequence,
(**: 1 :20 ::::**),
Field 7 is an optional protein name, (eg. :ferredoxin:),
Field 8 is an optional source of protein name, (eg. :Azotobacter vinelandii:),
Field 9 is an optional crystallographic resolution value, (eg. :1.90:),

Field 10 is an optional R-factor value, (eg. :0.19)¹⁴⁶

```
>P1;C_TM_N
```

```
sequence:C_TM_N:1::45:::0.00: 0.00
```

```
CTVMKDVALEWFLPPLYLLIAFLLLQGSSKINELVKLCKYSINE*
```

(Field-1 exhibits the specification, (**sequence:** (sequence))¹⁴⁶

Table 12.) Alnfile exhibiting a stitched technique; C-Tail residue 10 is stitched to TM residue 1 structure 2, TM residue 15 structure 2 is stitched to N-Tail residue 1 structure 3 resulting in a complete C_TM_N 45-residue model.

2.6.4.1.2.2 Multiple-Template Modeling, Multiple Templates per Target

A MODELLER multi-template approach may similarly stitch model via an alnfile exhibiting multiple-coordinates per target residue resulting in model building based on different types of restraints amongst different residues. A Clustal multiple template alignment input promotes this multiple coordinate modeling per target residue.

Clustal Omega

[Input form](#)[Web services](#)[Help & Documentation](#)[Bioinformatics Tools FAQ](#)

Tools > Multiple Sequence Alignment > Clustal Omega

Results for job clustalo-l20190927-220951-0933-44429844-p2m

[Alignments](#)[Result Summary](#)[Guide Tree](#)[Phylogenetic Tree](#)[Results Viewers](#)[Submission Details](#)

[Download Alignment File](#)[Show Colors](#)

CLUSTAL O(1.2.4) multiple sequence alignment

pdb 3SNO A	-----GXALEPQIKSA-----PTFVIL-IVEP	22
pdb 1FVP A	-----PSK--TMNNAETLRIIDEDTSIYDVINIDH	52
pdb 5MJI A	-----MALKALILNTTLRRSPSRSTQGLIDKAVPLYEKEGIEFEVVRVIDHD	48
sp Q96QZ0 PANX3_HUMAN	LPYSLALALLMYLPVLLWQYAA--VPALSSDLLFIISEL-----DKSYNRSIRLVQHML	162
pdb 5H1Q A	VPYVFALQAFLFYIPRFIWKAMI--AYS-GYDLAAAVKYV-----DRFWSENRD-KDDK	158

Table 13.) Clustal Omega multiple template alignment result exhibiting a multiple residue alignment towards Pannexin-3 target residue L162.⁸³

2.6.4.2 GalaxyWeb Molecular Modeling

GalaxyWeb's Galaxyhomomer oligomer protein prediction and refinement server specializes in polymer multimerization and orientation via an input monomer or protein sequence (monomers may be designed or PDB crystallized proteins). Both input methods may predict oligomers via detected templates or dockings, both are similarly model refined. Oligomeric states are input or via default server predicted.

Both sequence and monomer input methods firstly detect their oligomeric state via HHsearch within the protein structure database 'pdb70'. Final S-scores are then generated via both HHsearch sequence and secondary structure scores. Five final model oligomeric states and 100 oligomer templates each are generated via this search per method.

Subsequent to monomer or sequence state qualification, five total final oligomer models are built via a sequence and or structure-based similarity approach and or ab initio docking. During a sequence approach a target residue sequence is input and five best S score sequence and structural templates are detected and the sequence is template aligned. Subsequently GalaxyCassiopeia builds oligomer models via the alignment and template structure using Variable Target Function Method (VTFM) optimization (used in MODELLER) combined with FACTS solvation free energy, knowledge-based hydrogen bond energy, dipolar-DFIRE, molecular mechanics bonded and non-bonded energy terms. When a monomer is input the five best S score structure-based detected templates are selected towards oligomer modeling. A structure based method final oligomer model is completed via a superimposition of the input monomer onto each of the detected oligomer templates. Oligomeric templates generate best models when both sequence and monomer input methods lack a combined total of five oligomer templates, the remaining oligomer models are generated via the C_n -symmetry M-ZDOCK ab initio docking of a multiple-template-based GalaxyTBM predicted monomer structure or monomer input respectively. A final ab initio structural refinement re-modeling is promoted via GalaxyLoop and the overall structures are relaxed via GalaxyRefineComplex, three loop/termini refinement regions may be monomer input selected.¹³⁰

Template-based Oligomer Modeling Results (Sequence-based)

Model No	Oligomer template	Number of subunits	Interface area	Sequence identity	Loops/termini that may be refined	Re-submit for refinement
1	3brc	2-mer	2122.0	44.6	15-21	Submit

Template-based Oligomer Modeling Results (Structure-based)

Model No	Oligomer template	Number of subunits	Interface area	Sequence identity	Structure similarity (TM-score)	Loops/termini that may be refined	Re-submit for refinement
2	1zwy	2-mer	798.0	16.6	0.5682	59-74	Submit
3	2car	2-mer	209.9	10.2	0.5230	59-74	Submit
4	3tqu	2-mer	2193.4	9.6	0.5123	59-74	Submit

Ab initio Docking Results

Model No	Number of subunits	Interface area	Docking score	Loops/termini that may be refined	Re-submit for refinement
5	2-mer	628.9	625.491	59-74	Submit

Table 14.) GalaxyHomomer output page via a sequence input method using sequence and structure based template detection. Ab Initio Docking results displaying one of five-model Interface Area and Docking Scores, highest scores are selected. A highest Interface Area Score between adjacent monomer helices exhibits greatest helical energetically favored compact conformations influencing an thermodynamically favorable compact transmembrane pore size. Highest Docking Scores exhibit best cyclical symmetric (C_n) multi-mer structural prediction via M-ZDOCK algorithmic complementarity, electrostatics and desolvation between an input monomer (receptor) and created ligand (receptor rotated).^{130, 131}

2.7 Ligand-Target Docking Dynamic Simulation

Molecular Docking Assays are excellent ligand-receptor interaction/complex tools evaluating binding affinities towards drug discovery and protein modeling.¹³ Current small molecule docking algorithm MedusaDock endures simultaneous receptor ligand flexibility and adds water molecules explicitly and energy appropriately flexibly bridging the ligand to the protein via a specific best energy ligand (residue conformation) orientation and particular water arrangement promoting a most native ligand-receptor juxtaposition (MedusaScore incorporates a desolvation effect).^{47, 11, 147, 220} This MedusaDock local assay restricts itself to the spatial coordinates of the putative binding regions of a < 40-residue target protein and via algorithms generating 5,000-15,000 sampled target Binding Modes (BM), MedusaDock's CHARMM energies qualify a best BM (MedusaScore includes an explicit up to 3 Å hydrogen-bonding model).^{47, 64} CHARMM identifies target-ligand bonding via free energy minimization, adds disulfide bridges, protonates

residues at physiological pH etc.. Dock time is proportional to ligand rotatable bonds (<10 rotatable ligand-bonds preferred for best predicting results via lowering BMs) and ligand-target fit (shape complementarity). A software docking's interface client and server set the target and ligand and submit docking at physiological temperature. A greater fraction of the ligand being buried in the target results in a greater docking binding pocket identification and subsequent dock.⁶⁴

In silico docking free energy binding affinities evaluate ligand-target induced fit and molecular modeling regional potentials. Lower in silico free energy minimization values are directly proportional to greater ligand affinities and ligand-receptor hydrophobic interactions are optimized via hydrogen bonding increasing binding affinity and drug efficacy.²²⁰

Free Energy of Binding is additive:

$$\text{Formula 1.) } \Delta G_{\text{bind}} = \Delta G_{\text{solvent}} + \Delta G_{\text{conf}} + \Delta G_{\text{int}} + \Delta G_{\text{motion}}$$

where,

$\Delta G_{\text{solvent}}$ contribution via solvent, i.e. hydration free energy ΔG_{hyd} .

ΔG_{conf} contribution via conformational changes, i.e. receptor and ligand free energy changes respectively $\Delta G^r + \Delta G^l$.

ΔG_{int} contribution via proximity, i.e. electrostatic and van der Waals interactions ΔG^{r-l} amongst receptor and ligand.

ΔG_{motion} is the contribution via the motion of receptor and ligand once proximal, i.e. $\Delta G_{\text{rot}} + \Delta G_{\text{tr}} + \Delta G_{\text{vib}}$ freezing and internal rotational, translational/rotational and vibrational free energy changes respectively.⁴⁶

Total Energy (REMARK E_total) and Energy subtracting VDWR (REMARK E_without_VDWR) are considered via MedusaDocking Chemical PDB Files when analyzing ligand-receptor binding affinities. (E_without VDWR ameliorates imperfections, i.e. clashing molecular complexes, resulting in a more robust score more closely matching experimentally determined data.)⁴⁷ Weak affinities are < -20 kcal mol⁻¹ (kcal per mole), < -30 to -50 kcal mol⁻¹ exhibit high affinities and > -20 kcal mol⁻¹ exhibit poor affinities.^{46, 45}

Conclusion

Uncrystallized Pannexin-1 is a highly sophisticated ubiquitously expressed oligomeric transmembrane protein channel regulating homeostasis and physiological diseased states via open or closed gating. Therapeutically controlling Pannexin-1 channel gating may cure dire diseases such as AIDS, be a viable neuropathic pain reliever and is integral to other diseased states, accordingly a Pannexin-1 atomic structural model is needed together with a deep understanding of the interwoven array of Pannexin-1 physiological responses for best Pannexin-1 medicinal purposes.

In silico softwares are today an integral part of medicinal design via the molecular design of proteins coupled to pharmaceutical protein receptor dockings. Various in silico algorithmic protein databases may be combined towards discovering a beginning Pannexin-1 oligomer protein model exhibiting a satisfactory overall structure with reasonably designed medicinal-interacting pivotal domains. This beginning model and its binding partners may be further ameliorated via in silico molecular dynamic simulations, optimal results will control Pannexin-1 gating regulating homeostasis and physiology towards disease prevention.

Chapter 3

Research Method And Design

3.1 Overview and Objectives

3.1.1 Research Overview

A best molecular model of the uncrystallized transmembrane protein Pannexin-1 exhibiting a best overall structure and compact pore region matching experimental data was designed via computer software. In vitro discovered Pannexin-1 channel inhibitor binding events were computationally simulated via a dynamic docking software, these binding/molecular recognition events exhibited overall reasonable energy affinities proving fair pivotal regional accuracy of the Pannexin-1 protein model.

3.1.2 Research Objective

To in silico model a best uncrystallized Pannexin-1 protein exhibiting a fair model accuracy within pivotal domains responsible for its channel closure.

3.1.3 Future Research Objective

Future research will include subsequent refinement of the best host-partner(s), further elucidation of the Pannexin-1 region(s) of interest, key residues, water lattice and the validation of a stealth nano-system that controls Pannexin-1 pore gating. An exhaustive Molecular Dynamic Docking Simulation Assay will exhibit a Pannexin-1 channel pore closure via a host-partner Pannexin-1 pivotal regional binding event. In vitro studies will confirm the former validating a AuNP-conjugate as an effective delivery system and final in vivo studies will confirm Pannexin-1 closure via a stealth delivery nano-system exhibiting final clearance without toxicity.

3.2 Pannexin-1 Modeling, an Overview

Human Pannexin-1's 3-D crystallographic structure is yet to be determined, accordingly building a best Pannexin-1 via in silico 3-D modeling is a best beginning approach. Query sequence Pannexin-1's crystallographic template proteins were discovered via template discovery/alignment algorithms. Template topology consensus and slight hand pairwise matching optimally assisted a best selected multi-template threading alignment approach via

precisely aligning conserved transmembrane regions and pivotal residues. Template alignments and matching existing crystallographic 3D-structures were subsequently used to MODELLER model an A-chain of several Pannexin-1 alignments. One best Pannexin-1 A-chain subunit's 3-D coordinates were then used to build a best complete symmetric homo-oligomer Pannexin-1 via GalaxyWEB's oligomer prediction server. GalaxyWEB was further used to build a best symmetric similar homo-oligomer of Pannexin-1 via a sequence input. Each complete Pannexin-1 3-D model's pore and overall structure were compared and contrasted towards a best model selection.⁸⁵

3.2.1 Pannexin-1 Template Selection

The template discovery algorithms blastp, PSI-BLAST and HHblits were used to discover the best Pannexin-1 crystallized template proteins, the entire FASTA 426 amino acid sequence provided via UniProtKB-Q96RD7-1 (PANX1_HUMAN) was input towards this discovery.

MAIAQLATEYVFSDFLKEPTEPKFKGLRLELAVDKMVTCLAVGLPLLLISLAFAQEISIGT
 QISCFSPSSFSWRQAAFVDSYCWA AVQQKNSLQSESGNLPLWLHKFFPYILLFFAILLYLP
 PLFWRFAAAPHICSDLKFIMEELDKVYNRAIKAAKSARDLDMRDGACSVPGVTENLGQS
 LWEVSESHFKYPIVEQYLKTKKNSNNLIKYISCRLTLIIILLACIYLGYYFSLSSLSDEFV
 CSIKSGILRNDSTVPDQFQCKLIAVGIFQLLSVINLVVYVLLAPVVVYTLFVPFRQKTDVL
 KVEILPTFDVLHFKSEGYNDLSLYNLFLEENISEVKSYKCLKVLENIKSSGQGIDPMLLL
 TNLGMIMD VVDGKTPMSAEMREEQGNQTAELQGMNIDSETKANNGEKNARQRLLDS
 SC³⁸

This template discovery methodology query-ranged the entire Pannexin-1 isoform (1) 1-426 residue sequence to discover best domain templates.

3.2.1.1 NCBI Assay

NCBI blastp Parameters used:

Choose Search Set: Protein Data Bank proteins(pdb) selected towards finding already crystallized protein sets.

Algorithmic Parameters

General Parameters:

Max target sequences: 100

Expect threshold: 10 (chance matches)

Word size: 6 (max)

Scoring Parameters:

Matrix: BLOSUM62

Gap Costs: Existence: 11 Extension: 1

Computational adjustments: Conditional compositional score matrix adjustment

Program: BLASTP 2.9.0

NCBI PSI-BLAST Parameters:

Same as blastp save:

Word size: PSI 3 (max)

PSI/PHI/DELTA BLAST:

PSI-BLAST Threshold: 0.005¹¹¹

Sequence Input:

Pannexin-1 FASTA 426 amino acid sequence provided via UniProtKB-Q96RD7-1 (PANX1_HUMAN).³⁸

3.2.1.2 Phyre² HHBlits Assay

Phyre² Parameters Used:

Template Detection: HHpred 1.5.1

Secondary Structure Prediction: Psi-pred 2.5

PSI-Blast 3 Iterations

Disorder Prediction: Disopred 2.4

Transmembrane Prediction: Memsat SVM

Multi-Template Modeling and ab initio: Poing 1.0

Tool: Protein Homology/analogY Recognition Engine V 2.0¹³⁴

Sequence Input:

Query Pannexin-1 FASTA 426 amino acid sequence provided via UniProtKB-Q96RD7-1 (PANX1_HUMAN).³⁸

3.2.2 Pannexin-1 Target-Single Template Alignment Selection

Multiple Biomedical Informatics single template alignment methods (Clustal, Promals3D, Phyre2 and RaptorX/CNFPred) were cross-referenced, these alignments contributed to a final multiple template alignment.

3.2.2.1 Clustal

The basic Clustal pairwise sequence alignment Biomedical Informatics algorithm was firstly run to confirm the best-selected Innexin6 template's remote homology/low identity to Pannexin-1 via a protein library comparison target-template alignment.

Tool Clustal 0(1.2.4)

Clustal Parameter:

CLUSTALW

Sequences Input:

Query Pannexin-1 FASTA 426 amino acid sequence provided via UniProtKB-Q96RD7-1 (PANX1_HUMAN).³⁸

Template Sequence:

>5H1Q:AIPDBID|CHAIN|SEQUENCE

MASQVGAINSVNALISRVFVQPKGDLADRLNSRVTVVILAVSSALLSSHFIGDPITCWTP
AQFNAQWVNFVNQYCFVHGTYFVPLDQQLAEEEEERTKVSIIQYYQWVPYVFALQAFLF
YIPRFIWKAMIAYSGYDLAAVKYVDRFWSNRDKDDKFKTRLAAFEGRPSVYIWDGIR
LARKKRSRNMALFYTLSTVWQAVNAWIQFYILTQLLDSSIIYTLWGPSILGDLLQGNDWQ
TTGHFPRIVHCDNFNRRRPASVQLDTVLCVLTNLIIYEKLFIFLWFWLVFVAVVSTVNCFK
WIYYLCNKTKAQKTIKNYLSTAPIKSTISDDQFFSALGEDGLFIMDQMALNLGDIPASYLT
ISMRNICQDFIESEDYIDEERTPFVKSIIKHT⁴⁴

3.2.2.2 Promals3D

Promals3D, a secondary structure predictor towards remote homology, was run via input FASTA Pannexin-1 and Innexin6 sequences, this query-template alignment will exhibit secondary structural alignment features.

Promals3D Parameters used:

identity threshold: 0.6

secondary structure weight: 0.2

amino acid weight: 0.8¹¹⁷

Sequences Input:

Query Pannexin-1 FASTA 426 amino acid sequence provided via UniProtKB-Q96RD7-1 (PANX1_HUMAN).³⁸

Template Sequence:

>5H1Q:AIPDBID|CHAIN|SEQUENCE⁴⁴

3.2.2.3 Phyre²

Phyre² Secondary Structural Threading was run to align its best selected templates.

Phyre² Parameters:

(see section: **3.2.1.2 Phyre² HHBlits Assay**)

3.2.2.4 RaptorX/CNFPred

RaptorX Secondary Structural Threading was run to find and align its best selected templates.

RaptorX Parameters Used:

Sequence Input:

Query Pannexin-1 FASTA 426 amino acid sequence provided via UniProtKB-Q96RD7-1 (PANX1_HUMAN).³⁸

3.2.2.5 Consensus Pannexin-1 Structural Threading Alignment

A Methodology Consensus was manually formulated to move towards a best manual multiple

target-template alignment via secondary structural positioning for a target-template expressing a very distant homology i.e. Phyre², RaptorX and Promals3D.¹⁰⁵

3.2.3 Pannexin-1 Orientation and Positioning Selection

A methodology of cross-referencing algorithm prediction servers based upon hydrophobicity, disorder, solvent exposure and existing transmembrane proteins were run and compared to UniProtKB's Pannexin-1 and Innexin6 algorithmic topological analysis and UniProtKB's Connexin26 experimental topological analysis. Each topology algorithm ascertains Connexin26/Innexin6-Pannexin-1 topological similarity amongst themselves and ultimately amongst each-other assisting towards a precise alignments of the four transmembrane regions and topological domains via algorithmic corroboration and consensus. This topological alignment is imperative towards protein transmembrane orientation and positioning modeling via a precisely designed query-multiple template alignment.

3.2.3.1 Modeling Topology

Disordered dynamic hydrophilic coil and loop orientations and ordered membraneous residue positioning in Pannexin-1 and topologically related Connexin26 and best sequence template Innexin6 were methodologically cross-referenced. Connexin26 topology prediction will assist Pannexin-1-Innexin6 alignment via re-entrant residue discovery.

3.2.3.1.1 TMPred

TMPPred Topology Prediction Algorithm input Pannexin-1 and Connexin26 topological regional data to be compared against UniProtKB's Pannexin-1 and Connexin26 topological data.

TMPPred Parameters:

Output Format: html

Minimum: 14

Maximum: 41

Input Sequence Format: Plain Text⁶⁰

Sequences Input:

Query Pannexin-1 FASTA 426 amino acid sequence provided via UniProtKB-Q96RD7-1 (PANX1_HUMAN).³⁸

Template Connexin26:

>2ZW3:A|PDBID|CHAIN|SEQUENCE¹⁴⁵

UniProt Pannexin-1:

Topology¹¹⁰

UniProt CNX:

Topology¹²⁹

3.2.3.1.2 TMHMM

TMHMM Topology Prediction Algorithm input Pannexin-1 and Connexin26 topological regional data to be compared against UniProtKB's Pannexin-1 and Connexin26 topological data.

TMHMM Parameters:

Server 2.0

Output Format: Extensive with Graphics⁵⁰

Sequences Input:

Query Pannexin-1 FASTA 426 amino acid sequence provided via UniProtKB-Q96RD7-1 (PANX1_HUMAN).³⁸

Template Connexin26:

>2ZW3:A|PDBID|CHAIN|SEQUENCE¹⁴⁵

3.2.3.1.3 SOSUI

SOSUI Topology Prediction Algorithm input Pannexin-1 and Connexin26 topological regional data to be compared against UniProtKB's Pannexin-1 and Connexin26 topological data.

SOSUI System: SOSUI engine ver. 1.11⁷⁵

SOSUI Parameters:

Sequences Input:

Query Pannexin-1 FASTA 426 amino acid sequence provided via UniProtKB-Q96RD7-1 (PANX1_HUMAN).³⁸

Template Connexin26:

>2ZW3:AI|PDBID|CHAIN|SEQUENCE¹⁴⁵

3.2.3.1.4 RaptorX

RaptorX Solvent Exposure Prediction Algorithm input Pannexin-1 and Connexin26 topological regional data to be compared against UniProtKB's Pannexin-1 and Connexin26 topological data.

RaptorX System: v1.02²³

RaptorX Parameters:

Sequences Input:

Query Pannexin-1 FASTA 426 amino acid sequence provided via UniProtKB-Q96RD7-1 (PANX1_HUMAN).³⁸

Template Connexin26:

>2ZW3:AI|PDBID|CHAIN|SEQUENCE¹⁴⁵

3.2.3.1.5 Phyre²

Phyre² Re-Entrant Helices Prediction Algorithm input Pannexin-1 and Connexin26 topological regional data to be compared against UniProtKB's Pannexin-1 and Connexin26 topological data.

Phyre² Parameters Used:

Secondary Structure Prediction: Psi-pred 2.5

Disorder Prediction: Disopred 2.4

Transmembrane Prediction: Memsat SVM

Multi-Template Modeling and Ab Initio: Poing 1.0

Tool: Protein Homology/analogY Recognition Engine V 2.0¹³⁴

Phyre²:

Sequences Input:

Query Pannexin-1 FASTA 426 amino acid sequence provided via UniProtKB-Q96RD7-1 (PANX1_HUMAN).³⁸

Template Connexin26:

>2ZW3:A|PDBID|CHAIN|SEQUENCE¹⁴⁵

3.2.3.1.6 Consensus Topology Determination

Via combining the above topology prediction methods a Pannexin-1 and Connexin26 consensus topology determination methodology was manually created exhibiting Pannexin-1 transmembrane re-entrant helices positions and orientation.

3.2.3.1.7 Structural Threading and Topology Consensus

Via incorporating the former secondary structural alignment consensus method with UniProt Connexin26 topology a Pannexin-1 alignment exhibiting transmembrane helices positioning was predicted, these Pannexin-1 positions will be used towards re-entrant helices alignment.

3.2.3.1.8 Innexin6 Topology

The Innexin6 topology was determined via UniProt sequence algorithmic data and Phyre² analysis, this membrane positioning will be used towards a Pannexin-1-Innexin6 transmembrane final multiple template alignment.

UniProt Innexin-6:

Topology¹¹⁶

Phyre²:

Sequences Input:

Innexin-6 FASTA 389 amino acid sequence provided via UniProtKB-Q9U3N4 (INX6_CAEEL).⁸²

3.2.4 Pannexin-1 Target-Multiple Template Alignment Selection

The remote Pannexin-1 sequence homology warranted a multiple template approach. Two multiple template modeling approaches were performed and compared for best results, a Clustal multiple template/target approach and a single template/target approach using an Innexin6 structurally threaded top-template.

3.2.4.1 Multiple Template/Target Approach

Pannexin-1 and its six best sequence related templates discovered via the NCBI PSI-BLAST results were FASTA input into CLUSTAL Omega for a multiple template alignment approach.

Tool CLUSTAL 0(1.2.4) Multiple Sequence Alignment²³

CLUSTAL Parameter:

CLUSTALW

Sequences Input:

Query Pannexin-1 FASTA 426 amino acid sequence provided via UniProtKB-Q96RD7-1 (PANX1_HUMAN).³⁸

Template Innexin-6, 5H1Q, PDB,

>5H1Q:A|PDBID|CHAIN|SEQUENCE⁴⁴

Template Chain A, 3d Polymerase, 4Y3C_A, PDB,

>pdb|4Y3C|A Chain A, 3d Polymerase

GALERLPDGPRIHVPRKTALRPTVARQVFQPAFAPAVLSKFDPRTDADVDEVAFSKHTSN
QETLPPVFRMVAREYANRVFALLGRDNGRLSVKQALDGLGMDPMDKNTSPGLPYTTL
GMRRTDVVDWETATLIPFAAERLEKMNNKDFSDIVYQTFLKDELRIEKVQAAKTRIVD
VPPFEHCILGRQLLGKFASKFQTQPGLELGSAIGCDPDVHWTAFGVAMQGFERVYDVDY
SNFDSTHSVAMFRLLAEEFFSEENGFDPLVKDYLES LAISKHAYEEKRYLITGGLPSGCAA
TSMLNTVMNNIIRAGLYLTYKNFEFDDVKVLSYGDDLLVATNYQLNFDRVRTSLAKTG
YKITPANKTSTFPLESTLEDVVFLKRKFKEGPLYRPVMNREALEAMLSYYRPGTLSEKL
TSITMLAVHSGKQEYDRLFAPFREVGIVPTFESVEYRWRS LFW¹²⁸

Template Chain A, Large Tail Fiber Protein P34, 4UXF_A, PDB,

>pdb|4UXF|A Chain A, Large Tail Fiber Protein P34

MGSSHHHHHSQDPSQFIRRDIAQTVNGSLTLTQQTNLSAPLVSSSTGEFGGSLAANRTF
TIRNTGAPTSIVFEKGPASGANPAQSMSIRVWGNQFGGSDTTRSTVFEVGDDTSHHFYS
QRNKDGNIAFNINGTVMPININASGLMNVNGTATFGRSVTANGEFISKSANAFRAINGDY
GFFIRNDASNTYFLLTAAGDQTGGFNGLRPLLINNQSGQITIGELIIAKGVTINSGGLTVN
SRIRSQGTKTSDLYTRAPTSDTVGFWSIDINDSATYNQFPGYFKMVEKTNEVTGLPYLER
GEEVKSPGTLTQFGNTLDSLYQDWITYPTTPEARTTRWTRTWQKTKNSWSSFVQVFDGG
NPPQPSDIGALPSDNATMGNLITRDFLRIGNVRIVPDPVNKTVKFEWVE¹²⁷

Template Chain A, Long-tail Fiber Proximal Subunit, 5NXH_A, PDB,

>pdb|5NXH|A Chain A, Long-tail Fiber Proximal Subunit

SGLVESGTLWDHYTLNILEANETQRGTLRVATQVEAAAGTLDNVLITPKLLGTKSTEAQ
EGVIKVATQSETVTGTSANTAVSPKNLKWIAQSEPTWAATTAIRGFVKTSSGSITFVGNDT
VGSTQDLELYEKN SYAVSPYELNRVLANYLPLKAKAADTNLLDGLDSSQFIRRDIAQTVN
GSLTLTQQTNLSAPLVSSSTGEFGGSLAANRTFTIRNTGAPTSIVFEKGPASGANPAQMSI
RVWGNQFGGSDTTRSTVFEVGDDTSHHFYSQRNKDGNIAFNINGTVMPININASGLMN
VNGTATFGRSVTANGEFISKSANAFRAINGDYGFFIRNDASNTYFLLTAAGDQTGGFNGL
RPLLINNQSGQITIGELIIAKGVTINSGGLTVNSRIRSQGTKTSDLYTRAPTSDTVGFWSID
INDSATYNQFPGYFKMVEKTNEVTGLPYLERGEEVKSPGTLTQFGNTLDSLYQDWITYPT
TPEARTTRWTRTWQKTKNSWSSFVQVFDGGNPPQPSDIGALPSDNATMGNLITRDFLRIG
NVRIVPDPVNKTVKFEWVE¹¹⁹

Template Chain A, DNA polymerase lambda, 1NZP_A, PDB,

>pdb|1NZP|A Chain A, DNA polymerase lambda

MAQPSSQKATNHNH LITEKLEVLA KAYSVQGDKW RALGYAKAINALKSFHKPVTSYQE
ACSIPGIGKRMAEKIIEILESGHLRKL DH¹¹⁴

Template Chain A, Predicted amidohydrolase, dihydroorotase family, 3CJP_A, PDB,

>pdb|3CJP|A Chain A, Predicted amidohydrolase, dihydroorotase family

MSLIIDGHTHVILPVEKH IKIMDEAGVDKTILFSTSIHPETA VNLRDVKKEMKKLNDVVN
GKTNSMIDVRRNSIKELTNVIQAYPSRYVGFGNVPVGLSENDTNSYIEENIVNNKLVGIGE

LTPASGQIKSLKPIFKYSMDSGSLPIWIHAFNPLVLQDIKEIAELCKAFPKVPVILGHMGGN
WMTAVELAKEIQNLYLDTSAYFSTFVLKIVINELPLKCIFGTDMPFGDLQLSIEAIKKMSN
DSYVANAVLGDNISRLLNIEGHHHHHH¹¹³

3.2.4.2 Single Template/Target Approach

Several slightly adjusted multiple template/target alignments were modeled via the best selected templates and corresponding alignments discovered via Phyre² and NCBI PSI-BLAST. The best of these manual input single alnfile alignments used the two Phyre² discovered templates (5H1Q, 5H5P) and three of the NCBI PSI-BLAST discovered templates (1NZP, 4UXF, 4Y2C).

Conserved transmembrane regions, re-entrant membrane positions and pivotal residue constraints were alignment preserved, consensus contributed to alignments. The Phyre² Pannexin-1-Innexin6 threaded alignment (Table 27) remained the top-template and manual adjustments were slight towards maintaining alignment integrity.

UNCRYSTALLIZED TEMPLATE

Y10 predicted phosphorylation-site S residue neutrally aligned.

Inner membrane **S** polar residue constraint maintained, hydrophobic core and ss constraint maintained in TM.

Leu (L) more exhibited than Val and Ile, expected in alpha helices (L=25% vs. V and I total contribution=25%).²¹⁰

[N-Terminal-Tail-IV=~8%-----] [TM1-----IV=~14%]
PANNEXIN 1 (1) MAIAQLATEYVFSDFLLKEPTFKPKGLRLELAVDKMVT CIAVGIPLLIISLA AQEISIG (61)
INNEXIN-6 (7) -----AINSVNALISRVEFQPK-----GDLADRLNSRVTVVI-LAVSSAL LSSH-- (53)
 :::.....:.. ...:*:::~::~*::~::~:
[N-Terminal-Tail-----] [TM1-----]
#

```
1M, 2A, 3S, 4Q, 5V, 6G INX6_RESIDUES_UNCRYSTALLIZED INX6_RESIDUES_I52-G53
UNCRYSTALLIZED
```

Polar/Charged Residues (RKDEQNHSTYC)
Hydrophobic Residues (AILMFVPG)
Hydrophobic Residues Center Peaks (AIVL)
Amphipathic Residues Interface Residues (WYM)

(N-Tail)...AVDKMVTCLAVGLPLL...(TM1)¹⁵⁸

TM1 ~81% hydrophobic residues (IAVGLPLLLITSLAFAQEISIG) with central membrane peaks of (AIVL) ~80%, zero Panx1 TM gaps, and an energetically favorable polar S-residue residing within alpha-helical inner-membrane cores.¹⁰⁰

TM1-EL1 Boundary exhibits proper hydrophobic-hydrophilic boundary **IG-TQ**.

Residue constraints near pivotal functional residues aligned, functional residue constraints towards channel gating (W-A, R-Q and 67-86) aligned, structural residue constraints C-C aligned preserving disulfide bridges towards possible channel activity modulation.

Amphipathic **Tryptophan W74** acting as a Polarity Switch towards open channel WT Panx1 CBX blocking within conserved region 67-86 is aligned satisfactorily via hydrophobic-hydrophobic A-W alignment.

EL1 **R75** binds extracellular ATP inhibiting WT open Panx1, R is polar and aligned to a charged residue **R** satisfactorily.

Conserved region towards gating 67-86 aligned well, Identity Value 30% with a high ratio of residue with similar chemical properties and zero gaps.

[illegible]

Positively charged **R** and **K** charged residues and Trp (**W**) and Tyr (**Y**) exhibited at boundaries of TMs.^{100, 211}

The Pannexin-1 aligned First Extracellular Loop moderately but satisfactorily (considering the loop nature of glycine and proline and amphipathic nature of tryptophan) exhibited expected % charged/polar and Trp (W) interface residues importantly distinguishing proper TM1-EL1-TM2 residue boundary positioning.

Hydrophobic Residues Center Peaks (AIVL)
Amphipathic Residues Interface Residues (WYM)

EL1 ~56% (TQISCFSPSSF^WSRQAAFVDSYC^WAAVQ^GQKNSLQSESGNLPLWLH)¹⁵⁸


```

-----IV=13%][---TM3-IV=~10%-----]
PANNEKIN1 (207)NNLIKKYISCRLLTLIIILLACIYLGYYFSL (238)
INNEXIN-6 (186)RNMAFYTLSTVWQAVNAWIQEYILTQLLDSS (217)
:*:::.*.....*:::.*:::.*
---][---TM3-----][EL2--

```

#

TM3 exhibited zero alignment gaps and highly exhibited an expected hydrophobic residue % and central inner-membrane conserved polar residues importantly distinguishing proper TM residue positioning.

TM3 ~73% (LLTLIIILLLACIYLGYYFSL) with central membrane peaks of (AIVL) ~71% with one central polar C residue.

EL2 N255S aligned via chemical similarity to preserve asparagine glycosylation site i.e. polar residue alignment.

EL2-L237, L240, S247, K266 are pivotal residues towards a Probenecid and Food Dye blocking of a WT Panx1 open state, well aligned via similar residues.

Conserved Cysteine C246 and C265 in EL2 aligned to preserve disulfide bridges towards possible channel activity modulation.

```

[-----EL2-----IV=10%-----]
PANNEKIN1 (239)SL-----SDEF-----VCSIKSGILRNDSTVP-DQFQC--K (266)
INNEXIN6 (218) IYTLWGPSILGDLQGNQWQTTGHFPRIVHCDFNRRRPAS---VQLDTVLCVLT (268)
.:                      :.*      *. *:::.*:      *. *:::.* :
-----EL2-----
                                @      @

```

The Pannexin-1 aligned Second Extracellular Loop moderately but satisfactorily (considering the loop nature of glycine and proline) exhibited expected charged and polar residues distinguishing proper TM3-EL2-TM4 residue boundary positioning.

EL2 ~64% (SLSDDEFVCSIKSGILRNDSTVPDQFQCK)¹⁵⁸

```

[---TM4---IV=26%-----]
PANNEKIN1 (267)L-I-AVGIFQLLSVINLVVYVLL (287)
INNEXIN6 (269) LNIYYEKLFIPLFWIVFVAVVS (291)
* * :.*:.*:.*:.*:.*:.*:.*:.*:
--EL2-][--TM4-Phyre2---
                                @

```

Zero TM4 alignment gaps were exhibited within conserved pivotal transmembrane regions, ss TM4 residue constraints maintained, polar S, N inner membrane residue constraint maintained.

K381, T382, A386

Surrounding residue constraints aligned.

```

-----C-Tail---IV=5%-----]
PANNEXIN1 (383)----PMSAEMREEQGNQTAEALQGMNIDSETKANNGEKNAR----QRLLDSS (426)
4Y2C (131)ATLIPFAAERLEKMNNK (147)
--IV=40%-----]
*::**..*::*:
. ....:..*
4UXF_A (1245) [PSDIGALPSD] (1254)
5H5P (482) SETTANMRKKGKPNPLQR----- (500)
[-----IV=47%-----]
***:*** :*:: **
#### # ### # ##### ### ###

```

Surrounding residue constraints maintained.

Cysteine unmatched:

C42d binds TM1 F54 towards C-auto-inhibition, caspase cleavage releases this binding.

Table 15.) A multiple template alignment via two Phyre² and three NCBI PSI-BLAST single template/target alignments.^{229, 231, 84}

indicates constraints ascertained via interspecies Pannexin-1 homologs exhibiting high 99% homologies.²²²

@ indicates constraints ascertained via distant homologs exhibiting <20% homologies.²²³

[Download](#)
[GenPept](#)
[Graphics](#)

[▼ Next](#)
[▲ Previous](#)
[◀ Descriptions](#)

Chain A, DNA polymerase lambda [Homo sapiens]

Sequence ID: [INZP A](#) Length: 87 Number of Matches: 1

Range 1: 39 to 79
[GenPept](#)
[Graphics](#)

[▼ Next Match](#)
[▲ Previous Match](#)

Related Information
[Structure](#) - 3D structure displays

Score	Expect	Method	Identities	Positives	Gaps
28.9 bits(63)	3.6	Composition-based stats.	14/41(34%)	24/41(58%)	1/41(2%)
Query	150	YNRAIKAAKS-ARDLMDRGACSPVGTENLGSLWEVSES Y +AI A KS + + ACS+PG+ + + + E+ ES		189	
Sbjct	39	YAKAINALKSFHKPVTSYQEACSIPIGGRMAEKIIEILES		79	

Table 16.) NCBI PSI-BLAST 1NZP_A selected template-target alignment.⁸⁴

Download ▾ GenPept Graphics ▾ Next ▲ Previous ◀ Descriptions

Chain A, Large Tail Fiber Protein P34 [Escherichia virus T4]
Sequence ID: [4UXF_A](#) Length: 410 Number of Matches: 1
[See 14 more title\(s\) ▾](#)

Range 1: 248 to 310 [GenPept](#) [Graphics](#) ▾ Next Match ▲ Previous Match

Score	Expect	Method	Identities	Positives	Gaps
32.0 bits(71)	1.7	Compositional matrix adjust.	21/63(33%)	28/63(44%)	5/63(7%)

Query	301	QKTDVLKVYEILPTFDVLHFKSEGYNDLSLYNLF-----LEENISEVKSYKCLKVLENIK	355
Sbjct	248	Q T +Y P T D + F S ND + YN F + E +EV L+ E +K	307
Query	356	SSG 358	
Sbjct	308	SPG 310	

Related Information
[Structure](#) - 3D structure displays
[Identical Proteins](#) - Identical proteins to 4UXF_A

Table 17.) NCBI PSI-BLAST 4UXF_A selected template-target alignment.⁸⁴

Download ▾ GenPept Graphics ▾ Next ▲ Previous ◀ Descriptions

Chain A, Genome Polyprotein [Mengo virus]
Sequence ID: [4Y2C_A](#) Length: 460 Number of Matches: 1

Range 1: 94 to 147 [GenPept](#) [Graphics](#) ▾ Next Match ▲ Previous Match

Score	Expect	Method	Identities	Positives	Gaps
32.0 bits(71)	1.5	Compositional matrix adjust.	19/54(35%)	27/54(50%)	4/54(7%)

Query	346	KCLKVLENIKSSGGIDPMLLLTNLGMIMKMDVVDGKT----PMSAEMREEQGNO	395
Sbjct	94	+ L LE + + P L T LGM + DVVD +T P +AE E+ N+	147

Related Information
[Structure](#) - 3D structure displays

Table 18.) NCBI PSI-BLAST 4Y2C_A selected template-target alignment.⁸⁴

	406 . . . 410 420
Predicted Secondary structure	
Query Sequence	S E TKA NNGE K N A R Q R
Template Sequence	S E TTA NNXR K K G K PNP DQ R
Template Known Secondary structure	S S T T S B T T B TT
Template Predicted Secondary structure	
	482 490 500

Table 19.) Phyre² c5h5pA selected template-target alignment.⁸⁶

3.2.5 Pannexin-1 Molecular Modeling Methodology

MODELLER A-chain subunits were generated via the two former multiple template alignments with various A-chains generated via slight adjustments to the former Table 15 alignment. Single template alignments using Connexin26 and Innexin6 and a multiple template alignment using Connexin26-Innexin6 were similarly A-chain generated. All Coordinate Files were abstracted from the PDB (Connexin26 crystallized state seems to be in an open conformation, Innexin6 crystallized state open or closed state coordinates undetermined).^{179,218} GalaxyWeb subsequently oligomerized various pentamers, hexamers, heptamers and octamers of the best generated MODELLER A-chain monomer. These same oligomerizations were similarly GalaxyWeb generated via a Pannexin-1 FASTA sequence input methodology.

3.2.5.1 Multiple Template/Target MODELLER A-Chain

MODELLER modeling of an A-chain Pannexin-1 via a Clustal multiple 6-template alignment and respective PDB-3-D coordinate files.

Tool MODELLER Specific Version Number: 9v15 Installed

Graphic User Interface-None

Database Used-None

Default Parameters all used except number of models generated were 10 instead of one.

```
# Step 4: model building
#
# This script should produce two models, 1fdx_my.B99990001.pdb and
# 1fdx_my.B99990002.pdb.

from modeller import *
from modeller.automodel import *    # Load the automodel class

log.verbose()
env = environ() # To get different models from another script

# directories for input atom files
env.io.atom_files_directory = ['./']

a = automodel(env,
               alnfile='align3.ali',    # alignment filename
               knowns=('5h1q', '1nzp', '4uxf', '5nxh', '3cjp', '4y3c'), # codes
               sequence='Panx1')        # code of the target
a.starting_model= 1                    # index of the first model
a.ending_model  = 10                   # index of the last model
                                         # (determines how many models to calculate)

a.make()                               # do homology modelling
```

Table 20.) MODELLER script used to generate 10 Pannexin-1 models via the align3.ali file noted in results section 4.4.1 Clustal Multiple Template/Target Alignment File and the six-input known 3-D coordinate files (5h1q, 1nzp, 4uxf, 5nxh, 3cjp, 4y3c), Panx1 remains the sequence.¹⁴⁹

3.2.5.2 Single Template/Target MODELLER A-Chain

MODELLER modeling of an A-chain Pannexin-1 via a single template/target multiple 5-template alignment and respective PDB-3-D coordinate files.


```

# Step 4: model building
#
# This script should produce two models, 1fdx_my.899990001.pdb and
# 1fdx_my.899990002.pdb.

from modeller import *
from modeller.automodel import * # Load the automodel class

log.verbose()
env = environ() # To get different models from another script

# directories for input atom files
env.io.atom_files_directory = ['./']

a = automodel(env,
              alnfile='align2.ali', # alignment filename
              knowns=('5H1Q', '1NZP', '4UXF', '4Y2C', '5H5P'), # codes of the templates
              sequence='Pannexin-1') # code of the target
a.starting_model= 1 # index of the first model
a.ending_model = 10 # index of the last model
                  # (determines how many models to calculate)

a.make() # do homology modelling

```

Table 21.) MODELLER script used to generate 10 Pannexin-1 models via the align2.ali file noted in results section 4.4.2 Single Template/Target Alignment File and the five-input known 3-D coordinate files (5h1q, 1nzp, 4uxf, 4y2c, 5h5p), Panx1 remains the sequence.¹⁴⁹ (Several other A-chain models were generated via a slightly adjusted align2.ali file.)

3.2.5.3 GalaxyWeb Monomer Input

The multiple template align2.ali file MODELLER generated Panx1 subunit A-chain was subsequently multi-mer modeled via GalaxyWEB's GalaxyHomomer protein homo-oligomer software via five-default setting, 5, 6, 7, and 8 oligomeric state inputs. A default setting and multiple per-mutated ab initio loop/termini refinements were selected and input for each oligomeric state.

Loops or Termini to be Refined (5aa<=len<=20aa, **Optional)**
can be used only when monomer structure (PDB file) is provided.

Region 1	Start <input type="text" value="1"/>	End <input type="text" value="19"/>
Region 2	Start <input type="text" value="67"/>	End <input type="text" value="85"/>
Region 3	Start <input type="text" value="407"/>	End <input type="text" value="426"/>

Table 22.) Tails (1-19, 407-426) and gating regulating EL1 (67-85) refinement remodeling selected and input.⁷⁸

Python program
MySQL database

GalaxyHomomer Parameters (Coordinate-File Approach):

Inputs:

A-Chain Coordinate Files:

Pannexin-1.B99990001.pdb

Default Setting, 5, 6, 7, 8-Oligomeric State⁷⁸

3.2.5.4 GalaxyWeb Sequence Input

Five-default setting, 5, 6, 7 and 8-oligomeric states and a Panx1 FASTA amino-acid sequence were input into GalaxyWEB's GalaxyHomomer protein homo-oligomer tool.

GalaxyHomomer Parameters (FASTA Approach):

Inputs:

Pannexin-1 FASTA 426 amino acid sequence provided via UniProtKB-Q96RD7-1 (PANX1_HUMAN).³⁸

Default Setting, 5, 6, 7, 8-Oligomeric State⁷⁸

3.3 Ligand-Target Docking Dynamic Simulation Method

The discovered four inhibitor chemicals and one mimetic peptide were Medusa Guide-Docked into their in vitro experimental resulting determined Pannexin-1 EL-1, EL-2 and hexamer pore regions, affinities were subsequently determined. This MedusaDock local assay was restricted to the spatial coordinates of the putative binding regions of the best selected hexamer sequence model, all dockings were shape complementary and restricted to <10 rotatable ligand-bonds for best prediction results.⁶⁴

3.3.1 ¹⁰Panx1-Pore Docking Method

The Mimetic ¹⁰Panx1 was Guide-Docked to the Pannexin-1 hexamer pore region.

Tool MedusaDock v2.0

MedusaDock Parameters:

Input:

- 1.) Select receptor (Pannexin-1 hexamer sequence model uploaded)
- 2.) Select ligand (¹⁰Panx1 uploaded)
- 3.) Binding site set to Pannexin-1 pore-residues S93, Q95, S96 and E97
- 4.) Constraints set-energy guide docked (no restraints selected); used all default parameters.
- 5.) 1-10 Rounds Submitted¹⁸⁶

3.3.2 Target-EL1 Docking Method

All four Pannexin-1 EL-1 binding chemicals (CBX, Probenecid, Brilliant Blue FCF [BB FCF] and FD&C Green No. 3) were guide-docked to the Pannexin-1 EL1 67-86 region.

MedusaDock Parameters:

Input:

- 1.) Select receptor (Pannexin-1 hexamer sequence model uploaded)
- 2.) Select ligand (CBX, Probenecid, Brilliant Blue FCF [BB FCF] and FD&C Green No. 3 uploaded)
- 3.) Binding site set to Pannexin-1 EL1 67-86 region
- 4.) Constraints set-energy guide docked (no restraints selected); used all default parameters.
- 5.) 1-10 Rounds Submitted¹⁸⁶

3.3.3 Target-EL2 Docking Method

Discovered Pannexin-1 EL-2 binding chemicals (Probenecid, Brilliant Blue FCF [BB FCF] and FD&C Green No. 3) were guide-docked to the Pannexin-1 EL2 (237 (L), 240 (L), 247 (S), 266 (K)) targeted regions.

MedusaDock Parameters:

Input:

- 1.) Select receptor (Pannexin-1 hexamer sequence model uploaded)
- 2.) Select ligand (Probenecid, Brilliant Blue FCF [BB FCF] and FD&C Green No. 3 uploaded)
- 3.) Binding site set to Pannexin-1 EL2 (237 (L), 240 (L), 247 (S), 266 (K)) regions
- 4.) Constraints set-energy guide docked (no restraints selected); used all default parameters.
- 5.) 1-10 Rounds Submitted¹⁸⁶

Chapter 4

Results

4.1 Pannexin-1 Templates Selected

NCBI blastp results indicated homolog 5H1Q and 3CJP to be best selected templates. Innexin6 exhibits a best query coverage area with a strong E-value, however, its percent identity value is below 30% inferring a multiple template alignment approach. Although 3CJP exhibits an unfavorable E-value its query-coverage is useful towards a multiple template alignment.

☒ select all 2 sequences selected

[GenPept](#)
[Graphics](#)
[Distance tree of results](#)
[Multiple alignment](#)

	Description	Max Score	Total Score	Query Cover	E value	Per. Ident	Accession
<input checked="" type="checkbox"/>	Chain A, Innexin-6 [Caenorhabditis elegans]	42.4	42.4	26%	9e-04	26.45%	5H1Q_A
<input checked="" type="checkbox"/>	Chain A, Predicted amidohydrolase, dihydroorotase family [Clostridium acetobutylicum ATCC 824]	29.3	29.3	3%	9.4	52.94%	3CJP_A

Table 23.) NCBI blastp results.¹²⁵

PSI-BLAST results exhibited a run-iteration of 1 with a max 500 (one iteration was selected via default, a second iteration generated an alignment limited PSSM error i.e. not enough alignments left towards a subsequent iteration).

Run PSI-BLAST Iteration 2 with max number of sequences

500

Run

Sequences with E-value WORSE than threshold

☒ select all 10 sequences selected

PSI-BLAST iteration

	Description	Max score	Total score	Query cover	E value	Per. Ident	Accession	Select for PSI blast	Used to build PSSM	New added
<input checked="" type="checkbox"/>	Chain A, Genome Polyprotein [Mengo virus]	32.0	32.0	11%	1.5	35.19%	4Y2C_A	<input type="checkbox"/>		
<input checked="" type="checkbox"/>	Chain A, Genome Polyprotein [Mengo virus]	32.0	32.0	11%	1.5	35.19%	4NYZ_A	<input type="checkbox"/>		
<input checked="" type="checkbox"/>	Chain A, 3d Polymerase [Mengo virus]	32.0	32.0	11%	1.5	35.19%	4Y3C_A	<input type="checkbox"/>		
<input checked="" type="checkbox"/>	Chain A, Genome Polyprotein [Mengo virus]	32.0	32.0	11%	1.6	35.19%	4NZ0_A	<input type="checkbox"/>		
<input checked="" type="checkbox"/>	Chain A, Large Tail Fiber Protein P34 [Escherichia virus T4]	32.0	32.0	13%	1.7	33.33%	4UXF_A	<input type="checkbox"/>		
<input checked="" type="checkbox"/>	Chain A, Long-tail Fiber Proximal Subunit [Escherichia virus T4]	31.6	31.6	13%	2.4	33.33%	5NXH_A	<input type="checkbox"/>		
<input checked="" type="checkbox"/>	Chain A, DNA polymerase lambda [Homo sapiens]	28.9	28.9	9%	3.6	34.15%	1NZP_A	<input type="checkbox"/>		
<input checked="" type="checkbox"/>	Chain A, Large Tail Fiber Protein P34 [Escherichia virus T4]	30.8	30.8	13%	3.9	33.33%	4UXE_A	<input type="checkbox"/>		
<input checked="" type="checkbox"/>	Chain A, Long-tail Fiber Proximal Subunit [Escherichia virus T4]	30.4	30.4	13%	4.7	33.33%	5NXF_A	<input type="checkbox"/>		
<input checked="" type="checkbox"/>	Chain A, Predicted amidohydrolase, dihydroorotase family [Clostridium acetobutylicum ATCC 824]	29.3	29.3	3%	9.4	52.94%	3CJP_A	<input type="checkbox"/>		

Table 24.) Above PSI-BLAST Pannexin-1 discovered templates exhibiting high E-values albeit apropos towards a Pannexin-1 multiple template alignment approach.¹⁴⁴

Phyre² similarly returned a best Innexin6 template with a high Confidence of 99.9 and satisfactory % i.d. of 21, moreover seventy-one less confident templates were discovered via Phyre² including the low confidence scored 5.4 albeit high 60% i.d. c5h5pA to be used towards a multiple template alignment.


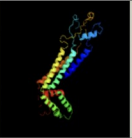
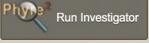

#	Template	Alignment Coverage	3D Model	Confidence	% i.d.	Template Information
1	c5h1qC			99.9	21	PDB header: transport protein Chain: C: PDB Molecule: innexin-6; PDBTitle: c. elegans inx-6 gap junction hemichannel 
66	c5h5pA		not modelled	5.4	60	PDB header: transcription Chain: A: PDB Molecule: myelin regulatory factor; PDBTitle: crystal structure of myelin-gene regulatory factor dna binding domain

Table 25.) Phyre² HH results exhibiting highly confident c5h1qc Innexin6 and c5h5pA to be used towards a Pannexin-1 top template and C-tail multiple template alignment respectively.⁹⁷

4.2 Pannexin-1 Single Target-Template Alignments

Multiple Biomedical Informatics produced the following alignment results to be used towards a multiple template alignment approach.

4.2.1 Clustal

Clustal Innexin6-Pannexin-1 alignment exhibited a BLAST suspected low identity of ~17% (sequence similarities should exhibit >25% identity ratios to avoid substantial alignment errors and lack of template hits¹⁴⁸).

Table 26.) Clustal Innexin6-Pannexin-1 alignment results (* = Identity Match).¹²⁰

Substantial gaps were exhibited within conserved 1st, 3rd and 4th conserved transmembrane regions (yellow-highlights) and pivotal residue Y309 and D379 verified phosphorylation and caspase cleavage sites (orange highlights) respectively.

CLUSTAL O(1.2.4) multiple sequence alignment

```

sp|Q96RD7|PANX1_HUMAN      MA--IAQLATEYVFSDFLLKEPTEPKFKGLRLELAVDKMVTCTIAVGLPLLLISLAFQEI 58
5H1Q:A|PDBID|CHAIN|SEQUENCE MASQVGAINSVNALISRVFVQPKGDLAD----RLNSRVTVVILAVS-----SALLLSSH 50
** :. : : :. : : :*. . . * . :*. * : :.

sp|Q96RD7|PANX1_HUMAN      SIGTQISCFSPPSSFSWRQAAFVDSYCWAAVQQKNS-----LQSESGNLPWLHKFFPY 111
5H1Q:A|PDBID|CHAIN|SEQUENCE FIGDPITCWTTPAQFNAQWVNFVNQYCFVHGTYFVPLDQQLAFEEEEERTKVS IQYYQWVPY 110
** *:*:*:*. : . *:*.*: . :. * : : : :*:**

sp|Q96RD7|PANX1_HUMAN      ILLFAILYLPPLFWRFAAAPHICSDLKFIMEELDKVYNRAIKAASARDLDMRDGACS 171
5H1Q:A|PDBID|CHAIN|SEQUENCE VFALQAFIFYIPRFWKAMIAYSQ-YDLAAVKYVDRFWSENRD-----KDDKFKTRLAA 164
: : * *:*:*: * :*: * * : :*:*. . . : * :. : :

sp|Q96RD7|PANX1_HUMAN      VPGVTENLGQSLWEVSESHFKYPIVEQYLKTKKNSNNLIKYISCRLLTLIIILLACIYL 231
5H1Q:A|PDBID|CHAIN|SEQUENCE FEG--RPSVYIWDGI-----RLARKKRSRNMALFYTLSTVWQAV-----NAWI 205
. * . . :*: * *:*.*: : * . : : : :

sp|Q96RD7|PANX1_HUMAN      GYFSLSSLSDE----FVCSIKSGIL----RNDSTVPDQFQCKLIAV-----GIFQLL 276
5H1Q:A|PDBID|CHAIN|SEQUENCE QFYIL-TQLLDSSIYTLWGPSILGDLQGNDWQTTGHFPRIVHCDFNRRRPASVQLDVTVL 264
*: :.* * . : ** :*: :. . . * :*: : : : *

sp|Q96RD7|PANX1_HUMAN      SVINLVVYVLLAP--VVVYTLFVPFRQKTDVLKV*EILPTFDVLHFKSEGYNDSLNLNF 334
5H1Q:A|PDBID|CHAIN|SEQUENCE CVLTNLNIYEKLFIFLWFVLFVAVVSTVNC-----FKWIYYLCNKT----- 306
.*.* : * : : :*: . :*: : * : : : :

sp|Q96RD7|PANX1_HUMAN      LEENISEVKS YKCLKVLEN----IKSSGQGIDPMLLLTN----LGMI----- 373
5H1Q:A|PDBID|CHAIN|SEQUENCE --KAQKTIKNYLSTAPIKSTISDDQFFSALGEDGLFIMDQMALNLGDIPASYLTISM RNI 364
: . :*. * : :. * . * : : : : * * *

sp|Q96RD7|PANX1_HUMAN      KMDVV-----DGKTPMSAEMREEQGNQTAEI.QGMNIDSETKA-----NNGEKNARQR 420
5H1Q:A|PDBID|CHAIN|SEQUENCE CQDFIESEDYIDEERTPFVKS IKHTQA-PDBIDCHAINSEQUENCEMASQVGAINSVNA 423
*.: : :*: . :. : : : : * : * : :

sp|Q96RD7|PANX1_HUMAN      LLDSS-----C----- 426
5H1Q:A|PDBID|CHAIN|SEQUENCE LISRVFVQPKGDLADRLNSRVTVVILAVSSALLLSSHFIGDPITCWTTPAQFNAQWVNFVN 483
*:. *

sp|Q96RD7|PANX1_HUMAN      ----- 426
5H1Q:A|PDBID|CHAIN|SEQUENCE QYCFVHGTYFVPLDQQLAFEEEEERTKVS IQYYQWVPYVFALQAFIFYIPRFWKAMIAYS 543

sp|Q96RD7|PANX1_HUMAN      ----- 426
5H1Q:A|PDBID|CHAIN|SEQUENCE GYDLAAVKYVDRFWSENRDKDKFKTRLAAFEGRPSVYIWDGIRLARKKRSRNMALFYT 603

sp|Q96RD7|PANX1_HUMAN      ----- 426
5H1Q:A|PDBID|CHAIN|SEQUENCE LSTVWQAVNAWIFQFYILTQLLDSSIYTLWGPSILGDLQGNDWQTTGHFPRIVHCDFNRR 663

sp|Q96RD7|PANX1_HUMAN      ----- 426
5H1Q:A|PDBID|CHAIN|SEQUENCE RPASVQLDVTLCVLTNLNIYEKLFIFLWFVLFVAVVSTVNCFKWIYYLCNKTAKQKTIK 723

sp|Q96RD7|PANX1_HUMAN      ----- 426
5H1Q:A|PDBID|CHAIN|SEQUENCE NYLSTAPIKSTISDDQFFSALGEDGLFIMDQMALNLGDIPASYLTISM RNICQDFIESED 783

sp|Q96RD7|PANX1_HUMAN      ----- 426
5H1Q:A|PDBID|CHAIN|SEQUENCE YIDEERTPFVKS IKHT 799

```

Accordingly although the pairwise Innexin6 alignment exhibits a low identity conventionally unsuitable towards single template homology modeling and moreover exhibits extensive gaps within pivotally conserved residues and membranous regions, this alignment was used towards a top template alignment adjustment within a fold-recognition multiple template alignment threading approach.

4.2.2 Promals3D

Promals3D Innexin6-Pannexin-1 fold alignment results similarly expressed a low identity of just ~14% and gaps within pivotal residues and transmembranes one and four. Accordingly, although Promals3D identity and gap results are unsatisfactory towards a single template alignment modeling methodology, this ss alignment was used towards a threading consensus.¹¹⁵

4.2.3 Phyre²

From the previous Phyre² multiple template predictor output, Phyre² aligned via structural threading Innexin6. In this prediction the alignment integrity has been heightened to 21% via Phyre²'s fold recognition algorithm.

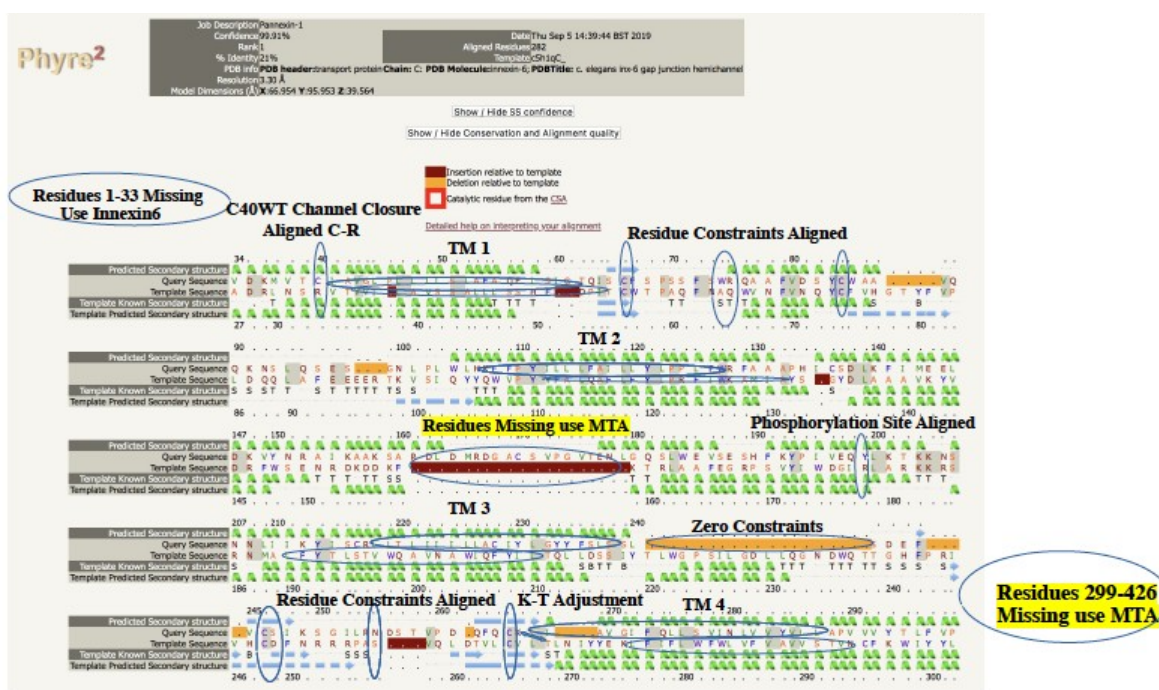


Table 27.) Phyre² Pannexin-1-Innexin6 template alignment secondary structural prediction exhibiting four conserved aligned transmembrane (TM) helices and pivotal residues throughout, bottom K-T to be manually adjusted to preserve residue integrity .¹¹¹

Phyre²'s Pannexin-1-Innexin6 alignment exhibits the best overall coverage area and alignment integrity, however, the Pannexin-1 front and back tail domains were absent. Accordingly this alignment was elected as a top template towards a multiple template alignment approach.

4.2.4 CNFpred

Similar to the previous template discovery methods CNFpred selected Innexin-6 as a best top template. Being a secondary structural predictor, the CNFpred alignment results were similar to Phyre²'s i.e. conserved alignments towards selected constraints. Although this algorithm's alignment results exhibited a low 14% sequence identity it was used towards a consensus structural threading alignment.⁶³

4.2.5 Consensus Target-Template Structural Threading

The above single template alignment methods were used towards the development of the below Table 28.) threading agreeing consensus multiple alignment illustrating helices positioning for a query Pannexin-1 exhibiting a distant homology.

ALPHAHELIX

TRANSMEMBRANEHELIX

BETA STRAND

BEND

TURN

UNCRYSTALLIZED_TEMPLATE

PANNEXIN 1 (1)MAIAQLATEYVFSDFLLEKEPTPEPKFKGLRLELAVDKMVTCTIAVGLPLLLI (50)

PHYRE2 MAIAQLATEYVFSDFLLEKEPTPEPKFKGLRLELAVDKMVTCTIAVGLPLLLI

PROMALS3D MAIAQLATEYVFSDFLLEKEPTPEPKFKGLRLELAVDKMVTCTIAVGLPLLLI

RAPTORX MAIAQLATEYVFSDFLLEKEPTPEPKFKGLRLELAVDKMVTCTIAVGLPLLLI

PANNEXIN 1 (51)SLAFAQEISIGTQISCFSPSSFSWRQAAAFVDSYCWAAVQQKNSLQSESGN (100)

PHYRE2 SLAFAQEISIGTQISCFSPSSFSWRQAAAFVDSYCWAAVQQKNSLQSESGN

PROMALS3D SLAFAQEISIGTQISCFSPSSFSWRQAAAFVDSYCWAAVQQKNSLQSESGN

RAPTORX SLAFAQEISIGTQISCFSPSSFSWRQAAAFVDSYCWAAVQQKNSLQSESGN

PANNEXIN1 (101)LPLWLHKFFPYILLFFAILLYLPPLFWRFAPPHICSDLKFIMEELDKVY (150)

PHYRE2 LPLWLHKFFPYILLFFAILLYLPPLFWRFAPPHICSDLKFIMEELDKVY

PROMALS3D LPLWLHKFFPYILLFFAILLYLPPLFWRFAPPHICSDLKFIMEELDKVY

RAPTORX LPLWLHKFFPYILLFFAILLYLPPLFWRFAPPHICSDLKFIMEELDKVY

PANNEXIN1 (151) NRAIKAAKSARDLDMRDGACSVPGVTENLGQSLWEVSESHFKYPIVEQYL (200)

PHYRE2 NRAIKAAKSARDLDMRDGACSVPGVTENLGQSLWEVSESHFKYPIVEQYL

PROMALS3D NRAIKAAKSARDLDMRDGACSVPGVTENLGQSLWEVSESHFKYPIVEQYL

RAPTORX NRAIKAAKSARDLDMRDGACSVPGVTENLGQSLWEVSESHFKYPIVEQYL

PANNEXIN1 (201) KTKKNSNNLI IKYISCRLLTLLI IILLACIYLGYYFSLSSLSDEFVCSIKS (250)

PHYRE2 KTKKNSNNLI IKYISCRLLTLLI IILLACIYLGYYFSLSSLSDEFVCSIKS

PROMALS3D KTKKNSNNLI IKYISCRLLTLLI IILLACIYLGYYFSLSSLSDEFVCSIKS

RAPTORX KTKKNSNNLI IKYISCRLLTLLI IILLACIYLGYYFSLSSLSDEFVCSIKS

PANNEXIN1 (251) GILRNDSTVPDQFQCKLI AVGIFQLLSVINLVVYVLLAPVVVYTLFVPFR (300)

PHYRE2 GILRNDSTVPDQFQCKLI AVGIFQLLSVINLVVYVLLAPVVVYTLFVPFR

PROMALS3D GILRNDSTVPDQFQCKLI AVGIFQLLSVINLVVYVLLAPVVVYTLFVPFR

RAPTORX GILRNDSTVPDQFQCKLI AVGIFQLLSVINLVVYVLLAPVVVYTLFVPFR

PANNEXIN1 (301) QKTDVLKVYEILPTFDVLHFKSEGYNDLSLYNLFLEENISEVKSYKCLKV (350)

PHYRE2 QKTDVLKVYEILPTFDVLHFKSEGYNDLSLYNLFLEENISEVKSYKCLKV

PROMALS3D QKTDVLKVYEILPTFDVLHFKSEGYNDLSLYNLFLEENISEVKSYKCLKV

RAPTORX QKTDVLKVYEILPTFDVLHFKSEGYNDLSLYNLFLEENISEVKSYKCLKV

PANNEXIN1 (351) LENIKSSGQGIDPMLLLTNLGM IKMDVVDGKTPMSAEMREEQGNQTAE LQ (400)

PHYRE2 LENIKSSGQGIDPMLLLTNLGM IKMDVVDGKTPMSAEMREEQGNQTAE LQ

PROMALS3D LENIKSSGQGIDPMLLLTNLGM IKMDVVDGKTPMSAEMREEQGNQTAE LQ

RAPTORX LENIKSSGQGIDPMLLLTNLGM IKMDVVDGKTPMSAEMREEQGNQTAE LQ

PANNEXIN1 (401) GMNIDSETKANNGEKNARQRL LDSSC (426)

PHYRE2 GMNIDSETKANNGEKNARQRL LDSSC

PROMALS3D GMNIDSETKANNGEKNARQRL LDSSC

RAPTORX GMNIDSETKANNGEKNARQRL LDSSC

4.3 Pannexin-1 Topology

4.3.1 TMPred Topology Prediction

4.3.1.1 Pannexin-1

Prediction parameters:

TM-helix length between 14 and 35

TMPRED.19992.5961.seq³⁷

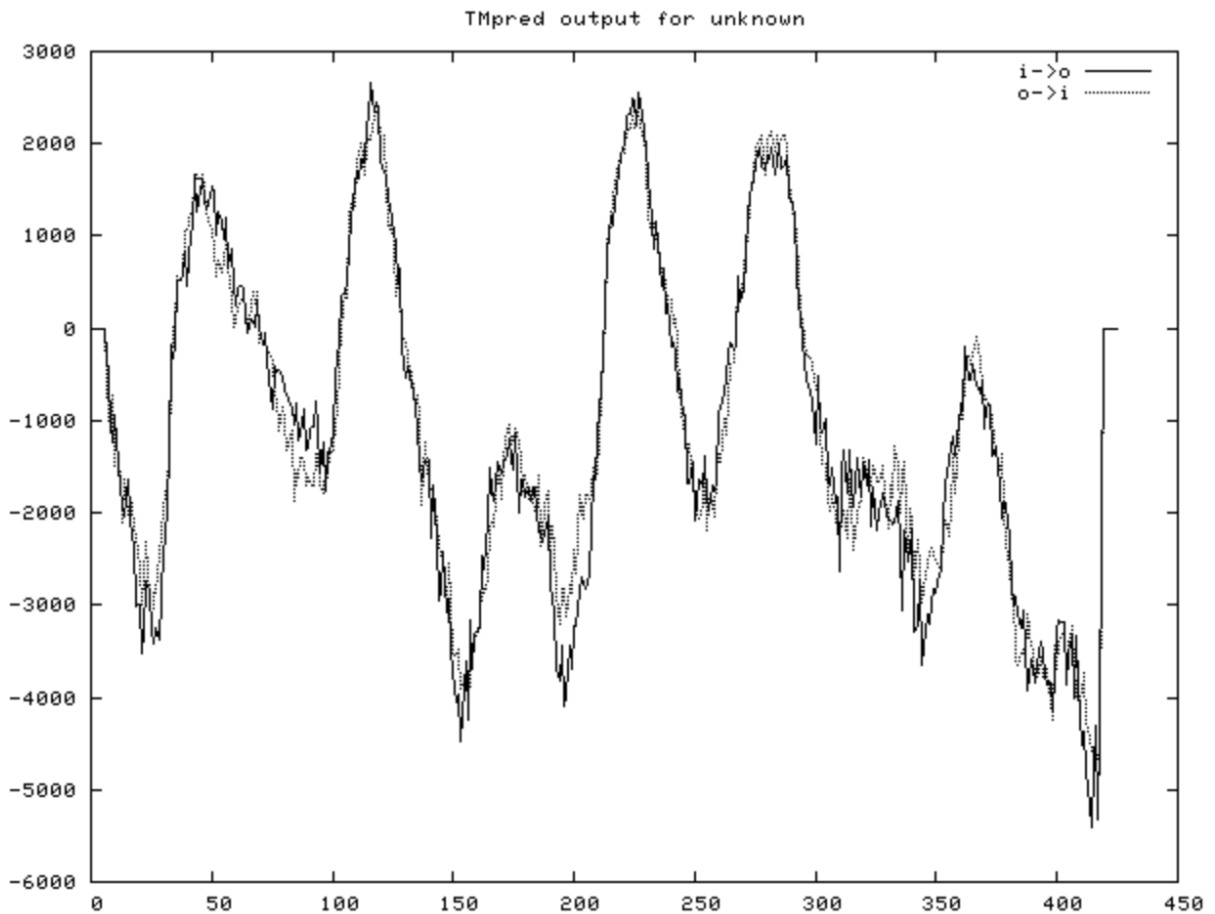


Table 29.) TMPred transmembrane spanning regional inside-outside (i→o), outside-inside (o→i) prediction.⁵¹ In this case my preferred election is towards the former TMPred's alternative model below orienting Pannexin-1's N and C termini in the cytosol scoring 8687 corroborating with UniProtKB's Pannexin-1 topological sequence analysis.

```

-----> STRONGLY preferred model: N-terminus outside
4 strong transmembrane helices, total score : 8705
# from    to length score orientation
1    37    55 (19)    1691 o-i
2   108   127 (20)    2661 i-o
3   218   235 (18)    2355 o-i
4   268   296 (29)    1998 i-o

-----> alternative model
4 strong transmembrane helices, total score : 8687
# from    to length score orientation
1    37    54 (18)    1663 i-o
2   108   127 (20)    2337 o-i
3   218   235 (18)    2553 i-o
4   267   296 (30)    2134 o-i

```

Table 30.) TMPred's 'alternative model' with all satisfactory scores of over 500 each corroborates with below UniProtKB's Pannexin-1 algorithmic topological transmembrane positioning.⁵¹

Topology					
Feature key	Position(s)	Description	Actions	Graphical view	Length
Topological domain ⁱ	1 – 40	Cytoplasmic Sequence analysis	Add BLAST		40
Transmembrane ⁱ	41 – 61	Helical PROSITE-ProRule annotation	Add BLAST		21
Topological domain ⁱ	62 – 106	Extracellular Sequence analysis	Add BLAST		45
Transmembrane ⁱ	107 – 127	Helical PROSITE-ProRule annotation	Add BLAST		21
Topological domain ⁱ	128 – 217	Cytoplasmic Sequence analysis	Add BLAST		90
Transmembrane ⁱ	218 – 238	Helical PROSITE-ProRule annotation	Add BLAST		21
Topological domain ⁱ	239 – 266	Extracellular Sequence analysis	Add BLAST		28
Transmembrane ⁱ	267 – 287	Helical PROSITE-ProRule annotation	Add BLAST		21
Topological domain ⁱ	288 – 426	Cytoplasmic Sequence analysis	Add BLAST		139

Table 31.) UniProtKB's Pannexin-1 sequence analysis topology coincides considerably with TMPred's prediction above i.e. oriented N and C termini inside, transmembrane regions and respective extracellular-cytoplasmic residue domains.¹¹⁰

4.3.1.2 Connexin26

Prediction parameters:

TM-helix length between 14 and 35

TMPRED.10830.6871.seq³⁷

```

-----> STRONGLY preferred model: N-terminus inside
4 strong transmembrane helices, total score : 7249
# from    to length score orientation
1    23    39 (17)    1877 i-o
2    76    96 (21)    1897 o-i
3   130   158 (29)    1218 i-o
4   190   215 (26)    2257 o-i

```

Table 32.) TMPred's Connexin26 STRONGLY preferred model similarly displays oriented cytosolic N and T termini, respective topological domains and lengths and transmembrane positioning as Pannexin-1.⁷⁷

Topology

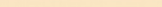




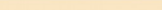




Feature key	Position(s)	Description	Actions	Graphical view	Length
Intramembrane ⁱ	2 – 13	1 Publication	Add BLAST		12
Topological domain ⁱ	14 – 20	Cytoplasmic 1 Publication			7
Transmembrane ⁱ	21 – 40	Helical 1 Publication	Add BLAST		20
Topological domain ⁱ	41 – 73	Extracellular 1 Publication	Add BLAST		33
Transmembrane ⁱ	74 – 94	Helical 1 Publication	Add BLAST		21
Topological domain ⁱ	95 – 135	Cytoplasmic 1 Publication	Add BLAST		41
Transmembrane ⁱ	136 – 156	Helical 1 Publication	Add BLAST		21
Topological domain ⁱ	157 – 189	Extracellular 1 Publication	Add BLAST		33
Transmembrane ⁱ	190 – 210	Helical 1 Publication	Add BLAST		21
Topological domain ⁱ	211 – 226	Cytoplasmic 1 Publication	Add BLAST		16

Table 33.) UniProtKB's Connexin26 transmembrane helices via mutational studies, topological lengths and termini cytosolic orientation correlate to TMPred's Connexin26.¹²⁹

4.3.2 TMHMM Topology Prediction

4.3.2.1 Pannexin-1

TMHMM transmembrane prediction results strongly demonstrating positive results of a TM protein via i.), an oriented cytosolic N-terminal via iii.) and topological and transmembrane spanning regions similar to UniProtKB's Pannexin-1 sequence positioning analysis in Table 31.) above.

i.) line 3.) Exp number of AAs in THMs: 90.50832, any resulting number > 18 very likely predicts a transmembrane protein (or signal peptide).

ii.) line 4.) Exp number, first 60 AAs: 20.66294, is the expected number of amino acids in transmembrane helices in the first 60 amino acids of the complete protein, any number > 3 warns of the N-term being a signal-peptide.

iii.) line 5.) Total prob of N-in: 0.96649, probability that the N-terminal is on the inside of the membrane. In the Pannexin-1 case, this ~97% value agrees with former topological algorithm predictor TMPred's positioning of the N terminal placed in the cytosol.⁵⁰

```
# pannexin-1 Length: 426
# pannexin-1 Number of predicted TMHs: 4
# pannexin-1 Exp number of AAs in TMHs: 90.50832
# pannexin-1 Exp number, first 60 AAs: 20.66294
# pannexin-1 Total prob of N-in: 0.96649
# pannexin-1 POSSIBLE N-term signal sequence
pannexin-1    TMHMM2.0    inside    1    37
pannexin-1    TMHMM2.0    TMhelix   38    60
pannexin-1    TMHMM2.0    outside   61   107
pannexin-1    TMHMM2.0    TMhelix  108   130
pannexin-1    TMHMM2.0    inside   131   212
pannexin-1    TMHMM2.0    TMhelix  213   235
pannexin-1    TMHMM2.0    outside  236   274
pannexin-1    TMHMM2.0    TMhelix  275   297
pannexin-1    TMHMM2.0    inside   298   426
```

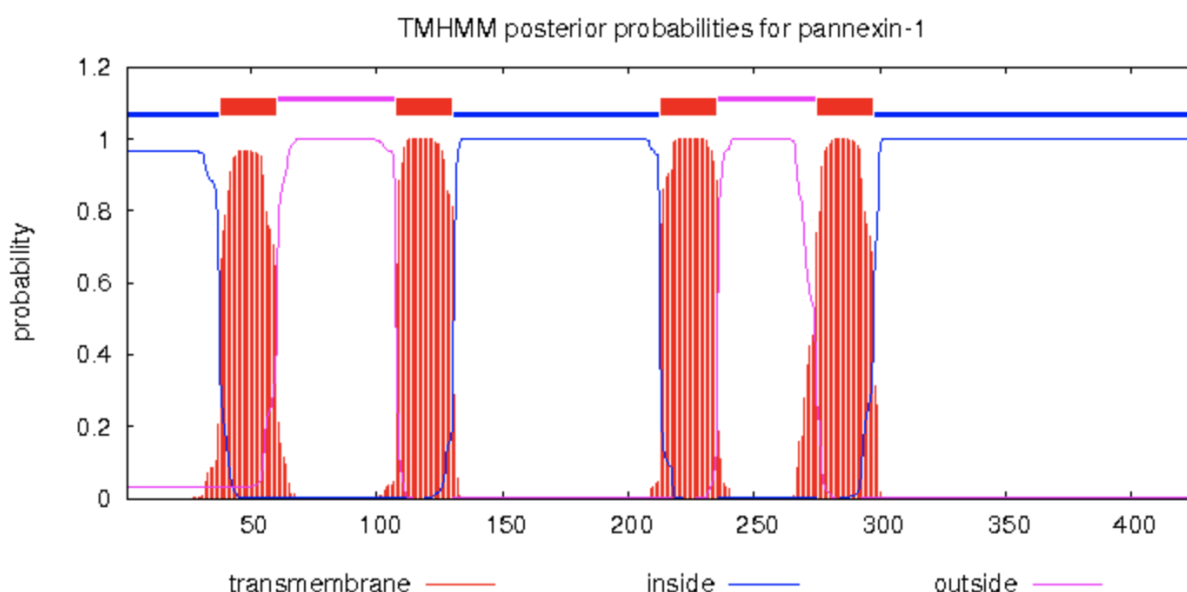


Table 34.) TMHMM topological and transmembrane probabilities similarly corroborating with TMPred's and UniProtKB's Pannexin-1 sequence analysis positioning.³⁶

4.3.2.2 Connexin26

- i.) line 3.) Exp number of AAs in THMs: 87.6082, any resulting number > 18 very likely predicts a transmembrane protein (or signal peptide) as Pannexin-1.
- iii.) line 5.) Total prob of N-in: 0.99323, probability that the N-term is on the inside of the membrane similar to Pannexin-1.⁵⁰

TMHMM result

[HELP](#) with output formats

```
# 2ZW3:A|PDBID|CHAIN|SEQUENCE Length: 226
# 2ZW3:A|PDBID|CHAIN|SEQUENCE Number of predicted TMHs: 4
# 2ZW3:A|PDBID|CHAIN|SEQUENCE Exp number of AAs in TMHs: 87.6082
# 2ZW3:A|PDBID|CHAIN|SEQUENCE Exp number, first 60 AAs: 20.00686
# 2ZW3:A|PDBID|CHAIN|SEQUENCE Total prob of N-in: 0.99323
# 2ZW3:A|PDBID|CHAIN|SEQUENCE POSSIBLE N-term signal sequence
2ZW3:A|PDBID|CHAIN|SEQUENCE TMHMM2.0 inside 1 20
2ZW3:A|PDBID|CHAIN|SEQUENCE TMHMM2.0 TMhelix 21 40
2ZW3:A|PDBID|CHAIN|SEQUENCE TMHMM2.0 outside 41 75
2ZW3:A|PDBID|CHAIN|SEQUENCE TMHMM2.0 TMhelix 76 98
2ZW3:A|PDBID|CHAIN|SEQUENCE TMHMM2.0 inside 99 131
2ZW3:A|PDBID|CHAIN|SEQUENCE TMHMM2.0 TMhelix 132 154
2ZW3:A|PDBID|CHAIN|SEQUENCE TMHMM2.0 outside 155 192
2ZW3:A|PDBID|CHAIN|SEQUENCE TMHMM2.0 TMhelix 193 215
2ZW3:A|PDBID|CHAIN|SEQUENCE TMHMM2.0 inside 216 226
```

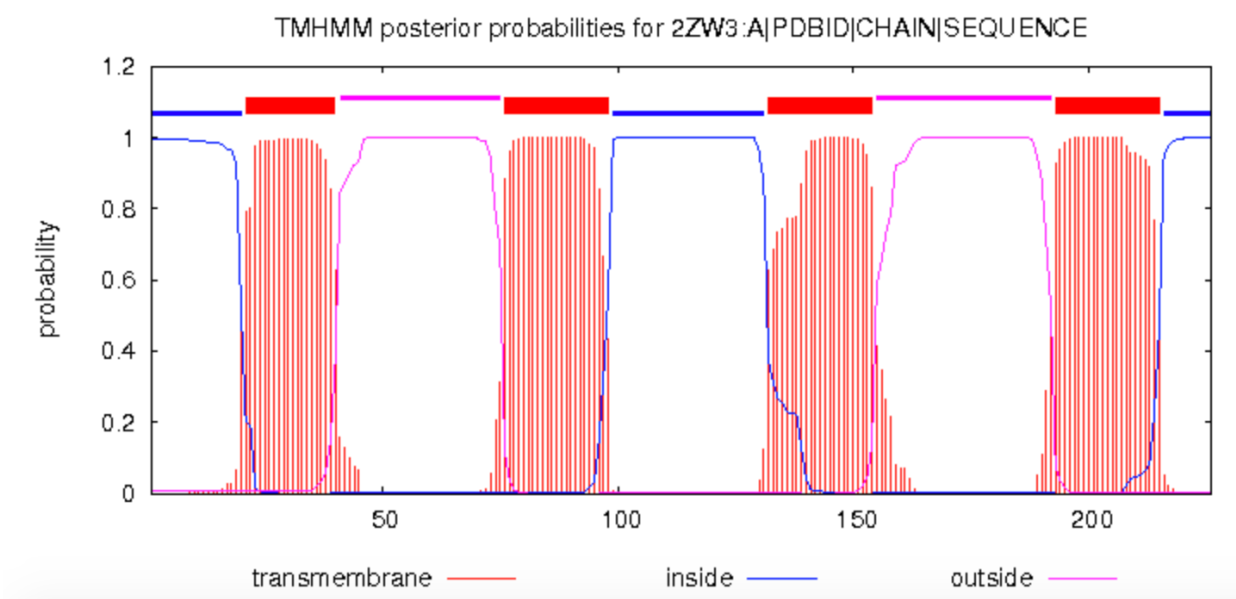


Table 35.) TMHMM's Connexin26 transmembrane and topological domain results are identical to UnitProKB's Connexin26 in Table 33.) and very similar to TMPred's Connexin26.³⁶

4.3.3 SOSUI Topology Prediction

4.3.3.1 Pannexin-1

SOSUI Result

Query title : None

Total length : 426 A. A.

Average of hydrophobicity : 0.203521

**This amino acid sequence is of a MEMBRANE PROTEIN
which have 4 transmembrane helices.**

No.	N terminal	transmembrane region	C terminal	type	length
1	38	VTCTAVGLPLLLISLAFQEISI	60	PRIMARY	23
2	106	HKFFPYILLFALLYLPLFWR	128	PRIMARY	23
3	210	IIKYISCRLLTLIIILLACIYLG	232	PRIMARY	23
4	270	VGIFQLLSVINLVVYVLLAPVVV	292	PRIMARY	23

Table 36.) SOSUI's Pannexin-1 hydrophobicity prediction displays four suggested ordered transmembrane regions corroborating very closely to UnitProtKB's, TMPred's and TMHMM's Pannexin-1 transmembrane sequence positioning.⁴³

4.3.3.2 Connexin26

SOSUI Result

Query title : None

Total length : 226 A. A.

Average of hydrophobicity : 0.288053

**This amino acid sequence is of a MEMBRANE PROTEIN
which have 4 transmembrane helices.**

No.	N terminal	transmembrane region	C terminal	type	length
1	20	IGKIWLTVLFIFRIMILVAAKE	42	PRIMARY	23
2	71	ISHIRLWALQLIFVSTPALLVAM	93	SECONDARY	23
3	139	SIFFRVIFEAAFMYVFYVMDGF	161	PRIMARY	23
4	193	VFMAVSGICILLNVTELCYLLI	215	PRIMARY	23

Table 37.) SOSUI's Connexin26 transmembrane positioning results agree with TMHMM's, UnitProtKB's and TMPred's Connexin26 sequence positioning.⁸⁸

4.3.4 RaptorX Topology Prediction

4.3.4.1 Pannexin-1

RaptorX's method results confirmed the existence of coils in Pannexin-1's front and back tails and a loop domain.

Section III. Detailed Prediction Results (you can see each result entry by clicking on it)

[-] Click to view the predicted structure property for the whole sequence

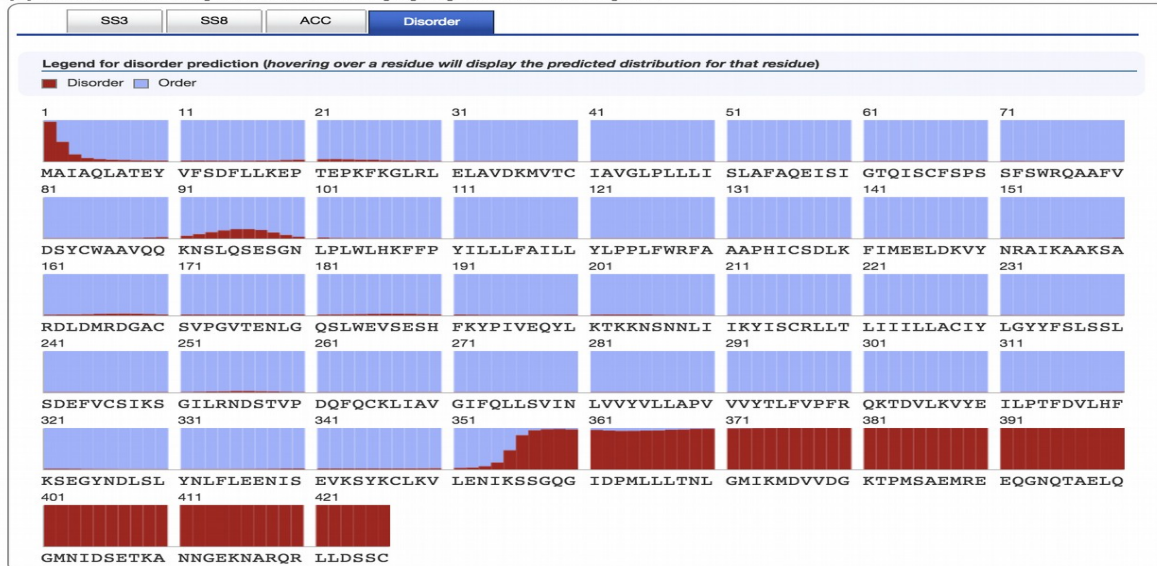


Table 38.) RaptorX prediction suggests disorderly regions in Pannexin-1 front and back tails and topological residues 90-100 inferring coil and loop presence respectively.⁴²

[-] Click to view the predicted structure property for the whole sequence

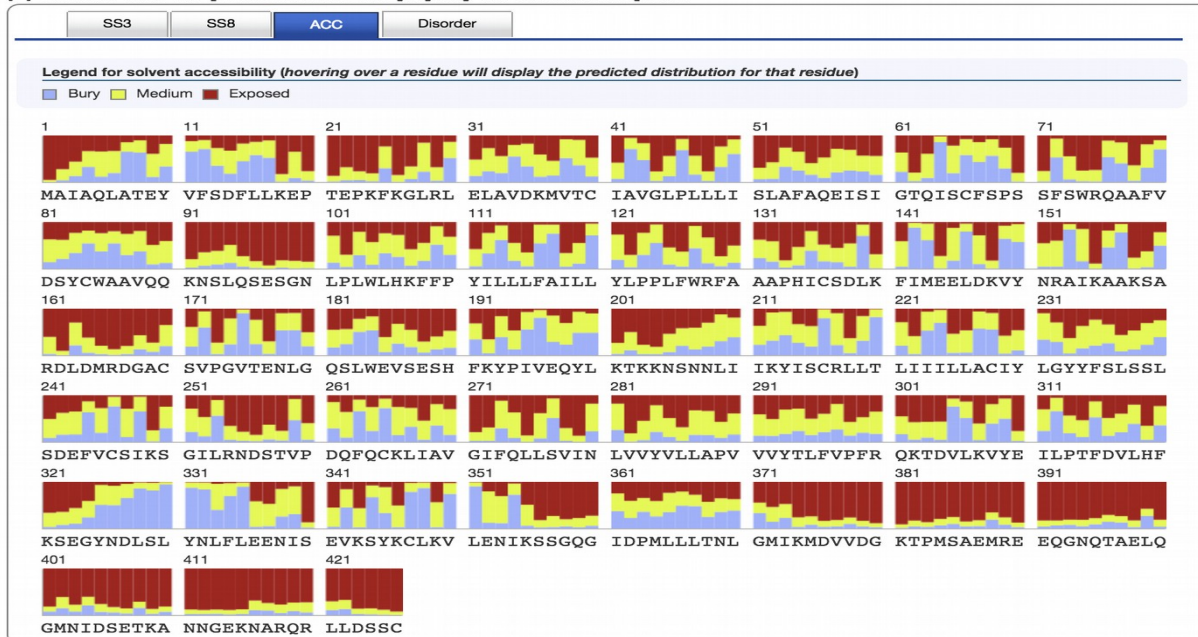


Table 39.) Further RaptorX’s strong inference of Pannexin-1 front and back tail coils and a loop region (residues 90-100) respectively via solvent exposure prediction.⁴²

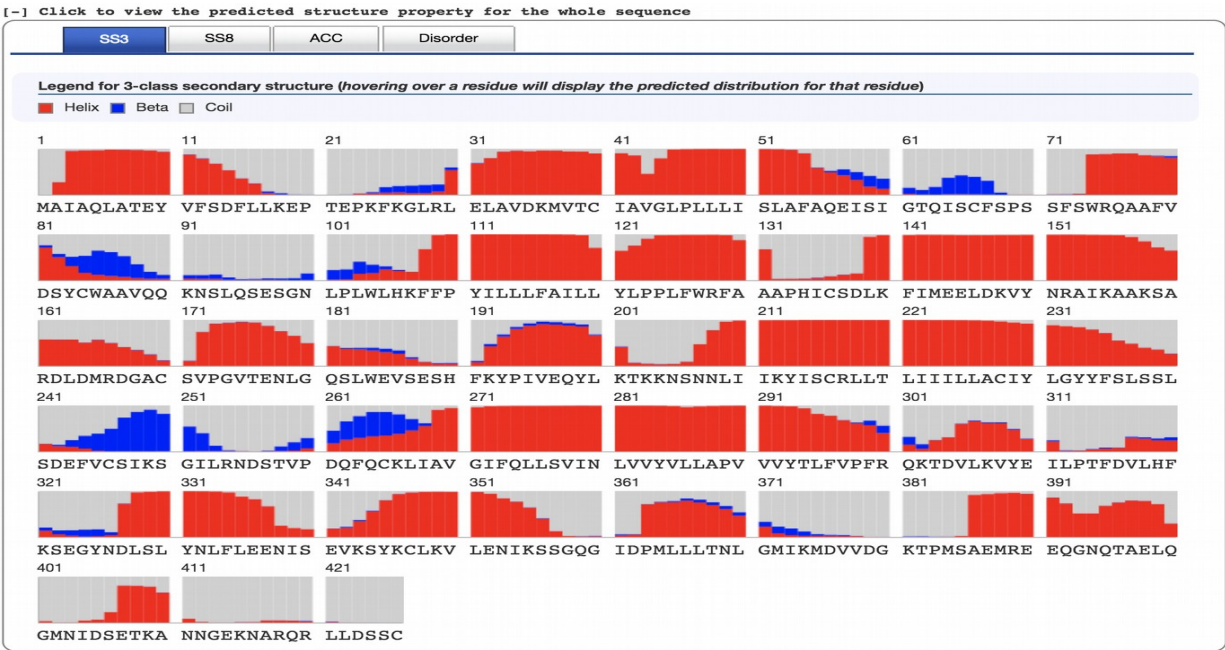


Table 40.) RaptorX 3-class secondary structural output confirming Pannexin-1 disorderly solvent exposed front and back tail coils and topological loop (residues 57-106).⁴²

4.3.4.2 Connexin26

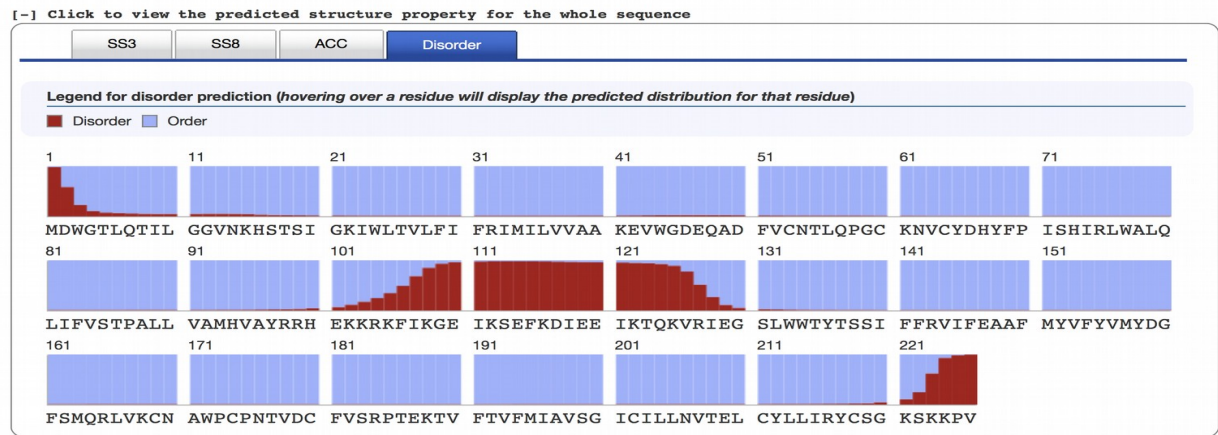


Table 41.) RaptorX prediction suggests disorderly regions in Connexin26 front and back tails (similar to Pannexin-1 coils) and first intracellular loop region (residues ~100-130); confirming TMPred’s, UniProtKB’s, TMHMM’s and SOSUI’s Connexin26 topological algorithms and exhibiting symmetry to RaptorX’s Pannexin-1 loop presence in its first intracellular domain.⁸⁹



Table 42.) RaptorX's strong inference of Connexin26 front and short back tails (similar to Pannexin-1 coils) and first intracellular topological loop region (residues ~100-130) via solvent exposure prediction.⁸⁹



Table 43.) RaptorX 3-class Connexin26 secondary structural output confirming disorderly solvent exposed front and short back tail coils and first intracellular topological loop region (residues ~100-130).⁸⁹

4.3.5 Phyre² Topology Prediction

4.3.5.1 Pannexin-1

Phyre²'s prediction of Pannexin-1 orientation and re-entrant helices agrees considerably with TMPred's, UnitProtKB's, TMHMM's and SOSUI's.

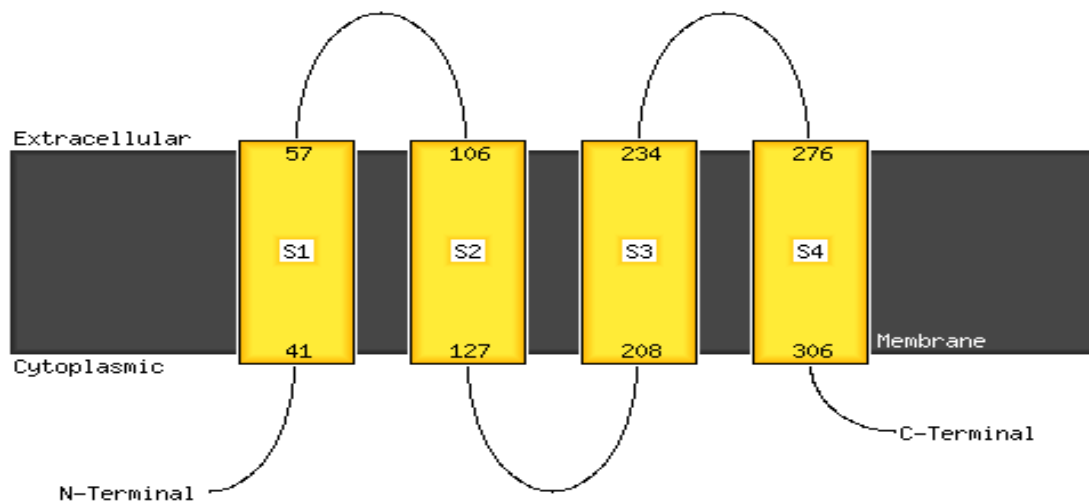


Figure 18.) Phyre² Pannexin-1 transmembrane helices topology prediction.¹¹²

4.3.5.2 Connexin26

Phyre² prediction exhibiting 4-transmembrane areas, two-cytosolic oriented tails and similar transmembrane residue lengths as Pannexin-1. Phyre² exhibits similar transmembrane residue positions as TMPred's, UnitProtKB's, TMHMM's and SOSUI's Connexin26.

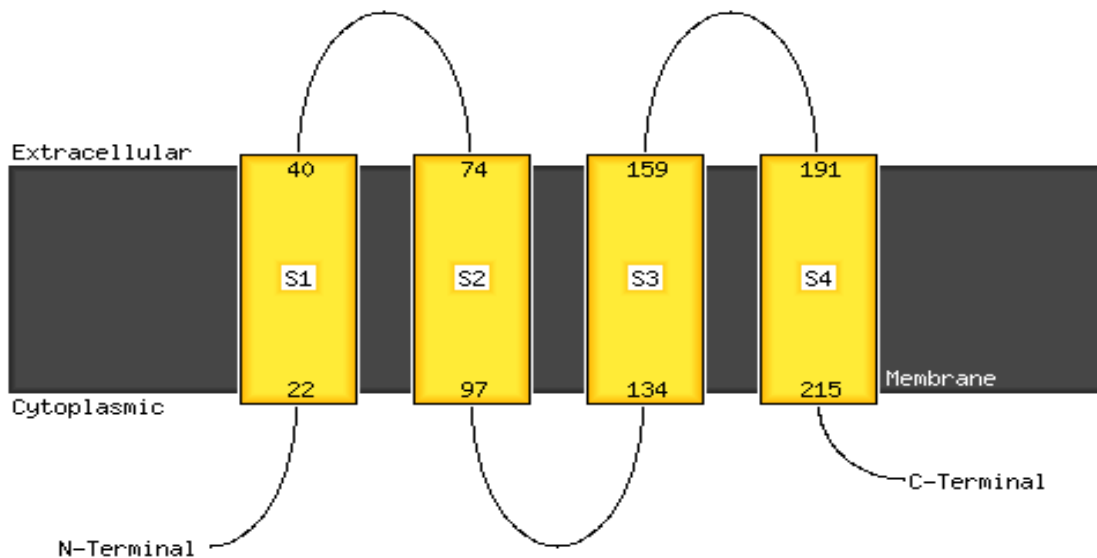


Figure 19.) Phyre²'s Connexin26 transmembrane helices topology prediction.⁸⁷

4.3.6 Topology Consensus

Table 44.) Below is a topological consensus summarizing Pannexin-1 and Connexin26 orientation and positioning agreements amongst themselves and each other via the former topology determining algorithms. (I-O and O-I is inside to outside and outside to inside cell respectively.)

i.) First Cytoplasmic/Topological 'In' N-Terminal Tail Region:

1	Algorithm	TM Region	Feature	From	To	Length	Direction	Protein
2	UniProtKB	N-terminal	Cytoplasmic	1	40	40	I	Pannexin-1
3	TMPred	N-terminal	Cytoplasmic	1	36	36	I	Pannexin-1
4	TMHMM	N-terminal	Cytoplasmic	1	37	37	I	Pannexin-1
5	SOSUI	N-terminal	Cytoplasmic	1	37	37	N/A	Pannexin-1
6	Phyre²	N-terminal	Cytoplasmic	1	40	40	I	Pannexin-1
7	UniProtKB	N-terminal	Cytoplasmic	1	20	20	I	Connexin-26
8	TMPred	N-terminal	Cytoplasmic	1	22	22	I	Connexin-26
9	TMHMM	N-terminal	Cytoplasmic	1	20	20	I	Connexin-26
10	SOSUI	N-terminal	Cytoplasmic	1	19	19	N/A	Connexin-26
11	Phyre²	N-terminal	Cytoplasmic	1	21	21	I	Connexin-26

ii.) First Helix Transmembrane Region, First Extracellular Second Topological Region and Second Helix Transmembrane Region respectively:

12								
13	UniProtKB	1	Helical	41	61	21	I-O	Pannexin-1
14	TMPred	1	Helical	37	54	18	I-O	Pannexin-1
15	TMHMM	1	Helical	38	60	23	I-O	Pannexin-1
16	SOSUI	1	Helical	38	60	23	N/A	Pannexin-1
17	Phyre²	1	Helical	41	57	17	I-O	Pannexin-1
18	UniProtKB	1	Helical	21	40	20	I-O	Connexin-26
19	TMPred	1	Helical	23	39	17	I-O	Connexin-26
20	TMHMM	1	Helical	21	40	20	I-O	Connexin-26
21	SOSUI	1	Helical	20	42	23	N/A	Connexin-26
22	Phyre²	1	Helical	22	40	19	I-O	Connexin-26
23								
24	UniProtKB	Topological	Extracellular	62	106	45	O	Pannexin-1
25	TMPred	Topological	Extracellular	55	107	53	O	Pannexin-1
26	TMHMM	Topological	Extracellular	61	107	47	O	Pannexin-1
27	SOSUI	Topological	Extracellular	61	105	45	N/A	Pannexin-1
28	Phyre²	Topological	Extracellular	58	105	48	O	Pannexin-1
29	UniProtKB	Topological	Extracellular	41	75	35	O	Connexin-26
30	TMPred	Topological	Extracellular	40	75	36	O	Connexin-26
31	TMHMM	Topological	Extracellular	41	75	35	O	Connexin-26
32	SOSUI	Topological	Extracellular	43	70	28	N/A	Connexin-26
33	Phyre²	Topological	Extracellular	41	73	33	O	Connexin-26

34								
35	UniProtKB	2	Helical	107	127	21	O-I	Pannexin-1
36	TMPred	2	Helical	108	127	20	O-I	Pannexin-1
37	TMHMM	2	Helical	108	130	23	O-I	Pannexin-1
38	SOSUI	2	Helical	106	128	23	N/A	Pannexin-1
39	Phyre²	2	Helical	106	127	22	O-I	Pannexin-1
40	UniProtKB	2	Helical	76	98	23	O-I	Connexin-26
41	TMPred	2	Helical	76	96	21	O-I	Connexin-26
42	TMHMM	2	Helical	76	98	23	O-I	Connexin-26
43	SOSUI	2	Helical	71	93	23	N/A	Connexin-26
44	Phyre²	2	Helical	74	97	24	O-I	Connexin-26

iii.) Second Cytoplasmic

45								
46	UniProtKB	Topological	Cytoplasmic	128	217	90	I	Pannexin-1
47	TMPred	Topological	Cytoplasmic	128	217	90	I	Pannexin-1
48	TMHMM	Topological	Cytoplasmic	131	212	82	I	Pannexin-1
49	SOSUI	Topological	Cytoplasmic	129	209	81	N/A	Pannexin-1
50	Phyre²	Topological	Cytoplasmic	128	207	80	I	Pannexin-1
51	UniProtKB	Topological	Cytoplasmic	99	131	33	I	Connexin-26
52	TMPred	Topological	Cytoplasmic	97	129	33	I	Connexin-26
53	TMHMM	Topological	Cytoplasmic	99	131	33	I	Connexin-26
54	SOSUI	Topological	Cytoplasmic	94	138	45	N/A	Connexin-26
55	Phyre²	Topological	Cytoplasmic	98	133	36	I	Connexin-26

iv.) Third Helix Transmembrane Region, Second Extracellular Fourth Topological Region and Fourth Helix Transmembrane Region respectively:

56								
57	UniProtKB	3	Helical	218	238	21	I-O	Pannexin-1
58	TMPred	3	Helical	218	235	18	I-O	Pannexin-1
59	TMHMM	3	Helical	213	235	23	I-O	Pannexin-1
60	SOSUI	3	Helical	210	232	23	N/A	Pannexin-1
61	Phyre²	3	Helical	208	234	27	I-O	Pannexin-1
62	UniProtKB	3	Helical	132	154	23	I-O	Connexin-26
63	TMPred	3	Helical	130	158	29	I-O	Connexin-26
64	TMHMM	3	Helical	132	154	23	I-O	Connexin-26
65	SOSUI	3	Helical	139	161	23	N/A	Connexin-26
66	Phyre²	3	Helical	134	159	26	I-O	Connexin-26
67								
68	UniProtKB	Topological	Extracellular	239	266	28	O	Pannexin-1
69	TMPred	Topological	Extracellular	236	266	31	O	Pannexin-1
70	TMHMM	Topological	Extracellular	236	274	39	O	Pannexin-1
71	SOSUI	Topological	Extracellular	233	269	37	N/A	Pannexin-1
72	Phyre²	Topological	Extracellular	235	275	41	O	Pannexin-1
73	UniProtKB	Topological	Extracellular	155	192	38	O	Connexin-26
74	TMPred	Topological	Extracellular	159	189	31	O	Connexin-26
75	TMHMM	Topological	Extracellular	155	192	38	O	Connexin-26
76	SOSUI	Topological	Extracellular	162	192	31	N/A	Connexin-26
77	Phyre²	Topological	Extracellular	160	190	31	O	Connexin-26

78								
79	UniProtKB	4	Helical	267	287	21	O-I	Pannexin-1
80	TMPred	4	Helical	267	296	30	O-I	Pannexin-1
81	TMHMM	4	Helical	275	297	23	O-I	Pannexin-1
82	SOSUI	4	Helical	270	292	23	N/A	Pannexin-1
83	Phyre ²	4	Helical	276	306	31	O-I	Pannexin-1
84	UniProtKB	4	Helical	193	215	23	O-I	Connexin-26
85	TMPred	4	Helical	190	215	26	O-I	Connexin-26
86	TMHMM	4	Helical	193	215	23	O-I	Connexin-26
87	SOSUI	4	Helical	193	215	23	N/A	Connexin-26
88	Phyre ²	4	Helical	191	215	25	O-I	Connexin-26

v.) Final Cytoplasmic/Topological C-Terminal Tail Region:

89								
90	UniProtKB	T-Terminal	Cytoplasmic	288	426	139	I	Pannexin-1
91	TMPred	T-Terminal	Cytoplasmic	297	426	130	I	Pannexin-1
92	TMHMM	T-Terminal	Cytoplasmic	298	426	129	I	Pannexin-1
93	SOSUI	T-Terminal	Cytoplasmic	293	426	134	N/A	Pannexin-1
94	Phyre ²	T-Terminal	Cytoplasmic	307	426	120	I	Pannexin-1
95	UniProtKB	T-Terminal	Cytoplasmic	216	226	11	I	Connexin-26
96	TMPred	T-Terminal	Cytoplasmic	216	226	10	I	Connexin-26
97	TMHMM	T-Terminal	Cytoplasmic	216	226	11	I	Connexin-26
98	SOSUI	T-Terminal	Cytoplasmic	216	226	11	N/A	Connexin-26
99	Phyre ²	T-Terminal	Cytoplasmic	216	226	11	I	Connexin-26

4.3.7 Structural Threading Topology Consensus

The former and below structural threading positioning consensus together were used to build a Pannexin-1-Connexin26 alignment exhibiting accurate re-entrant membrane residue positioning to be used towards building a re-entrant residue accurate final multiple template alignment.

```

ALPHAHELIX
TRANSMEMBRANEHELIX
BETAstrand
BEND
TURN
UNCRYSTALLIZED_TEMPLATE

PANNEXIN 1 (1) MAIAQLATEYVFSDFLLEKEPTEPKFKGLRLELAVDKMVTCTIAVGLPLLLI (50)
PHYRE2          MAIAQLATEYVFSDFLLEKEPTEPKFKGLRLELAVDKMVTCTIAVGLPLLLI
PROMALS3D       MAIAQLATEYVFSDFLLEKEPTEPKFKGLRLELAVDKMVTCTIAVGLPLLLI
RAPTORX         MAIAQLATEYVFSDFLLEKEPTEPKFKGLRLELAVDKMVTCTIAVGLPLLLI
UniProt (TM_1)  IAVGLPLLLI

CONNEXIN-26     MDWGTLTQTILGGVKNKHSTSIGKIWLTVLFIFRIMILVVAKEVWGDEQAD
UniProt (TM_1)  GKIWLTVLFIFRIMILVVA

PANNEXIN 1 (51) SLAFAQEISIGTQISCFSPSSFSWRQAAAFVDSYCWAAVQQKNSLQSESGN (100)
PHYRE2          SLAFAQEISIGTQISCFSPSSFSWRQAAAFVDSYCWAAVQQKNSLQSESGN
PROMALS3D       SLAFAQEISIGTQISCFSPSSFSWRQAAAFVDSYCWAAVQQKNSLQSESGN
RAPTORX         SLAFAQEISIGTQISCFSPSSFSWRQAAAFVDSYCWAAVQQKNSLQSESGN
UniProt (TM_1)  SLAFAQEISIG

CONNEXIN-26     FVCNTLQPGCKNVCYDHYFPISHIRLWALQLIFVSTPALLVAMHVAYRRH
UniProt (TM_2)  LWALQLIFVSTPALLVAMHVAYR

PANNEXIN1 (101) LPLWLHKFFPYILLFFAILLYLPPLFWRFRAAAPHICSDLKFIMEELDKVY (150)
PHYRE2          LPLWLHKFFPYILLFFAILLYLPPLFWRFRAAAPHICSDLKFIMEELDKVY
PROMALS3D       LPLWLHKFFPYILLFFAILLYLPPLFWRFRAAAPHICSDLKFIMEELDKVY
RAPTORX         LPLWLHKFFPYILLFFAILLYLPPLFWRFRAAAPHICSDLKFIMEELDKVY
UniProt (TM_2)  KFFPYILLFFAILLYLPPLFW

CONNEXIN-26     EKKRKFKIKGEIKSEFKDIEEIKTQKVRIEGSLWWTYTSSIFFRVIFEAAF
UniProt (TM_3)  LWWTYTSSIFFRVIFEAAF

```

```

PANNEGIN1 (151) NRAIKAAKSARDLDMRDGACSVPGVTENLGQSLWEVSESHFKYPIVEQYL (200)
PHYRE2          NRAIKAAKSARDLDMRDGACSVPGVTENLGQSLWEVSESHFKYPIVEQYL
PROMALS3D       NRAIKAAKSARDLDMRDGACSVPGVTENLGQSLWEVSESHFKYPIVEQYL
RAPTORX         NRAIKAAKSARDLDMRDGACSVPGVTENLGQSLWEVSESHFKYPIVEQYL

CONNEXIN-26     MYVFYVMDGFSMQRLVKCNAPCPNTVDCFVSRPTEKTVFTVFMIASG
UniProt(TM_3)   MYVF                               UniProt(TM_4) VFMIASG

PANNEGIN1 (201) KTKKNSNNLIKYISCRLLTLIIILLACIYLGYYFSLSSLSDEFVCSIKS (250)
PHYRE2          KTKKNSNNLIKYISCRLLTLIIILLACIYLGYYFSLSSLSDEFVCSIKS
PROMALS3D       KTKKNSNNLIKYISCRLLTLIIILLACIYLGYYFSLSSLSDEFVCSIKS
RAPTORX         KTKKNSNNLIKYISCRLLTLIIILLACIYLGYYFSLSSLSDEFVCSIKS
UniProt(TM_3)   LTLIIILLACIYLGYYFSLSSLS

CONNEXIN-26     ICILLNVTELCYLLIRYCSGKSKKPV
UniProt(TM_4)   ICILLNVTELCYLLI

PANNEGIN1 (251) GILRNDSTVPDQFQCKLIAVGIFQLLSVINLVVYVLLAPVVVYTLFVPFR (300)
PHYRE2          GILRNDSTVPDQFQCKLIAVGIFQLLSVINLVVYVLLAPVVVYTLFVPFR
PROMALS3D       GILRNDSTVPDQFQCKLIAVGIFQLLSVINLVVYVLLAPVVVYTLFVPFR
RAPTORX         GILRNDSTVPDQFQCKLIAVGIFQLLSVINLVVYVLLAPVVVYTLFVPFR
UniProt(TM_4)   LIAVGIFQLLSVINLVVYVLL

PANNEGIN1 (301) QKTDVLKVYEILPTFDVLHFKSEGYNDLSLYNLFLEENISEVKSYSKCLKV (350)
PHYRE2          QKTDVLKVYEILPTFDVLHFKSEGYNDLSLYNLFLEENISEVKSYSKCLKV
PROMALS3D       QKTDVLKVYEILPTFDVLHFKSEGYNDLSLYNLFLEENISEVKSYSKCLKV
RAPTORX         QKTDVLKVYEILPTFDVLHFKSEGYNDLSLYNLFLEENISEVKSYSKCLKV

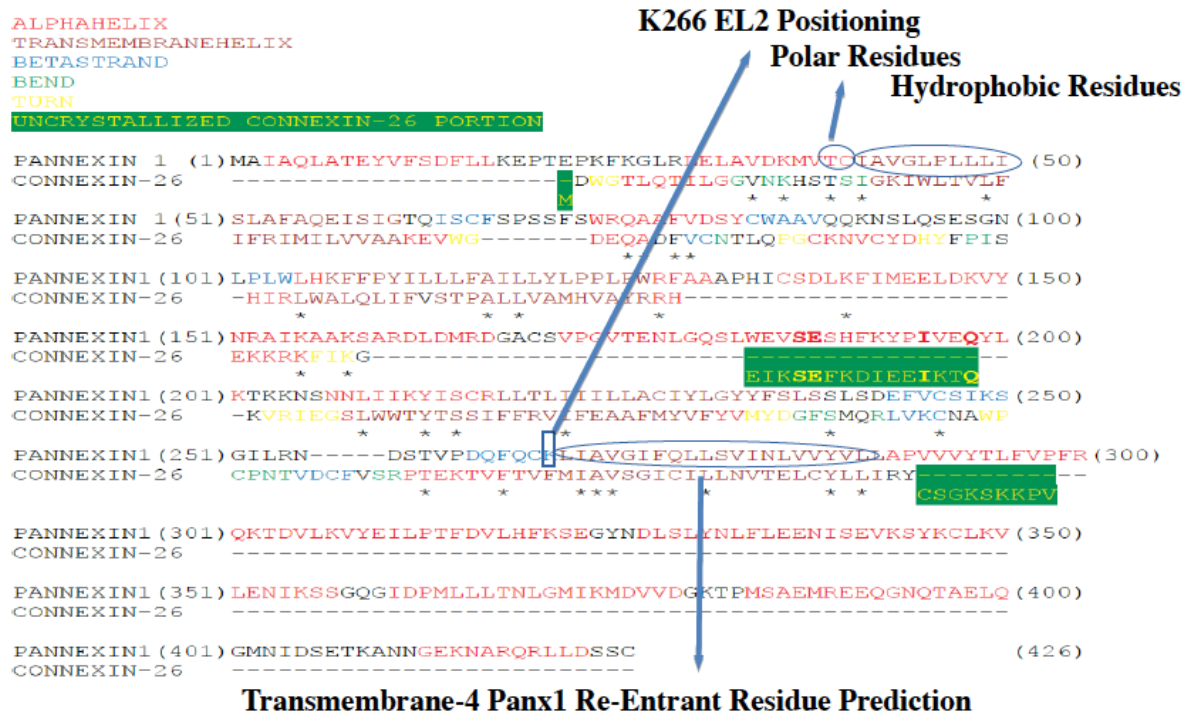
PANNEGIN1 (351) LENIKSSGQGIDPMLLLTNLGMKMDVVDGKTPMSAEMREEQGNQTAEIQ (400)
PHYRE2          LENIKSSGQGIDPMLLLTNLGMKMDVVDGKTPMSAEMREEQGNQTAEIQ
PROMALS3D       LENIKSSGQGIDPMLLLTNLGMKMDVVDGKTPMSAEMREEQGNQTAEIQ
RAPTORX         LENIKSSGQGIDPMLLLTNLGMKMDVVDGKTPMSAEMREEQGNQTAEIQ

PANNEGIN1 (401) GMNIDSETKANNGEKNARQRLDSSC (426)
PHYRE2          GMNIDSETKANNGEKNARQRLDSSC
PROMALS3D       GMNIDSETKANNGEKNARQRLDSSC
RAPTORX         GMNIDSETKANNGEKNARQRLDSSC

```

Table 45.) Above a Topology Consensus Alignment of Pannexin-1 and Connexin26 exhibiting transmembrane helices positioning via ss methods, CONNEXIN-26 PDB crystallized data and UniProt experimental transmembrane positioning.^{110, 105, 106}

Table 46.) A re-entrant helices alignment with slight residue adjustments amongst the Pannexin-1-Connexin26 topological relatives exploiting threading/ss and transmembrane positioning consensus. Note all four transmembrane regions exhibit zero gaps and align via default all intra-extracellular domains. TMs express high hydrophobic residue %s with hydrophobic central peak residues and amphipathic W interface residues, loops and coils exhibit charged and polar residues. Residue constraints are maintained eg. residue K266 pivotal towards chemical blocker interactions properly topologically exhibited in the EL2 domain not TM4 precluding an Innexin6 4th TM residue misalignment. Similarly pivotal polar residues 39T and 40C are properly aligned to a non-membraneous TM1 conserving 40C action as a channel closer.



4.3.8 Innexin6 Topology

Innexin6 below exhibiting four spanning transmembranes with respective positions.

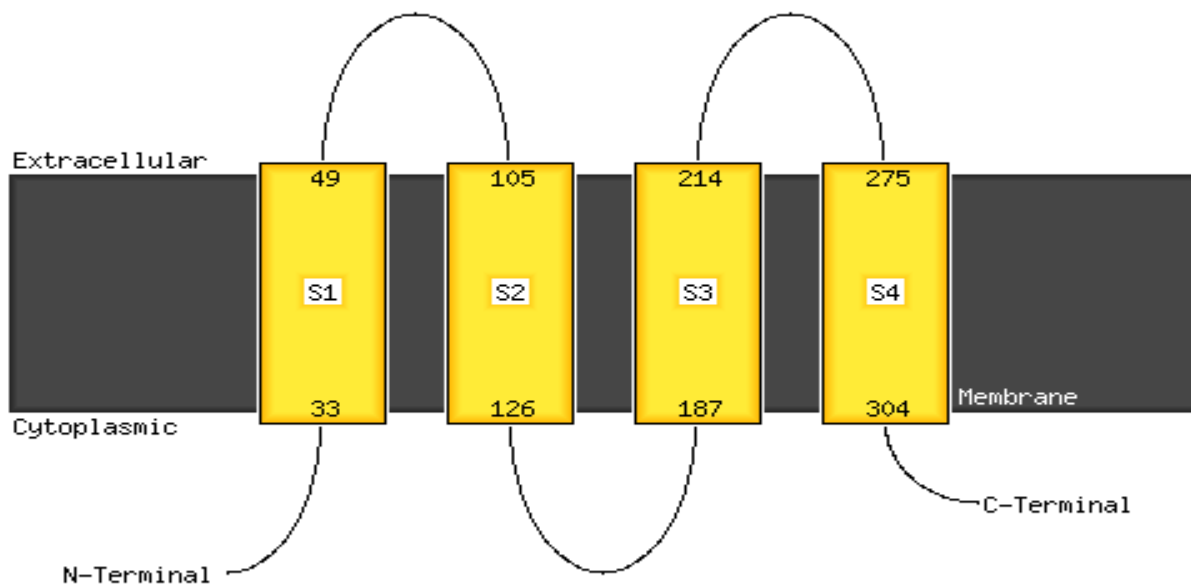


Figure 20.) Phyre2 Innexin6 transmembrane topology helix prediction in accordance with below Innexin6 UniProtKB sequence analysis.⁸²





















Topology						
Feature key	Position(s)	Description	Actions		Graphical view	Length
Transmembrane ⁱ	36 – 56	Helical  PROSITE-ProRule annotation 	 Add	 BLAST		21
Transmembrane ⁱ	111 – 131	Helical  PROSITE-ProRule annotation 	 Add	 BLAST		21
Transmembrane ⁱ	190 – 210	Helical  PROSITE-ProRule annotation 	 Add	 BLAST		21
Transmembrane ⁱ	276 – 296	Helical  PROSITE-ProRule annotation 	 Add	 BLAST		21

Table 47.) UniProtKB’s Innexin6 positions via algorithmic sequence analysis.¹¹⁶

4.4 Pannexin-1 Multiple Template Alignments

Two multiple template alnfiles generated for MODELLER input.

4.4.1 Multiple Template/Target Alignment File

```
>P1;5h1q
structureX:5h1q: 7 :A:369 :A:::-1.00:-1.00
-----AINSVN-----ALISRVFVQPK
GD--LADRLNSRVTVVILAVSSALLSSHF--DPITCWTPAQFNAQWVNFVNQYCFVHGT
YFVP--L--DQQLAFEEEE--RTKVSIIQYQWVPYVFALQALFYIPRFIWK
MIAYSGYDLAAAVKYVDRFWSNRDGD--DKFKTRL-----AAFEGRPVYIWDG
IRLARKKRSRNMALFYTLSTVWQAVNAWIQFYILTQLLDSSIIYTLWGSPSILGDL
-----QGNDWQTTGHFPRIV-----HCDNF
RRRPAS-----VQLDVLVCV-----LTLNIIYYEKLFIPLFWFLV
FVAVSTVNCFKWIYY--LCN--KTKAQKTIKNYLSAPIKSTISDDQF----FSALGEDGL
FIMDQMALNLGDIPAS-----YLTISMNRNICQDF-----
-----I-----
-----*

>P1;4uxf
structureX:4uxf: 893 :A:1289:A:::
-----
-----PSQFIRRDIAQTVNGSL-TLTQQTNLAPLVSSSTGEFGGSLAANRTFT
IRNTGAPTSI--VFEKG-----PASGANPAQSMISIRVWGNQFGGSDTTRST
VFEVGDDTSHHFYSQRN-----KDGNIAFNNGTVMPIINASGLMNVNG--TATFG
R-----SVTANGEFISKSANAFRAINDYG----F-FI--RNDA-SNTYFL-----
LTAAGDQTGGFNGLRPLLIN-----NQSG-----QITIG-EG
IIAKGVTINSGLTNSRIRSQGKTSIDLYTRAPT--SDTVGF-----WSIDIN--
-----DSATYNQFPGYFKMV-EKTNEVTGLPYLERGEVKSPTLTQFGNTLDSLY
QDWITYPTTPEARTTRWTRTWQKTKNSWSSFVQVFDGNGPPQ-----PSDIGALP
SDN---ATMGNTIIRDFLRIGNVRIVPDPVNKTVKFEWVE---*

>P1;5nxh
structureX:5nxh: 744 :A:1289:A:::
-----EANETORGTLRVATQVEAAAG-----T--LDNVLITPK
K---LLGKSTEAQEGVI--KVATQSEVTGTSTANTAVSPKNLKWIAQSEP---TWAATT
AIRGF--VKTSSGSITFVGNDTVGSTQDLELYEKNSYAVSPYELNR-VLANYLPLKAKAA
DTNL--LDGLDSSQFIRRDIAQTVNGSL-TLTQQTNLAPLVSSSTGEFGGSLAANRTFT
IRNTGAPTSI--VFEKG-----PASGANPAQSMISIRVWGNQFGGSDTTRST
VFEVGDDTSHHFYSQRN-----KDGNIAFNNGTVMPIINASGLMNVNG--TATFG
R-----SVTANGEFISKSANAFRAINDYG----F-FI--RNDA-SNTYFL-----
LTAAGDQTGGFNGLRPLLIN-----NQSG-----QITIG-EG
IIAKGVTINSGLTNSRIRSQGKTSIDLYTRAPT--SDTVGF-----WSIDIN--
-----DSATYNQFPGYFKMV-EKTNEVTGLPYLERGEVKSPTLTQFGNTLDSLY
QDWITYPTTPEARTTRWTRTWQKTKNSWSSFVQVFDGNGPPQ-----PSDIGALP
SDN---ATMGNTIIRDFLRIGNVRIVPDPVNKTVKFEWVE---*

>P1;3cjp
structureX:3cjp: 3 :A:264:A:::
-----LI-----IDGHTHVILPVEKHIMDEAGVDKT-----ILFSTS
I-----HPETAVNLR--D-----VKKEM-----
KKLNDVVNGKTNMIDVRR-NSIKELTNVIAQYPSRYVGFGN-----VPVGLSEN
DTNS--YI-----EENIVNNKL-----VG
IGELTPASGQ----IKSLK-----PI-FKYSMDSGSLPIWIHAFNPLVLQ---D
IKEIAEL-CKAFPKVP-----VILGHMGGSNWMTAVEL-----AKEIQNLYLD-TSAY-
-----FSTFV-----LKI-----
VI-NELPLKCIF--GT-----DMPFGDL
-----QLSIEA-----IKK-M--SND-----
-----SYVANA-VLGDNISR-----LL
N-----I-----*
-----*
```

```
>P1:1nzp  
structureX:1nzp:    242 :A:327:A:::  
  
-----  
  
-----  
  
-----  
  
-----  
  
-----AQ-----  
  
-----  
  
-----PS-SQKATNHNHHITEKLEVLAKAYSV  
QGDKWRALGYAKAINALKSFHKPV-TSYQEACSIPIGIGR-----MAEKII  
E-----  
  
-----TIESGHIRK-IDH-----*
```

```

>P1:Panx1
sequence:Panx1:1      : 426      :::::
-----MATAQLATEVVFSDFL-----LKEPTEP-----KFKGLRLLEAVDKMVTICIA
✓-----GLPLLLI-----SLAFAQEIS-----IGTKISCFSPSSFWRAQAFVDSYCAWAQV
QKNS-----LQSESNL-----PLWLHG-----FFPYILLLFAITLYLPLFWRF
AAA-----PHICSDLKFIMEELDKVYNRAIKAAKSARDL-----
-----D-----MRDGACSVPGV-----TE-----
-----NLGQSLWEVSESHFKYP-----
-----IVEQYLKTKKNSNNLI-----KYISCRLLTIILACIYLGYYS
LSSLDEFCVCSI-----KSGILRNDSTVPDQFQCKLIVAGFIQLLS-----VINLV-VYV
LLAPVVV-----YTFLFVP-----F-RQKTDVLKVYEITPT-FDVLHFKE-----
-----GYNDLSLYNLFLEENISEVKSCKLVLENIKSSG-----QGIDPML
LLT-----NLGMICKMDVVDGKTPMSAEMREFEQNGQTAELEGQMN
IDSETKANNGEKNAO-----RLLDSSC-----*

```

4.4.2 Single Template/Target Alignment File

94

```

>P1;4UXF
structureX:4UXF: 1127 :A:1254:A:: ::
-----
-----
-----
-----
-----QGTKTSDLYTRAPTSDTV
GFWSIDINDSATYNQFPGYFKMVEKTNEVTGLPYLERGEEVKSPG-----
-----PSDIGALPSD-----
-----*

>P1;4Y2C
structureX:4Y2C: 100 :A:147:A:::
-----
-----
-----
-----
-----EGMDPMDKNTSPGL
PYTTLGMRRTDVVDWETATLIPFAAERLEKMNNK-----
-----*

>P1;5H5P
structureX:5H5P: 482 :A:500:A:::
-----
-----
-----
-----
-----SETTANMRKKGKPN
PDQR-----*

>P1:Pannexin-1
sequence:Pannexin-1: : : : 0.00: 0.00
MAIAQLATEYVFSDFLKEPTEPKFKGLRLELAVDKMVTCTIAVGLPLLLISLAFQAEIS
IGTQISCFSPSSFWRQAAFVDSYCWAA----VQKNSLQSES---GNLPLWLHKFFPY
ILLFATLLYLPLFWRFAAAPHICSDLKFIMEELDKVYNRAIKAAS-ARDLDMRDGA
CSVPGVTENLGQSLWEVSESHFKYPIVEQYLKTKKNSNNLIKYISCRLLTLIIILLAC
IYLGYYFSLSSL-----SDEF----VCSIKSGILRNDSTVP-DQF
QC--KL-I-AVGIFQLLSVINLVVYVLLAPVVVYTLFVPFRQKTDVLKVYEILPTFDVL
HFKSEGYNDLSLYNLF-----LEENISEVKSYSKLVLENIKSSGQIDPM-----L
LLTNLGMIMDVVDGKT---PMSAEMREEQGNQTAEQGMNIDSETKANNGEKNAR--
--QRLLDSSC*

```

Table 49.) A 5-template result single alignment file designated ‘align2.ali’ (Methods Table 15.), query remains the sequence.¹⁵⁰

4.5 MODELLER A-Chain Models

MODELLER calculated ten similar 3-D models for each of the multiple template alignments, one best-fit model of each was selected via energy profiling. The A-chain monomer based on the former align2.ali single template/target alignment took precedence towards oligomerization.

4.5.1 Multiple Template/Target Monomer

Because Clustal is a pairwise alignment algorithm not aligning via secondary structural folds, imperative towards transmembrane protein Pannexin-1 alignment, its generated A-chain monomer exhibited a topology not matching template Connexin26 and Innexin6 EM ribbon generated topology models.

4.5.2 Single Template/Target Monomer

The align2.ali file target template alignment based on secondary structural folds took precedence towards generating a best A-chain monomer exhibiting an expected tetra-transmembrane configuration with respective coiled tails and three-loops, all other slightly adjusted single template/target alignments, similar to Clustal, generated skewed topologies.

>> Summary of successfully produced models:

Filename	molpdf

Pannexin-1.B99990001.pdb	3512.81323
Pannexin-1.B99990002.pdb	3717.61914
Pannexin-1.B99990003.pdb	4068.33667
Pannexin-1.B99990004.pdb	3745.99121
Pannexin-1.B99990005.pdb	3679.26147
Pannexin-1.B99990006.pdb	3874.66064
Pannexin-1.B99990007.pdb	3978.54883
Pannexin-1.B99990008.pdb	3668.39819
Pannexin-1.B99990009.pdb	3823.51099
Pannexin-1.B99990010.pdb	4078.27271

Table 50.) Of the 10 Pannexin-1 A-chain monomers generated via MODELLER using the align2.ali file, structural file Pannexin-1.B99990001.pdb was elected as the best model via its lowest moldpdf score of 3512.81323.¹⁵⁹

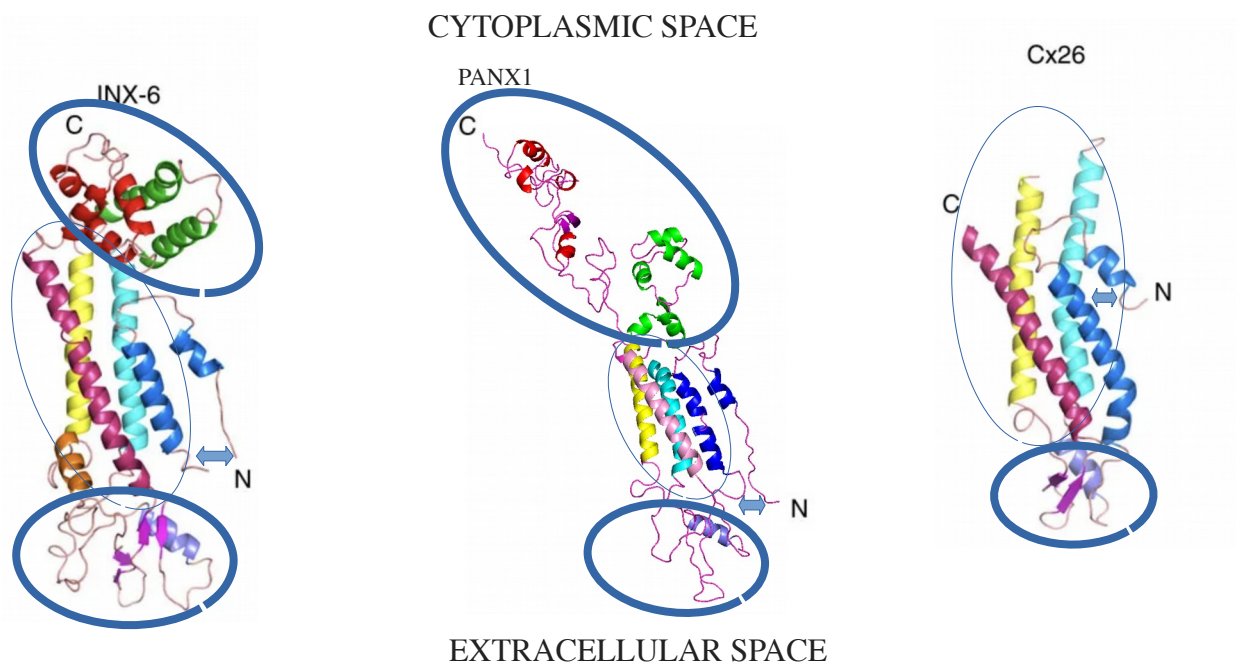


Figure 21.) Pymol visual of best elected Pannexin-1 A-chain based on the align2.ali file alignment exhibiting 4-symmetrically compact transmembranes (thin blue ellipses) and loops and tails (thick blue ellipses) (TM1-N-tail helix blue, TM2 cyan, TM3 yellow, TM4 pink, EL1 helix purple, IL1 helices green, c-tail helices red, beta sheets magenta, primary structure light magenta) comparable to respective sequence and topology templates Innexin6 and Connexin26 (Innexin6 and Connexin26 illustrated via EM ribbon models.) Note the N-tail tucked within the membraneous region (blue double-arrow) as experimentally determined, residue positions match experimental data.^{63, 22, 171, 198}

4.5.3 Single/Multiple Template-Target Monomers

Single template aligned Innexin6 and Connexin26 and multiple template aligned Innexin6-Connexin26 generated unsuccessful skewed topological A-chains.

4.6 Galaxy Oligomer Models

Input A-chain subunit Pannexin-1.B99990001.pdb and refinement settings Tails (1-19, 407-426), gating regulating EL1 (67-85) (Table 22.) Galaxyhomomer generated a best elected hexamer amongst all oligomers and refinements generated.⁷⁸ Although this hexamer exhibited symmetry,

a compact outer-pore region and satisfactory diameters, its inflated lower pore-structure and loops and coils exhibiting steric clashes precluded this model from subsequent docking selection. Galaxy FASTA sequence inputs similarly generated an overall best elected hexamer oligomer and overall best Pannexin-1 model exhibiting consistent satisfactory diameters and an overall structure matching experimental data, this model was subsequently selected towards docking simulations. (MolProbity model validation software exhibited a 78th percentile score out of a best 100% towards clashes, rotamer and Ramachandran evaluations for the sequence input generated Panx1 hexamer, the monomer input generated hexamer's MolProbity score was substantially lower.)²¹⁹

Adding to the bulk of the literature reports supporting a hexamer structure, both the sequence and monomer input generated oligomer modeled pentamers, heptamers and octamers (via oligomeric state selection and default setting) exhibited structural problems at the subunit interfaces and steric clashes within the coils and tails resulting in pore and oligomer diameters not fitting reported sizes, moreover generated oligomers outside of the hexamers exhibited inner pore lining TM1 and EL1 domains not matching SCAM experimental data.

4.6.1 GalaxyHomomer Hexamers

Both monomer and sequence inputs resulted in an Ab Initio Docking methodology via default due to zero oligomer templates discovered within the structural database.

4.6.1.1 Galaxy Scores

Ab initio Docking Results

Model No	Number of subunits	Interface area	Docking score	Loops/termini that may be refined	Re-submit for refinement
1	6-mer	11958.7	1126.893	N/A	Submit
2	6-mer	14887.0	1062.338	N/A	Submit
3	6-mer	9655.0	947.809	N/A	Submit
4	6-mer	8308.4	924.505	N/A	Submit
5	6-mer	9890.0	890.033	N/A	Submit

Table 51.) Ab initio docking results displaying interface area and docking scores towards a best selected Pannexin-1 hexamer generated via an input monomer, best score 2 was selected.⁷⁸

Ab initio Docking Results

Model No	Number of subunits	Interface area	Docking score	Loops/termini that may be refined	Re-submit for refinement
1	6-mer	16432.5	1330.357	251-257	Submit
2	6-mer	13422.6	1274.161	251-257	Submit
3	6-mer	13675.6	1041.152	251-257	Submit
4	6-mer	6187.8	884.699	251-257	Submit
5	6-mer	7913.5	801.861	251-257	Submit

Table 52.) Ab initio docking results displaying interface area and docking scores generated via a FASTA input, highest score 1 was selected.⁷⁶

4.6.1.2 Monomer vs. FASTA Hexamers

The FASTA input GalaxyHomomer more closely matched Pannexin-1 experimental data.

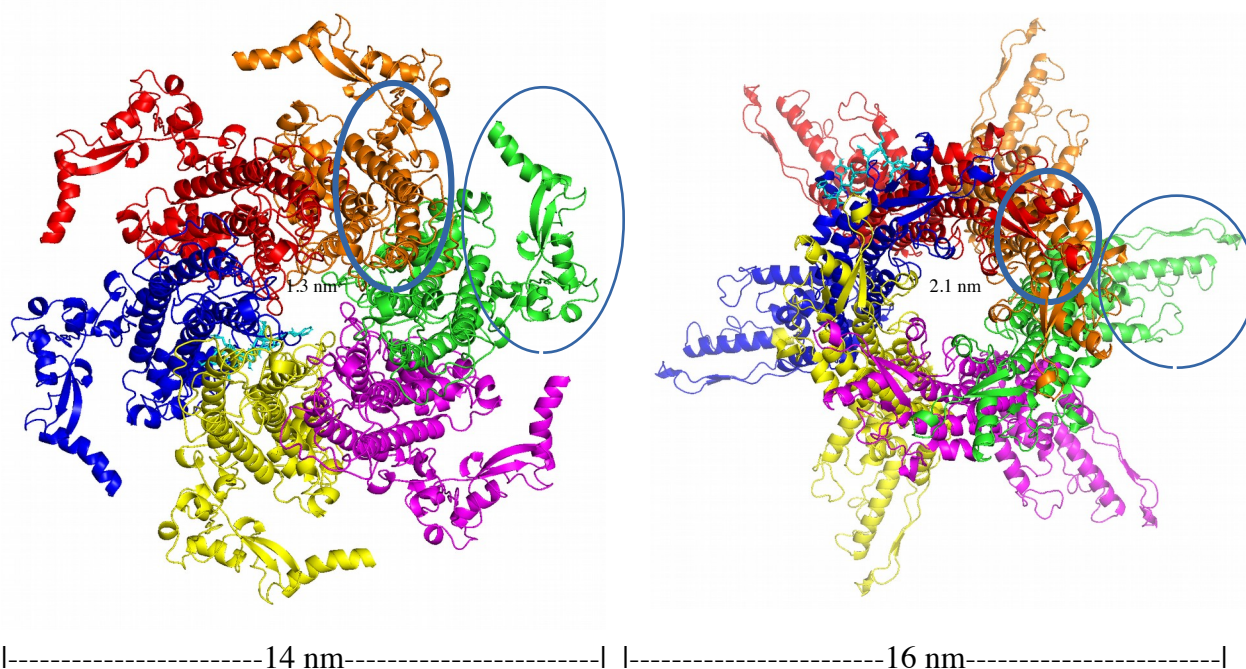


Figure 22.) Pymol visual of monomer and FASTA Galaxy generated hexamers respectively viewed from the extracellular space. Both exhibit fair diameters, monomer membraneous tucked N-terminal (monomer residues 1-12 cyan stick model) exhibited, the FASTA model's lower helices exhibit a much greater thermodynamically favorable compact conformation (thick blue ellipses) with substantially more optimized tails and loops (thin blue ellipses).⁷³

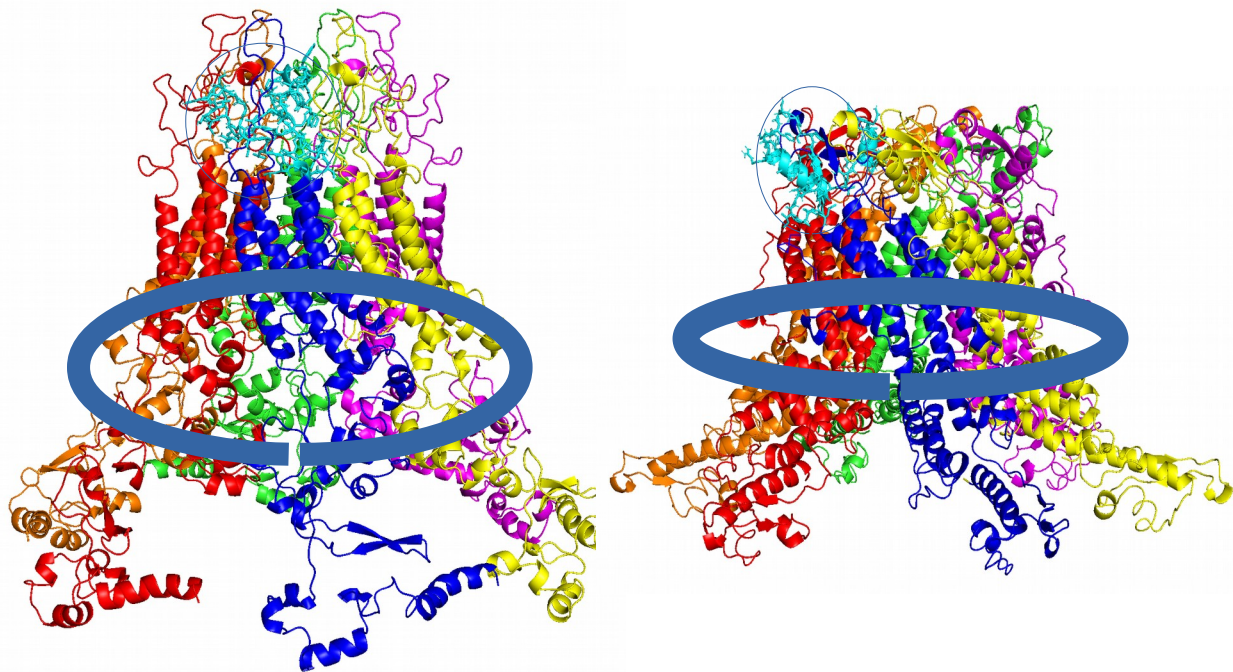


Figure 23.) Respective monomer and FASTA Galaxy generated Pannexin-1 models side-view via Pymol exhibiting residues 57-107 EL1 in stick cyan in apropos extracellular space. FASTA input exhibits a greater lower compact helices conformation precipitating a more compact transmembrane region throughout (thick blue-ellipses). EL1 regions via the FASTA version exhibit a greater optimized conformation via charged residue repulsions within the loops (thin blue-circles).⁷⁹

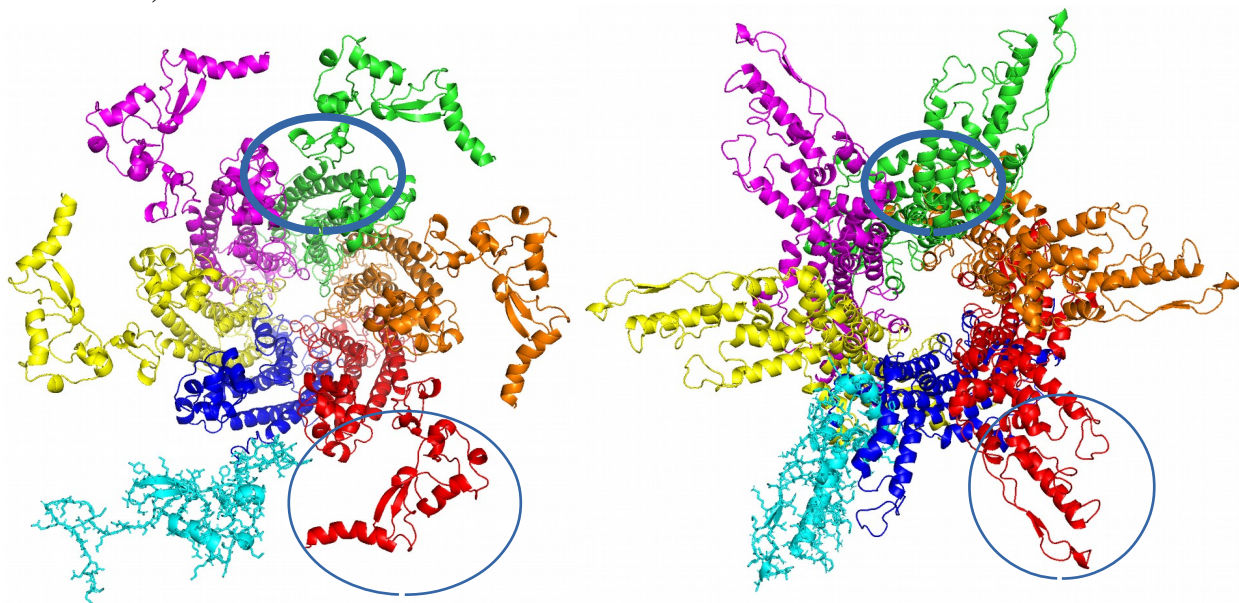


Figure 24.) Cytoplasmic view, respective monomer and FASTA generated hexamers with FASTA model generation exhibiting substantially greater lower helices compaction (thick blue-circles) and greater coil/tail electrostatic repulsion (thin blue-circles) promoting consistent pore and oligomer sizes respectively and a better overall thermodynamic structure (residues 306-426 C-tail as cyan stick model.)⁸⁰

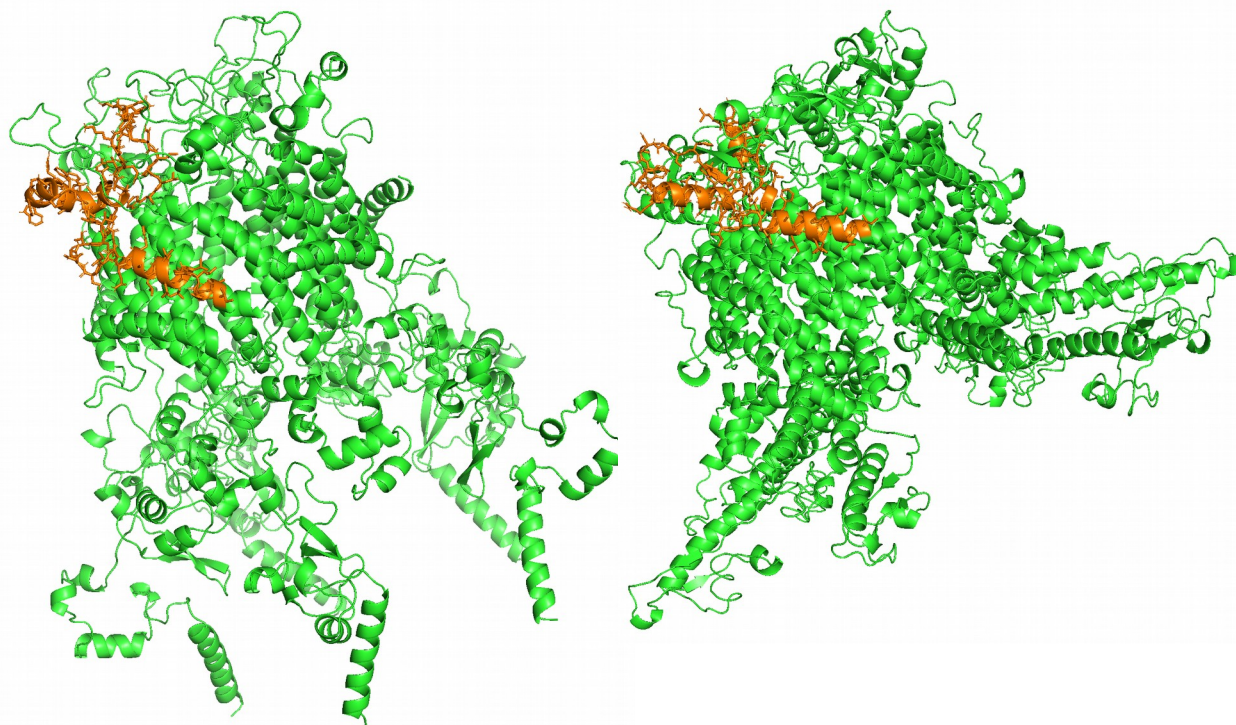


Figure 25.) Monomer and FASTA hexamer elected models respectively exhibiting a TM1 and EL1 outer pore lining (orange stick model) matching experimental SCAM data.⁸¹

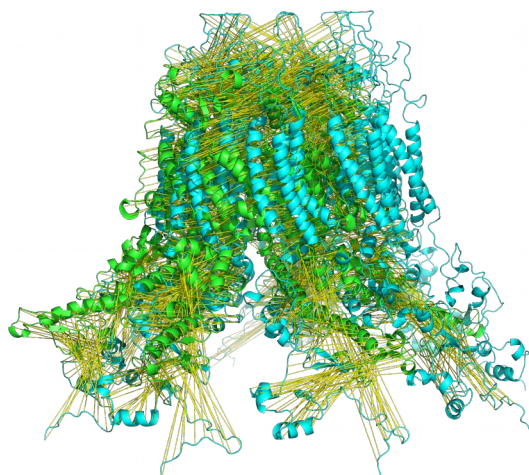


Figure 26.) Pymol monomer and sequence based hexamers superimposed exhibiting residue-residue correspondence (yellow-sticks). Green sequence based hexamer exhibiting a consistently compact pore region and optimized loops and tails, cyan monomer based hexamer exhibits steric clashes amongst its loops and coils and inflated lower transmembrane helices.

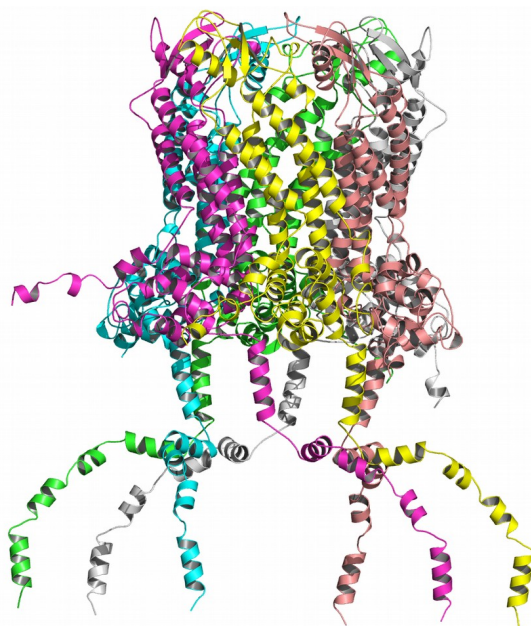


Figure 27.) GalaxyHomomer Pannexin-1 FASTA input method predicted symmetrical Pannexin-1 hexamer homo-oligomer model exhibiting consistently compact intra-membraneous helices with dynamic disordered optimized tails and loops, side-view.⁷⁴

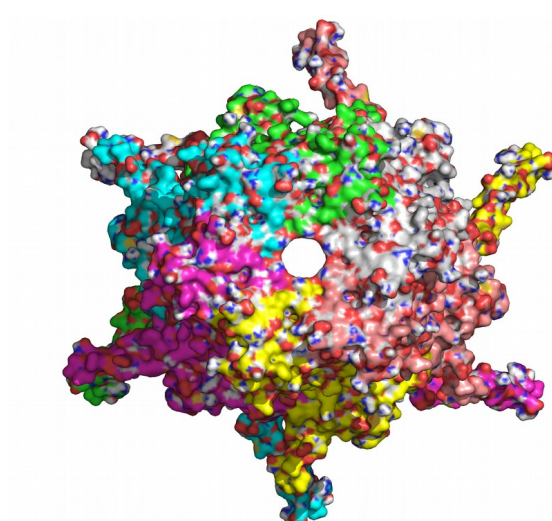


Figure 28.) GalaxyHomomer FASTA input method predicted symmetrical Pannexin-1 hexamer model viewed from the extracellular space exhibiting an apropos compact pore size via energetically favorable compact helical conformations.⁷²

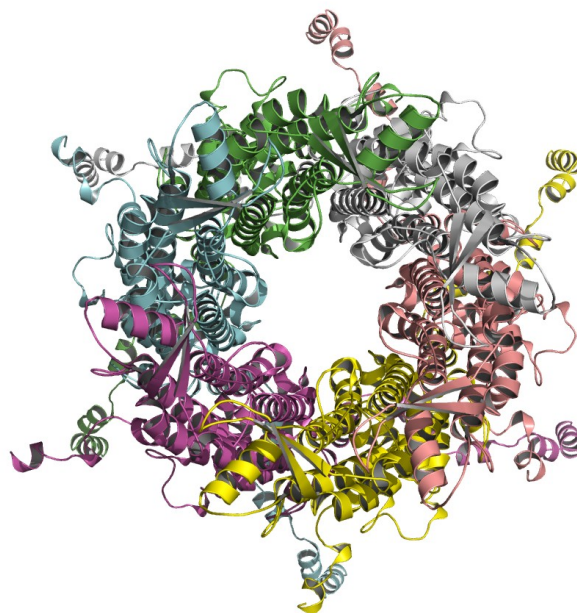


Figure 29.) GalaxyHomomer FASTA input method predicted symmetrical Pannexin-1 hexameric model viewed from the extracellular space exhibiting dynamic disordered optimized tails and loops and highly compact helices resulting in oligomer and consistently compact pore sizes matching Pannexin-1 experimental data.⁷¹

4.7 Ligand-Target Experimental and Docking Dynamic Simulation Results

4.7.1 Experimental Results

Experimental alanine mutant results proved food-dye and probenecid binding sites and or gating structural activity within the Panx1 EL1-74 and EL2-237, 240, 247, 266 residues.⁶⁹

Experimental mutant results proved CBX binding sites and or gating structural activity within the Panx1 EL1-74 and Conserved Region EL1 67-86.¹⁵

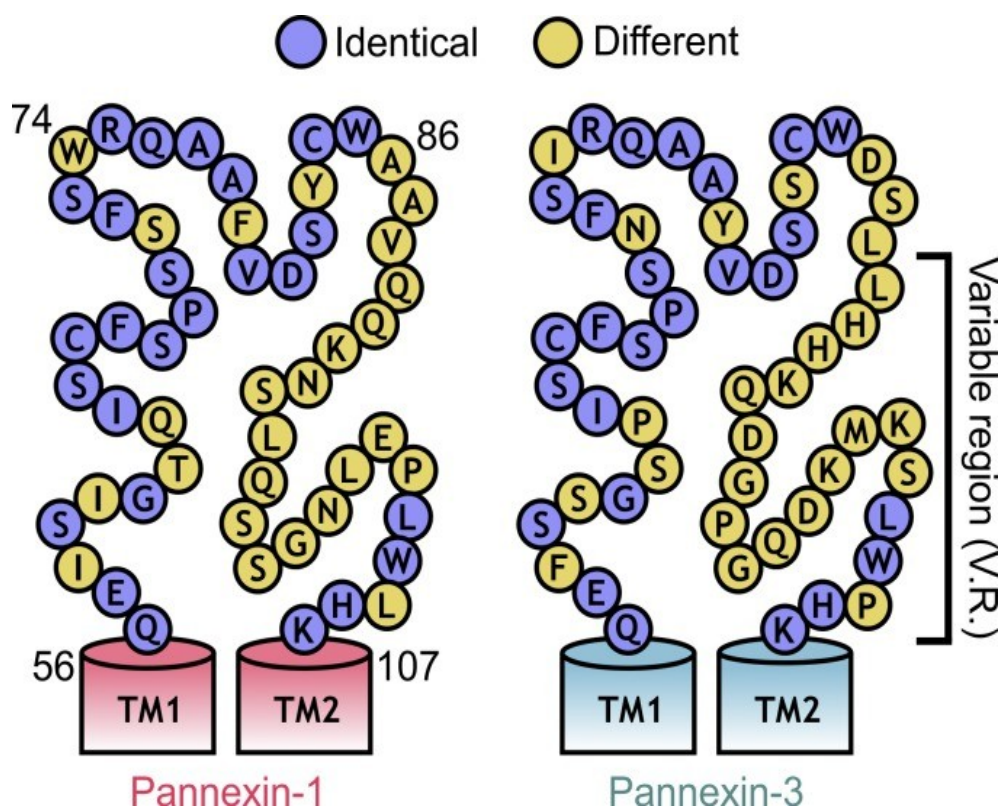


Figure 30.) Pannexin-1 Extracellular Loop Region 1 (EL1) with both conserved and non-conserved residues outlined. CBX has proven that the conserved region promotes Pannexin-1 gating activity.⁶⁷

Experimental dye and channel current results have demonstrated the ¹⁰Panx1 mimetic peptide to most likely steric block the hexamer pore region (¹⁰Panx1 may activate a docking gate via a cryptic binding needing further elucidation).^{2,8,66}

4.7.2 In Silico Results

In silico dockings overall exhibited weak to high affinity binding free energy values using the proven partners known to experimentally block the Pannexin-1 channel inferring an overall fair regional modeling accuracy. Similar to Adenosine Receptor activation, conserved internal water molecules pivotally connect the extracellular cavity to the intra-Pannexin-1 space via H-bonding

to ligands and conserved Panx1 residues promoting a most native ligand-receptor apropos juxtaposition (MedusaDock via default discovers and docks to a best/lowest energy ligand binding residue-specific conformation). Ligand-receptor dockings also exhibited electrostatic or polar interactions and steric effective nonbonding and steric match via a steric augmentation of products exhibiting a smallest steric strain.^{222, 224, 226}

4.7.2.1 Pore Docking Results

The Mimetic ¹⁰Panx1 docked to the modeled hexamer pore region hydrogen-bonding and steric effectively nonbonding to residues S93, Q95, S96 and E97, four Panx1 subunits exhibited bonds. Mimetic ¹⁰Panx1 exhibited a high binding affinity inferring a high pore modeling accuracy, ligand binding partially steric blocked the hexamer pore-region matching experimental data.

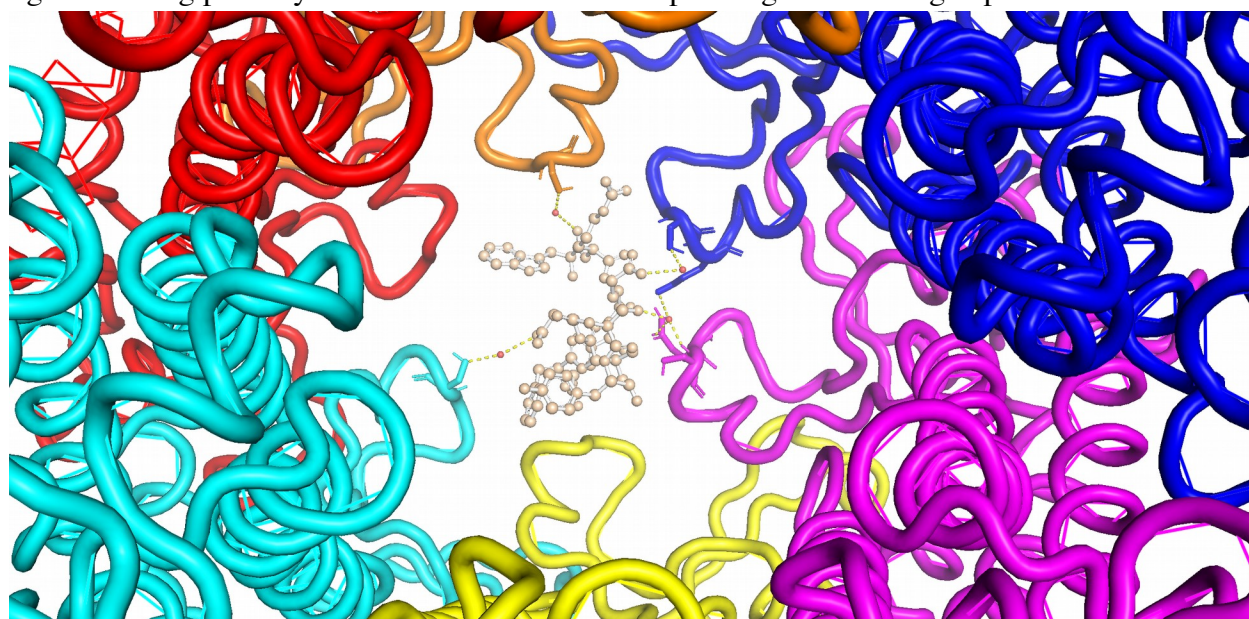


Figure 31.) A cytoplasmic view of Mimetic ¹⁰Panx1 bound to the Panx1 non-conserved EL1 Pore Region via a hydrogen-bonding water arrangement (red-dots are water molecules).¹²⁶

High binding affinity exhibited in the Panx1-EL1 pore region:

PAX_10PANX.pdb

REMARK E_{total}: -44.4728 kcal mol⁻¹

REMARK E_{without_VDWR}: -46.38 kcal mol⁻¹¹⁸⁶

4.7.2.2 EL-1 Docking Results

EL-1 docking results exhibited outer Pannexin-1 polar interactions and nonbonding steric effects amongst all four-chemicals. Binding position indicates a gating allosteric event.

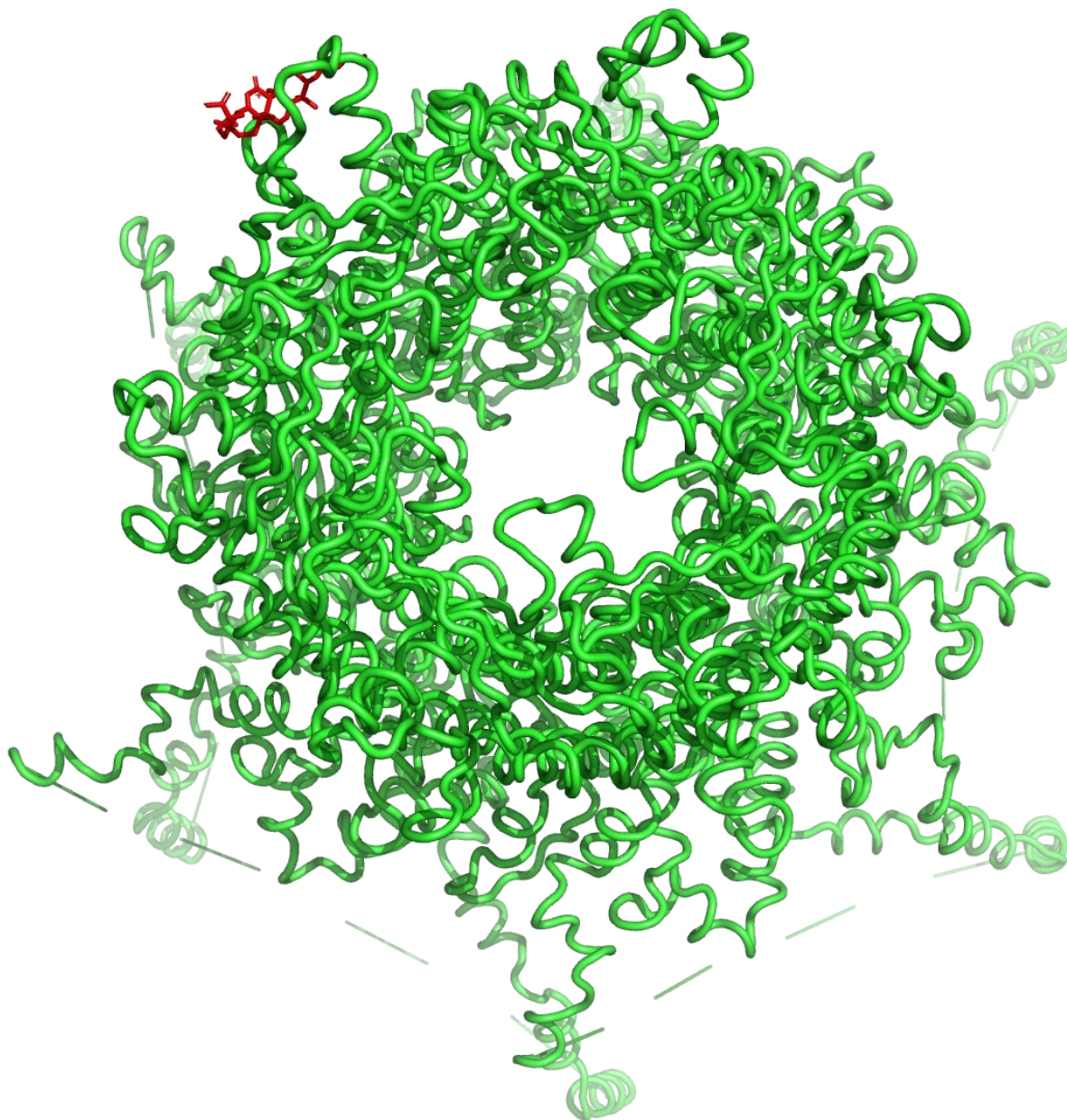


Figure 32.) CBX nonbonding steric effect on the outer Panx1 EL-1 experimentally proven region.⁴⁹

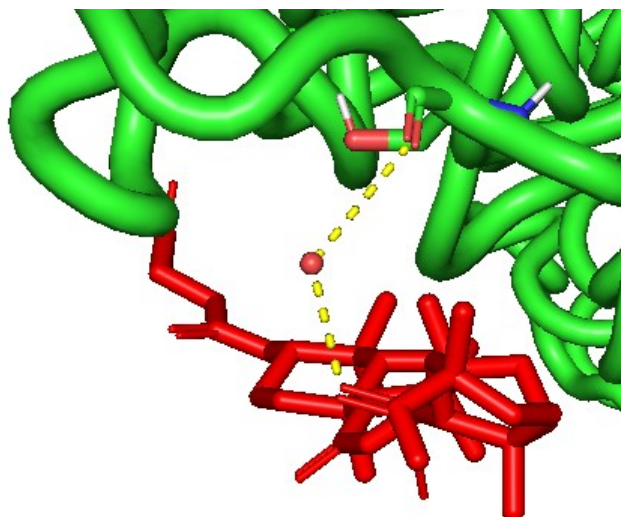


Figure 33.) Above Pannexin-1-CBX interaction inflated exhibiting 3 Å H-bonding red-dot water molecule to CBX, a polar interaction of water to pivotal residue 68 > 3.1 Å in the EL1 and CBX hydrophobic to Panx1 hydrophobic residue steric effective nonbonding.⁴⁸

Poor to high binding affinities exhibited in the Panx1-EL1 region inferred an overall fair EL1 modeling accuracy.

PAX_Carbenoxolone.pdb

REMARK E_total: -23.4778 kcal mol⁻¹

REMARK E_without_VDWR: -25.3025 kcal mol⁻¹

PAX_brilliantblue.pdb:

REMARK E_total: -27.5987 kcal mol⁻¹

REMARK E_without_VDWR: -29.5413 kcal mol⁻¹

PAX_Fastgreen.pdb

REMARK E_total: -31.5298 kcal mol⁻¹

REMARK E_without_VDWR: -34.8731 kcal mol⁻¹

PAX_Probenecid.pdb

REMARK E_total: -15.3546 kcal mol⁻¹

REMARK E_without_VDWR: -15.5225 kcal mol⁻¹ ¹⁸⁶

4.7.2.3 EL-2 Docking Results

Probenecid and green and blue food dyes docked to the experimentally determined Panx1 EL2-237, 240, 266 region via polar interactions and nonbonding steric effects.

Poor to high binding affinities exhibited in the Panx1-EL2 region inferred an overall fair EL2 modeling accuracy.

PAX_Probenecid.pdb

REMARK E_total: -15.949 kcal mol⁻¹

REMARK E_without_VDWR: -16.0732 kcal mol⁻¹

PAX_Fastgreen.pdb

REMARK E_total: -26.6799 kcal mol⁻¹

REMARK E_without_VDWR: -31.2314 kcal mol⁻¹

PAX_brilliantblue.pdb

REMARK E_total: -31.8357 kcal mol⁻¹

REMARK E_without_VDWR: -33.294 kcal mol^{-1 186}

Chapter 5

Discussion

5.1 Interpretation of Main Findings

Pannexin-1 is a ubiquitous transmembrane protein regulating homeostasis and pathology via autocrine/paracrine channel signaling. The significance of solving this beginning Pannexin-1 structure in silico will contribute to subsequent studies further elucidating the physicochemical characteristics, binding properties and gating mechanisms of the Panx1 channel. Together these contributions along with a deeper understanding of Pannexin-1's homeostatic conduits will lead to a therapeutic gating controlling a multitude of physiological functions.

Experimental evidence indicates the Pannexin-1 to be a symmetrical un-apposed hemichannel homo-hexamers. An input MODELLER generated Panx1 sub-unit and Panx1 amino acid sequence GalaxyHomomer generated hexamers most closely matching established documented experimental evidence, both exhibited topologies and orientations similarly matching published data. All other oligomeric states generated exhibited structural problems at the subunit interfaces and steric clashes within the coils and tails resulting in pore and oligomer diameters not fitting reported sizes. Between the input sub-unit and sequence based hexamers, the later exhibited a best overall structure via a consistently thermodynamic compact pore region with highly optimized coils and loops.

A GalaxyHomomer sequence input method generates monomers via a multiple-template based GalaxyTBM tool. GalaxyTBM generated a more favorable potential docking sub-unit than MODELLER via its overall approach of least contaminating templates, conservative core modeling and MODELLER CSA heightened optimization. GalaxyTBM specially selected a 2HDI_B template compatible to its selected top template 5h1q (Innexin6). Moreover 2HDI_B was the only other template selected covering residues (353-426), this precluded template contamination via conflicting constraints upon convergence precipitated when greater than three templates are selected (the MODELLER generated A-chain used five-templates). GalaxyTBM models conserved cores first and ab initio models ULR (Unreliable Local Regions) loops and coils subsequently increasing modeling accuracy (MODELLER models all regions

simultaneously). GalaxyTBM updated MODELLER CSA more rigorously optimizes (minimizes forces between atoms) in multiple template cases minimizing conflicting template restraints/contamination during model building resulting in a better converged monomer.²²³

Pannexin-1 pore closure can be precipitated in vitro via a mimetic peptide steric block or via a conformational change within the pore region via Pannexin-1 chemical inhibitors. Overall Medusa flexible guide docking results within this study exhibited moderate ligand-receptor affinities using experimentally determined data inferring a fair regional modeling accuracy. Medusa explicit water addition and each ligand exhibiting <10 rotatable bonds further strengthened results via exhibiting a more closely resembling native ligand-receptor juxtaposition and a lowering of binding modes respectively.

Mimetic ¹⁰Panx1 exhibited a high affinity ($-46.38 \text{ kcal mol}^{-1}$) to the Pannexin-1 pore region. Moreover, via Pymol Visualization, this docking event exhibited experimentally inferred steric block. Accordingly, the designed Pannexin-1 model pore region within this study is non-trivial. The precise design of the conserved region of the Panx1 Extracellular Loop Region 1 (EL1) is pivotal, particularly non-conserved residue W74, due to its proven Pannexin-1 pore gating activity via conformational change. Food dyes and CBX together exhibited fair docking affinities in this region pushing the validity of the Panx1 EL1 model, however, Probenecid's affinity of $-15.5225 \text{ kcal mol}^{-1}$ may warrant a greater EL1 elucidation. CBX is a known and proven regulator of Pannexin-1 closure via EL1 binding sites and gating structural activity. CBX docking is nonbonding steric/hydrophobic and polar, hydrophobic interactions stabilize ligand receptor binding and hydrogen bonding optimizes these hydrophobic effects.²²⁰ Together these two weak intermolecular interactions increased ligand receptor binding affinity enough to infer a fair EL1 regional modeling. Similarly exhibiting chemical inhibitor binding sites and gating structural activity, the Panx1 EL2 region was overall docked reasonably well via chemical inhibitors inferring a fair modeling of the EL2 region. Probenecid's poor affinity value of $-16.0732 \text{ kcal mol}^{-1}$ similarly may warrant EL2 model refinement or may alternatively strengthen EL1 and EL2 model results via Probenecid docking affinity value corroboration i.e. in this case maybe a finely tuned steric nonbonding conformation may be required to successfully trigger a finer gating mechanism.

Chapter 6

Conclusion

6.1 Final Statement

The main hypothesis of this study is predicated upon the modeling of a yet uncrystallized transmembrane protein called Pannexin-1 that controls a multitude of functions towards physiology and homeostasis. Pannexin-1 was designed in silico exhibiting a thermodynamically compact pore region, expected overall hexameric structure and validated regional accuracy. The pivotal regional domains responsible for gating were validated via overall moderate in silico docking affinities exhibited by various chemicals and one mimetic peptide known to experimentally block the Pannexin-1 channel. This proven protein design may be used in future studies to control Pannexin-1 gating to combat disease.

6.2 Limitations

Pannexin-1 experimental blocking action is yet elusive and may be only gating regulated, the modeled Panx-1 EL1/2 regions are located distal to the pore. The largest inhibitor, Mimetic ¹⁰Panx1 exhibiting a high affinity and pore steric block in silico, may instead bind a cryptic site regulating pore-gating. Moreover ¹⁰Panx1 being a larger ligand may have generated false positives via force field scoring inaccuracies being proportional to ligand-receptor contact area.⁴⁷ Inaccurately placed ligand-receptor interface waters may additionally have generated false positive affinity values.²²⁵

This preliminary data is yet limited and expresses a beginning Pannexin-1 model. The Pannexin-1 model is not co-crystallized and therefore does not include any potentially pivotal water molecule arrangements within the Panx1 model structure which would transfer its 3-D space adding to its 3-D accuracy. Pannexin-1 pore conformational closure via the former inhibitors has not yet been exhibited via Molecular Dynamic Simulations, accordingly this designed Pannexin-1 model requires further validation exhibiting structural changes towards pore closure.

6.3 Future Research

This investigated software designed Pannexin-1 hexamer model is a start towards future Pannexin-1 regional-inhibitor/promoter modifications. A lengthy and exhaustive subsequent study using Molecular Dynamic Simulations will discover the pivotal residue inhibitor/promoter/ and arranged water electro-steric interactions involved in Pannexin-1 gating via exhibiting structural changes within the channel. Subsequently a nanoparticle may be engineered exhibiting a tag that triggers a Panx1 conformational closure, this development will lead to in vitro and in vivo testings.

REFERENCES

1. Public Health Research Institute [Internet]. [Newark, New Jersey: New Jersey Medical School]; 2017. Rutgers New Jersey Medical School Faculty and Research, Eliseo A. Eugenin, Ph.D.; [cited 2017 Sept 5]; [16 webpages]. Available from: http://phri.org/research/res_pieugenin.asp#ra
2. Velasquez Stephani, Eugenin A. Eliseo. Role of Pannexin-1 hemichannels and purinergic receptors in the pathogenesis of human diseases. *Frontiers in Physiology* [Internet]. 2014 March- [cited 2017 Sept 5]. Available from: <https://www.ncbi.nlm.nih.gov/pmc/articles/PMC3953678/>
3. [Model/Role Panx 1 Purinergic Receptors][illustration]. [Published Online]: [Front Physiol]; 2014. 1 illustration: color.
4. [Elemental ATP release Purinergic signaling model][illustration]. [Published Online]: [Front Physiol]; 2014. 1 illustration: color.
5. Mukhopadhyay Rajendrani, Team effort to figure out a rare genetic disease. *Journal of Biological Chemistry* [Internet]. 2016 June/July- [cited 2017 Sept 6]. Available from: <http://www.asbmb.org/asbmbspecial/201606/JournalNews/JBCPannexin/>
6. [Panx 1 Mutated][illustration]. [ASBMB]: [JBC]; 2016. 1 illustration: color.
7. [Panx 1 Channels in Lipid Bilayer/Panx1 Opening via Cleavage][illustration]. [ASBMB]: [JBC]; 2016. 1 illustration: color.
8. Orellana J.A., Velasquez S., Williams D.W., Saez J.C., Berman J.W., Eugenin E.A.. Pannexin1 hemichannels are critical for HIV infection of human primary CD4+ T lymphocytes. *Journal of Leukocyte Biology* [Internet]. 2013 September- [cited 2017 Sept 11]. Available from: <https://www.ncbi.nlm.nih.gov/pmc/articles/PMC3747122/>

9. Hazelton E. Joy, Berman W. Joan, Eugenin A. Eliseo. Purinergic Receptors are Required for HIV-1 Infection of Primary Human Macrophages. *Journal Immunology* [Internet]. 2012 May- [cited 2017 Sept 14]. Available from: <https://www.ncbi.nlm.nih.gov/pmc/articles/PMC3508684/>
10. Seror Claire, Melki Marie-Therese, Subra Frederic, Raza Qasim Syed, Bras Marlene, Saidi Helga, Nardacci Roberta, Voisin Laurent, Paoletti Audrey, Law Frederic, Martins Isabelle, Arnedola Alessandra, Abdul-Sater A. Ali, Ciccocanti Fabiola, Delelis Olivier, Niedergang Florence, Thierry Sylvain, Said-Sadier Najwane, Lamaze Christophe, Metivier Didier, Estaquier Jerome, Fimia Maria Gian, Falasca Laura, Casetti Rita, Modjtahedi Nazanine, Kanellopoulos Jean, Mouscadet Jean-Francois, Ojcius M. David, Piacentini Mauro, Gougeon Marie-Lise, Kroemer Guido, Perfettini Jean-Luc. Extracellular ATP acts on P2Y2 purinergic receptors to facilitate HIV-1 infection. *Journal Exp Med.* [Internet]. 2011 Aug- [cited 2017 Sept 18]. Available from: <https://www.ncbi.nlm.nih.gov/pmc/articles/PMC3171090/>
11. Ding Feng, Yin Shuangye, Dokholyan V. Nikolay. Rapid Flexible Docking a Stochastic Rotamer Library of Ligands. *J Chem Inf Model* [Internet]. Sep 27 2010-[cited 2019 June 9]. Available from: <https://www.ncbi.nlm.nih.gov/pmc/articles/PMC2947618/>
12. [Cascade (pannexin-1—>ATP—> P2Y2—> Pyk2)][illustration]. [Published Online]: [Journal Exp Med.]; 2011. 1 illustration: color.
13. Bolia Ashini, Gerek Z. Nevin, Ozkan S.Banu. BP-Dock: A Flexible Docking Scheme for Exploring Protein-Ligand Interactions Based on Unbound Structures. *J Chem Inf Model* [Internet]. March 24 2014-[cited 2019 June 9]. Available from: <https://www.ncbi.nlm.nih.gov/pmc/articles/PMC4857727/>
14. Eugenin Eliseo. Role of Connexin/Pannexin containing channels in infectious diseases. *FEBS Lett.* [Internet]. 2014 January- [cited 2017 Sept 22]. Available from: <https://www.ncbi.nlm.nih.gov/pmc/articles/PMC4229019/>
15. Michalski K., Karate T.. Carbenoxolone inhibits Pannexin1 channels through interactions in the first extracellular loop. *J. Gen Physiol.* [Internet]. 2016 February- [cited 2017 Sept 25]. Available from: <https://www.ncbi.nlm.nih.gov/pmc/articles/PMC4727946/>

16. [Panx1 EM Diameter Images][images]. [Published Online]: [JBC]; 2010. 4-Images: black and white.
17. Ehrlich S. Lorna, Carter A. Carol. HIV Assembly and Budding: Ca^{2+} Signaling and Non-ESCRT Proteins Set the Stage. *Mol Biol Int.* [Internet]. 2012-[cited 2017 April 11]. Available from: <https://www.ncbi.nlm.nih.gov/pmc/articles/PMC3384956/>
18. Temesgen Zelalem, Siraj S. Dawd. Raltegravir: first in class HIV integrase inhibitor. *The Clin Risk Manag.* [Internet]. 2008 Apr.- [cited 2017 Oct 3]. Available from: <https://www.ncbi.nlm.nih.gov/pmc/articles/PMC2504063/>
19. Dimitrov S. Dimiter, Broder C. Christopher, Berger A. Edward, Blumenthal Robert. Calcium Ions Are Required for Cell Fusion Mediated by the CD4-Human Immunodeficiency Virus Type 1 Envelope Glycoprotein Interaction. *Journal Of Virology.* [Internet]. 1993-[cited 2018 April 11]. Available from: <https://jvi.asm.org/content/jvi/67/3/1647.full.pdf>
20. Xiling Zhang, Shan Gao, Masayoshi Tanaka, Zhen Zhang, Yanru Huang, Takahiko Mitsui, Manabu Kamiyama, Schuichi Koizumi, Jianglin Fan, Masayuki Takeda, Jian Yao. Carbenoxolone inhibits TRPV4 channel-initiated oxidative urothelial injury and ameliorates cyclophosphamide-induced bladder dysfunction. *Journal of Cellular and Molecular Medicine.* [Internet]. 2017-[cited 2018 April 8]. Available from: <https://onlinelibrary.wiley.com/doi/full/10.1111/jcmm.13100>
21. Penuela Silvia, Gehi Ruchi, Laird W. Dale. The biochemistry and function of pannexin channels. *Biochimica et Biophysica Acta (BBA)-Biomembranes.* [Internet]. 2013-[cited 2018 April 8]. Available from: <https://www.sciencedirect.com/science/article/pii/S0005273612000211>
22. [Figure 3: Similarity between the INX-6 and Cx26 monomers.][illustration]. [NY, USA]: [Springer Nature]; 2016. 1 illustration: color.
23. RaptorX [Internet]. [Chicago, Il: Toyota Technological Institute at Chicago]; 2012. RaptorX: protein structure prediction server, Section II. Engine; [cited 2019 Oct 2]; [1 screens].

Available from: https://github.com/realbigws/RaptorX_Property_Fast

24. Peng Jian, Xu Jinbo. A multiple-template approach to protein threading. *Proteins*. 2012-[cited 2019 June]. Available from: <https://www.ncbi.nlm.nih.gov/pmc/articles/PMC3092796/>
25. Prochnow Nora, Abdulazim Amr, Kurtenbach Stefan, Wildforster Verena, Dvorianchikova Galina, Hanske Julian, Parwez-Petrash Elisabeth, Dermietzel Rolf, Shestopalov I. Valery, Vaughan-Manahan Denise, Zoidl Georg. Pannexin1 Stabilizes Synaptic Plasticity and Is Needed for Learning. *PLOS ONE*. [Internet]. 2012-[cited 2019 March 23]. Available from: <https://journals.plos.org/plosone/article?id=10.1371/journal.pone.0051767>
26. Ramirez Alejandro, Arbuckle R. Melissa. Synaptic Plasticity: The Role of Learning and Unlearning in Addiction and Beyond. *Biol. Psychiatry*. [Internet]. 2017-[cited 2019 March 23]. Available from: <https://www.ncbi.nlm.nih.gov/pmc/articles/PMC5347979/>
27. Weaver L. Janelle, Arandjelovic Sanja, Brown Gregory, Mendu K. Suresh, Schappe S. Michael, Buckley W. Monica, Chiu Yu-Hsin, Shu Shaofang, Kim K. Jin, Chung Joyce, Krupa Julia, Todorovic-Jevtovic Vesna, Desai N. Bimal, Ravichandran S. Kodi, Bayliss A. Douglas. Hematopoietic Pannexin 1 Function is Critical for Neuropathic Pain. *Scientific Reports*. [Internet]. 2017-[cited 2019 March 21]. Available from: <https://www.ncbi.nlm.nih.gov/pmc/articles/PMC5307344/>
28. Billaud Marie, Chiu Yu-Hsin, Lohman W. Alexander, Parpaite Thibaud, Butcher T. Joshua, Mutchler M. Stephanie, DeLalio J. Leon, Artamonov V. Mykhaylo, Sandilos K. Joanna, Best K. Angela, Somlyo V. Avril, Thompson J. Roger, Le H. Thu, Ravischandran S. Kodi, Bayliss A. Douglas, Isakson E. Brant. A Molecular Signature in the Pannexin 1 Intracellular Loop Confers Channel Activation by the $\alpha 1$ Adrenoreceptor in Smooth Muscle Cells. [Internet]. 2015-[cited 2019 March 21]. Available from: <http://stke.sciencemag.org.proxy.libraries.rutgers.edu/content/8/364/ra17>
29. Delalio Leon. Regulation of Blood Pressure Homeostasis by Pannexin 1 Channels. *LIBRAETD* [Internet]. 2019-[cited 2019 March 21]. Available from: https://libraetd.lib.virginia.edu/public_view/mp48sd20f

30. Chekeni B. Faraaz, Elliot R. Michael, Sandilos K. Joanna, Walk F. Scott, Kinchen M. Jason, Lazarowski R. Eduardo, Armstrong J. Allison, Penuela Silvia, Laird W. Dale, Salvesen S. Guy, Isakson E. Brant, Bayliss A. Douglas, Ravichandran S. Kodi. Pannexin 1 channels mediate 'find-me' signal release and membrane permeability during apoptosis. *Nature*. [Internet]. 2010-[cited 2019 March 20]. Available from: <https://www.ncbi.nlm.nih.gov/pmc/articles/PMC3006164/>
31. Calcium Signaling in Apoptosis: 2019. abcam [Internet]. 2019-[cited 2019 March 20]. Available from: <https://www.abcam.com/cancer/calcium-signaling-in-apoptosis>
32. Hossmann KA. Periinfarct Depolarizations. *Cerebrovasc brain metab Rev*. [Internet]. 1996-[cited 2019 March 19]. Available from: <https://www.ncbi.nlm.nih.gov/pubmed/8870974>
33. Anrather Josef, Iadecola Costantino. Inflammation and Stroke: An Overview. *Neurotherapeutics*. [Internet]. 2016-[cited 2019 March 19]. Available from: <https://www.ncbi.nlm.nih.gov/pmc/articles/PMC5081118/>
34. Excitotoxicity and Cell Damage: 2019. Science Daily [Internet]. 2019-[cited 2019 March 19]. Available from: <https://www.sciencedaily.com/terms/excitotoxicity.htm>
35. Subach, Joel. Pannexin-1 and Physiology and Pathology [Internet]. Message to Frederick Coffman. 2019 March [cited 2019 March 19]. [2 paragraphs].
36. SACS [Internet]. [San Francisco, Ca: University of California San Francisco]; 2015. SACS: Transmembrane Prediction Site, TMHMM Transmembrane Probabilities; [cited 2018 March 19]; [1 screen]. Available from: <http://www.cbs.dtu.dk/services/TMHMM/>
37. Tmpred [Internet]. [Lausanne, Switzerland: Swiss Institute of Bioinformatics]; 2017. TMpred: Prediction of Transmembrane Regions and Orientation, TMpred Parameters; [cited 2018 Mar 19]; [1 screens]. Available from: https://embnet.vital-it.ch/software/TMPRED_form.html
38. UniProt [Internet]. [Oxford, UK: University of Oxford]; 2018. UniProt Consortium: A

Knowledge Resource for Proteins (SIB), Pannexin-1 Isoform(1) FASTA; [cited 2018 May 31]; screen]. Available from: available from: <https://www.uniprot.org/uniprot/Q96RD7.fasta>

39. Leung Wilson. Lab Week 8-An In-Depth Introduction to NCBI BLAST. Washington: [publisher unknown]; [cited 2017-2018]; 18 p. Report No.: 8.

40. BLAST Help [Internet]. [Bethesda, MD: National Center for Biotechnology Information]; 2011. BLAST Help, raw score; [cited 2019 May 30]; [1 webpage]. Available from: <https://www.ncbi.nlm.nih.gov/books/NBK62051/>

41. Fassler Jan, Cooper Peter. BLAST Glossary: 2011-[cited 2019 May 30]. Available from: <https://www.ncbi.nlm.nih.gov/books/NBK62051/>

42. RaptorX [Internet]. [Chicago, Il: Toyota Technological Institute at Chicago]; 2012. RatporX: protein structure prediction server, Section II. Pannexin-1 Summary Prediction Results; [cited 2018 Mar 18]; [4 screens]. Available from: http://raptorx.uchicago.edu/StructurePrediction/myjobs/60804446_309260/

43. OMIC TOOLS [Internet]. [Le-Petit-Quevily, France: omicX | Seine Innopolis]; 2018. SOSUI: Transmembrane helix prediction: SOSUI Pannexin-1 Result: [cited 2018 March 19]; [1 screen]. Available from: http://harrier.nagahama-i-bio.ac.jp/sosui/sosui_submit.html

44. PDB [Internet]. [Piscataway, NJ; La Jolla, Ca: Rutgers, SDSC]; 2018. PDB: A Knowledge Resource to Understand Biological Macromolecular Structures (PDB), 5H1Q FASTA; [cited 2018 Mar 15]; [1 screens]. Available from: <https://www.rcsb.org/structure/5H1Q>

45. Subach, Joel. Free Energy Question [Internet]. Message to: Venkat Reddy. 2019 Feb [cited 2019 Feb 11]. [1 paragraph].

46. Ajay, Murcko A. Mark. Computational Methods to Predict Binding Free Energy in Ligand-Receptor Complexes. Journal Of Medicinal Chemistry. [Internet]. 1995-[cited 2019 Jan 29]. Available from: <https://pubs-acscs-org.proxy.libraries.rutgers.edu/doi/pdf/10.1021/jm00026a001>

47. Yin Shuangye, Biedermannova Lada, Vondrasek Jiri, Dokholyan V. Nikolay. MedusaScore: An Accurate Force-Field Based Scoring Function for Virtual Drug Screening. *J Chem Inf Model*. [Internet]. 2009-[cited 2019 Jan 29]. Available from: https://link.springer.com/protocol/10.1007%2F978-1-4939-8630-9_5
48. PyMOL [Internet]. [Mannheim, Germany: Schrodinger]; 2018: PyMOL: A Molecular Visualization Program Towards Bio-Molecular Systems, CBX-Panx-1 EL1 Steric Interaction [cited 2019 Jan 21]; [1 screen]. Available from: <https://pymol.org/2/>
49. PyMOL [Internet]. [Mannheim, Germany: Schrodinger]; 2018: PyMOL: A Molecular Visualization Program Towards Bio-Molecular Systems, CBX-Panx-1 EL1 Interaction [cited 2019 Jan 21]; [1 screen]. Available from: <https://pymol.org/2/>
50. SACS [Internet]. [San Francisco, Ca: University of California San Francisco]; 2015. SACS: Transmembrane Prediction Site, TMHMM2.0 User's guide; [cited 2018 March 19]; [1 screen]. Available from: <http://www.cbs.dtu.dk/services/TMHMM/>
51. Tmpred [Internet]. [Lausanne, Switzerland: Swiss Institute of Bioinformatics]; 2017. Tmpred: Prediction of Transmembrane Regions and Orientation, Tmpred output for Pannexin-1; [cited 2018 Mar 19]; [1 screen]. Available from: https://embnet.vital-it.ch/software/TMPRED_form.html
52. Nugent Timothy, Jones T. David. Transmembrane protein topology prediction using support vector machines. *BMC Bioinformatics*. 2009-[cited 2018 March]. Available from: <https://bmcbioinformatics.biomedcentral.com/articles/10.1186/1471-2105-10-159>
53. Wang Shen, Weng Shunyan, Ma Jianzhu, Tang Qingming. DeepSCF-D: Predicting Protein Order/Disorder Regions by Weighted Deep Convolution Neural Fields. *Int J Mol Sci*. 2015-[cited 2018 March]. Available from: <https://www.ncbi.nlm.nih.gov/pmc/articles/PMC4581195/>
54. Z. Dosztanyi. Prediction of protein disorder based on IUPred. *Protein Sci*. 2018-[cited 2018 March 18]. Available from: <https://www.ncbi.nlm.nih.gov/pubmed/29076577>

55. Oldfield C., Dunker A. Keith. (2014). Intrinsically Disordered Proteins and Intrinsically Disordered Protein Regions. Annual Review of Biochemistry. 2014-[cited 2018 March 18]. Available from: <https://www.annualreviews.org/doi/abs/10.1146/annurev-biochem-072711-164947>

56. Lakoucheva M. Lilia, Brown J. Celeste, Lawson J. David, Obradovic Zoran, Dunker A. Keith. Intrinsic Disorder in Cell-signaling and Cancer-associated Proteins, Journal of Molecular Biology. Oct-2002-[cited 2018 March 18]. Available from: <https://www.sciencedirect.com/science/article/pii/S0022283602009695?via%3Dihub>

57. OMIC TOOLS [Internet]. [Le-Petit-Quevily, France: omicX | Seine Innopolis]; 2018. SOSUI: Transmembrane helix prediction: Membrane protein analysis: [cited 2018 March 18]; [1 screen]. Available from: <https://omictools.com/sosui-tool>

58. SACS [Internet]. [San Francisco, Ca: University of California San Francisco]; 2015. SACS: Transmembrane Prediction Site, SACS; [cited 2018 March 18]; [1 screen]. Available from: <http://www.sacs.ucsf.edu/Links/transmem.html>

59. Silverstein P. Todd. The Real Reason Why Oil and Water Don't Mix. Journal of Chemical Education. 1998-[cited 2018 March 18]. Available from: <https://www.docdroid.net/EnMrRWi/the-real-reason-why-oil-and-water-dont-mix.pdf#page=3>

60. Tmpred [Internet]. [Lausanne, Switzerland: Swiss Institute of Bioinformatics]; 2017. TMpred: Prediction of Transmembrane Regions and Orientation, TMpred Parameters; [cited 2018 Mar 19]; [1 screens]. Available from: https://embnet.vital-it.ch/software/TMPRED_form.html

61. Petsko A. Gregory, Ringe Dagmar. Protein Structure and Function [Internet]. London (UK): New Science Press Ltd.; 2004. Membrane Protein Structure; [cited 2018 March 17]; [1 p.]. Available from: https://books.google.com/books?id=bCI5u_19N_oC&pg=PA25&lpg=PA25&dq=helix+edge+strand+non+edge+strand&source=bl&ots=aF4aF0mYKd&sig=fNWGkxtxioPamWNP-1gmjAgOXHI&hl=en&sa=X&ved=0ahUKEwiBx7WtouXZAhVRxVkKHRCRCe0Q6AEIWDA

[#v=onepage&q=helix%20edge%20strand%20non%20edge%20strand&f=false](#)

62. Chen M. Kuang-Yui, Sun Jiaming, Salvo S. Jason, Baker David, Barth Patrick. High Resolution Modeling of Transmembrane Helical Protein Structures from Distant Homologues. *Plos Comput Biol.* 2014-[cited 2018 March 17]. Available from: <https://www.ncbi.nlm.nih.gov/pmc/articles/PMC4031050/>
63. PyMOL [Internet]. [Mannheim, Germany: Schrodinger]; 2018: PyMOL: A Molecular Visualization Program Towards Bio-Molecular Systems, align2.ali alignment A-chain [cited 2019 Oct 4]; [1 screen]. Available from: <https://pymol.org/2/>
64. Grosdidier Aurelien, Zoete Vincent, Michielin Olivier. SwissDock, a protein-small docking web service based on EADock DSS. *Nucleic Acid Research* [Internet]. Jul 1 2011-[cited 2018 Nov 28]. Available from: <https://www.ncbi.nlm.nih.gov/pmc/articles/PMC3125772/>
65. Ma Jianzhu. Software [Internet]. La Jolla (Ca): UCSD, Biomedical Research Facility; 2016 May 24 [updated 2016 March 14; cited 2018 March 17]. Available from: <http://ttic.uchicago.edu/~majianzhu/software.html>
66. Wang Junjie, Ma Meiyun, Locovei Silviu, Keane W. Robert, Dahl Gerhard. Modulation of membrane channel currents by gap junction protein mimetic peptides: size matters. *American Journal of Physiology Cell Physiology* [Internet]. 2007 Sep 1-[cited 2018 Nov 17]. Available from: https://www.physiology.org/doi/full/10.1152/ajpcell.00097.2007?url_ver=Z39.88-2003&rfr_id=ori%3Arid%3Acrossref.org&rfr_dat=cr_pub%3Dpubmed
67. [Sequence composition of the first extracellular loops of Panx1 and Panx3][illustration]. [NY, USA]: [Rockefeller University Press]; 2016. 1 illustration: color.
68. Willebrords Joost, Maes Michael, Yanguas Crespo Sara, Vinken Mathieu. Inhibitors of connexin and pannexin channels as potential therapeutics. *Pharmacol Ther.* [Internet]. 2017 Jul 15-[cited 2018 Nov 15]. Available from: <https://www.ncbi.nlm.nih.gov/pmc/articles/PMC5802387/>

69. Wang Junjie, Jackson George David, Dahl Gerhard. The food dye FD&C Blue No. 1 is a selective inhibitor of the ATP release channel Panx1. JGP Journal of General Physiology [Internet]. 2013 May-[cited 2018 Nov 14]. Available from: <https://www.ncbi.nlm.nih.gov/pmc/articles/PMC3639576/>
70. Silverman William, Locovei Silviu, Dahl Gerhard. Probenecid, a gout remedy, inhibits pannexin 1 channels. American Journal Physiology Cell Physiology [Internet]. 2008 Sep-[cited 2018 Nov 14]. Available from: <https://www.ncbi.nlm.nih.gov/pmc/articles/PMC2544448/>
71. PyMOL [Internet]. [Mannheim, Germany: Schrodinger]; 2018: PyMOL: A Molecular Visualization Program Towards Bio-Molecular Systems, Pannexin1 FASTA Model Pore-Size [cited 2018 April 25]; [1 screen]. Available from: <https://pymol.org/2/>
72. PyMOL [Internet]. [Mannheim, Germany: Schrodinger]; 2018: PyMOL: A Molecular Visualization Program Towards Bio-Molecular Systems, Pannexin1 FASTA Model Pore-Size [cited 2018 April 25]; [1 screen]. Available from: <https://pymol.org/2/>
73. PyMOL [Internet]. [Mannheim, Germany: Schrodinger]; 2018: PyMOL: A Molecular Visualization Program Towards Bio-Molecular Systems, Monomer vs. FASTA Pannexin-1 Models, Extracellular View [cited 2019 Oct 11]; [1 screen]. Available from: <https://pymol.org/2/>
74. PyMOL [Internet]. [Mannheim, Germany: Schrodinger]; 2018: PyMOL: A Molecular Visualization Program Towards Bio-Molecular Systems, Pannexin1 FASTA Model Side-View [cited 2018 April 25]; [1 screen]. Available from: <https://pymol.org/2/>
75. OMIC TOOLS [Internet]. [Le-Petit-Quevily, France: omicX | Seine Innopolis]; 2018. SOSUI: Transmembrane helix prediction: SOSUI Parameters: [cited 2019 Oct 2]; [1 screen]. Available from: http://harrier.nagahama-i-bio.ac.jp/sosui/sosui_submit.html
76. GalaxyWEB [Internet]. [Seoul, Republic of Korea: Seoul National University]; 2018. GalaxyWEB Homo Oligomer, Pannexin1 FASTA Prediction; [cited 2018 April 24]; [1 screen]. Available from: <http://galaxy.seoklab.org>

77. Tmpred [Internet]. [Lausanne, Switzerland: Swiss Institute of Bioinformatics]; 2017. TMpred: Prediction of Transmembrane Regions and Orientation, TMpred output for Connexin26; [cited 2018 Mar 19]; [1 screens]. Available from: https://embnet.vital-it.ch/software/TMPRED_form.html
78. GalaxyWEB [Internet]. [Seoul, Republic of Korea: Seoul National University]; 2018. GalaxyWEB Homo Oligomer, Pannexin1 Input Monomer Prediction; [cited 2018 April 24]; [1 screen]. Available from: <http://galaxy.seoklab.org>
79. PyMOL [Internet]. [Mannheim, Germany: Schrodinger]; 2018: PyMOL: A Molecular Visualization Program Towards Bio-Molecular Systems, Monomer vs. FASTA Pannexin-1 Models, Side View [cited 2019 Oct 11]; [1 screen]. Available from: <https://pymol.org/2/>
80. PyMOL [Internet]. [Mannheim, Germany: Schrodinger]; 2018: PyMOL: A Molecular Visualization Program Towards Bio-Molecular Systems, Monomer vs. FASTA Pannexin-1 Models, Cytoplasmic View [cited 2019 Oct 11]; [1 screen]. Available from: <https://pymol.org/2/>
81. PyMOL [Internet]. [Mannheim, Germany: Schrodinger]; 2018: PyMOL: A Molecular Visualization Program Towards Bio-Molecular Systems, Monomer vs. FASTA Pannexin-1 Models, TM1, EL1 [cited 2019 Oct 11]; [1 screen]. Available from: <https://pymol.org/2/>
82. Phyre2 [Internet]. [London, UK: Imperial College]; 2018. PROMALS: web portal for protein modeling, prediction analysis, Innexin-6 transmembrane helices topology prediction; [cited 2018 April 12]; [1 screens]. Available from: <http://www.sbg.bio.ic.ac.uk/phyre2/html/page.cgi?id=index>
83. Clustal Omega [Internet]. [Cambridgeshire, UK: EMBL-EBI]; 2018. Clustal Omega: A Knowledge Resource for Biomedical Sciences, CLUSTAL Panx3 Multiple Template Alignment; [cited 2019 Sep 27]; [1 screen]. Available from: <https://www.ebi.ac.uk/Tools/psa/>
84. NCBI [Internet]. [Bethesda, MD: National Library of Medicine]; 2017. NCBI: A Knowledge Resource for Biotechnology Information (NCBI), PSI-BLAST Alignments; [cited 2019 Sep 23]; [6 screens]. Available from: <https://blast.ncbi.nlm.nih.gov/Blast.cgi>

85. MODELLER [Internet]. [San Francisco, California: UCSF]; 2014. Modeller: A Knowledge Resource Towards 3-D Protein Homology or Comparative Modeling, Protein structure modeling with MODELLER; [cited 2018 March 21]; [30 pages]. Available from: https://salilab.org/pdf/Webb_MethodsInMolBiol_2013.pdf
86. Phyre² [Internet]. [London, UK: Imperial College]; 2018. PROMALS: web portal for protein modeling, prediction analysis, c5h5pA Alignment; [cited 2019 Sep 24]; [1 screens]. Available from: <http://www.sbg.bio.ic.ac.uk/phyre2/html/page.cgi?id=index>
87. Phyre² [Internet]. [London, UK: Imperial College]; 2018. PROMALS: web portal for protein modeling, prediction analysis, Connexin26 transmembrane helices topology prediction; [cited 2018 Mar 21]; [1 screens]. Available from: <http://www.sbg.bio.ic.ac.uk/phyre2/html/page.cgi?id=index>
88. OMIC TOOLS [Internet]. [Le-Petit-Quevilly, France: omicX | Seine Innopolis]; 2018. SOSUI: Transmembrane helix prediction: SOSUI Connexin26 Result: [cited 2018 March 21]; [1 screen]. Available from: http://harrier.nagahama-i-bio.ac.jp/sosui/sosui_submit.html
89. RaptorX [Internet]. [Chicago, Il: Toyota Technological Institute at Chicago]; 2012. RatporX: protein structure prediction server, Section II. Connexin26 Summary Prediction Results; [cited 2018 Mar 21]; [4 screens]. Available from: http://raptorx.uchicago.edu/StructurePrediction/myjobs/73868546_309294/
90. Chiu Yu-Hsin, Medina B. Christopher, Leonhardt A. Susan, Kiessling Volker, Bennett C. Brad, Jin Xueyao, Shu Shaofang, Tamm K. Lukas, Yeager Mark, Ravichandran S. Kodi, Bayliss A. Douglas. A quantized mechanism for activation of pannexin channels. Nat Commun. 2017 Jan-[cited 2017 Oct 26]. Available from: <https://www.ncbi.nlm.nih.gov/pmc/articles/PMC5290276/>
91. Coddou Claudio, Yan Zonghe, Obsil Tomas, Toro-Huidobro J. Pablo, Stojikovic S. Stanko. Activation and Regulation of Purinergic P2X Receptor Channels. Pharmacol Rev. 2011 Sep-[cited 2017 Oct 29]. Available from: <https://www.ncbi.nlm.nih.gov/pmc/articles/PMC3141880/>

92. Erb Laurie, Weisman A. Gary. Coupling of P2Y receptors to G proteins and other signaling pathways. Wiley Interdiscip Rev Membr Transp Signal. 2012 Nov-Dec-[cited 2017 Oct 29]. Available from: <https://www.ncbi.nlm.nih.gov/pmc/articles/PMC4358762/>
93. Jones R. Karlie, Choi Uimook, Gao Ji-Lang, Thompson D. Robert, Rodman E. Larry, Malech L. Harry, Kang M. Elizabeth. A Novel Method for Screening Adenosine Receptor Specific Agonists for Use in Adenosine Drug Development. Sci Rep. 2017 Mar-[cited 2017 Oct 30]. Available from: <https://www.ncbi.nlm.nih.gov/pmc/articles/PMC5357845/>
94. Pirrainen Henni, Ashok Yaswanth, Nanekar T. Rahul, Jaakola Pekka-Veli. Structural features of adenosine receptors; From crystal to function. Biochimica et Biophysica Acta. 2011 May-[cited 2017 Oct 30]. Available from: <http://www.sciencedirect.com/science/article/pii/S0005273610001707>
95. [3-D A2A Receptor:Antagonist ZM241385 complex][illustration]. [Amsterdam, Netherlands]: [Elsevier]; 2011. 1 illustration: color.
96. [Structural Details of A2A Receptor:Antagonist ZM241385][illustration]. [Amsterdam, Netherlands]: [Elsevier]; 2011. 1 illustration: color.
97. Phyre² [Internet]. [London, UK: Imperial College]; 2018. PROMALS: web portal for protein modeling, prediction analysis, Detailed Template Information; [cited 2019 Sep 24]; [1 screens]. Available from: <http://www.sbg.bio.ic.ac.uk/phyre2/html/page.cgi?id=index>
98. ALDRICH Materials Science. POLYMERIC DRUG DELIVERY TECHNIQUES Translating Polymer Science for Drug Delivery. [Internet]. 2015-[cited 2017 Nov 10]. Available from: <https://www.sigmaaldrich.com/materials-science/drug-delivery/drug-delivery-welcome.html>
99. Freitas A., Robert, Nanomedicine, Volume I: Basic Capabilities [Internet]. Landes Bioscience, Georgetown, TX, c1999. Chapter 4.2.9, Diagnosis; [cited 2017 Nov 11]; [about 2 screens]. Available from: <http://kriorus.ru/sites/kriorus/files/nanomed/NANOMEDI.PDF>

100. MacCallum L. Justin, Bennet W.F. Drew, Tieleman D. Peter. Distribution of Amino Acids in a Lipid Bilayer from Computer Simulations. *Biophysics Journal*. 2008-[cited 2019 July 30]. Available from: <https://www.ncbi.nlm.nih.gov/pmc/articles/PMC2292383/>
101. Penuela Silvia, Harland Luke, Simek Jamie, Laird W. Dale. Pannexin channels and their links to human disease. *Biochem*. 2014-[cited 2019 Aug 1]. Available from: <https://login.proxy.libraries.rutgers.edu/login?url=http://www.biochemj.org%2fcontent%2f461%2f3%2f371>
102. ViPR [Internet]. [place unknown: publisher unknown]; 2016. NIAID Virus Pathogen Database and Analysis Resource (ViPR), HIV; 2017 Oct 21 [cited 2017 Nov 13]; [1 webpage]. Available from: https://www.viprbrc.org/brc/antiviralDrug_search.spg?method=ShowCleanSearch&decorator=reo
103. Viral Zone [Internet]. [Geneve 4, Switzerland: SwissProt group]; 2011. Viralzone: A Knowledge Resource to Understand Virus Diversity (Viral Zone), Virus Fact Sheet, HIV Resource; [cited 2017 Nov 13]; [1 webpage]. Available from: <https://viralzone.expasy.org/4976>
104. PDB [Internet]. [Piscataway, NJ; La Jolla, Ca: Rutgers, SDSC]; 2017. PDB: A Knowledge Resource to Understand Biological Macromolecular Structures (PDB), Pannexin-1; [cited 2017 Nov 13]; [1 webpage]. Available from: <http://www.rcsb.org/pdb/protein/Q96RD7>
105. PDB [Internet]. [Piscataway, NJ; La Jolla, Ca: Rutgers, SDSC]; 2018. PDB: A Knowledge Resource to Understand Biological Macromolecular Structures (PDB), Connexin26 Sequence; [cited 2019 July 29]; [1 screens]. Available from: <https://www.rcsb.org/pdb/explore/remediatedSequence.do?structureId=2ZW3>
106. UniProt [Internet]. [Oxford, UK: University of Oxford]; 2018. UniProt Consortium: A Knowledge Resource for Proteins (SIB), Connexin26 Topology; [cited 2019 July 29]; [1 screen]. Available from: <https://www.uniprot.org/uniprot/P29033>
107. Barbe T. Michael, Monyer Hannah, Bruzzone Roberto. Cell-Cell Communication Beyond Connexins: The Pannexin Channels. *Physiology*. 2106-[cited 2019 Aug 4]. Available from:

<https://www.physiology.org/doi/full/10.1152/physiol.00048.2005>

108. Sosinsky E. Gina, Boassa Daniela, Dermietzel Rolf, Duffy S. Heather, Laird W. Dale, MacVicar Brian, Naus C. Christian, Penuela Silvia, Scemes Eliana, Spray C. David, Thompson J. Roger, Zhao Hong-Bo, Dahl Gerhard. Pannexin channels are not gap junction hemichannels. Channels. 2011-[cited 2019 Aug 4]. Available from: <https://www.ncbi.nlm.nih.gov/pmc/articles/PMC3704572/>

109. Penuela Silvia, Bhalla Ruchi, Gong Xiang-Qun, Cowan N. Kyle, Celetti J. Steven, Cowan J. Bryce, Bai Donglin, Shao Qing, Laird W. Dale. Pannexin 1 and pannexin 3 are glycoproteins that exhibit many distinct characteristics from the connexin family of gap junction proteins. Journal of Cell Science. 2007-[cited 2019 Aug 4]. Available from: <https://jcs.biologists.org/content/120/21/3772>

110. UniProt [Internet]. [Oxford, UK: University of Oxford]; 2018. UniProt Consortium: A Knowledge Resource for Proteins (SIB), Pannexin-1 Topology; [cited 2018 March 17]; [1 screen]. Available from: <https://www.uniprot.org/uniprot/Q96RD7>

111. Phyre² [Internet]. [London, UK: Imperial College]; 2018. Phyre²: web portal for protein modeling, prediction analysis, Panx1-5H1Q Alignment; [cited 2019 Sep 24]; [1 screen]. Available from: <http://www.sbg.bio.ic.ac.uk/phyre2/html/page.cgi?id=index>

112. Phyre² [Internet]. [London, UK: Imperial College]; 2018. PROMALS: web portal for protein modeling, prediction analysis, Pannexin-1 transmembrane helices topology prediction; [cited 2018 Mar 17]; [1 screens]. Available from: <http://www.sbg.bio.ic.ac.uk/phyre2/html/page.cgi?id=index>

113. NCBI [Internet]. [Bethesda, MD: National Library of Medicine]; 2017. NCBI: A Knowledge Resource for Biotechnology Information (NCBI), FASTA Chain A, Predicted amidohydrolase, dihydroorotase family, 3CJP_A; [cited 2019 Sep 23]; [1 screen]. Available from: https://www.ncbi.nlm.nih.gov/protein/3CJP_A?report=fasta

114. NCBI [Internet]. [Bethesda, MD: National Library of Medicine]; 2017. NCBI: A Knowledge Resource for Biotechnology Information (NCBI), FASTA Chain A, DNA polymerase Lambda, 1NZP_A; [cited 2019 Sep 23]; [1 screen]. Available from: https://www.ncbi.nlm.nih.gov/protein/1NZP_A?report=fasta
115. PROMALS3D [Internet]. [Place Unknown: Publisher Unknown]; 2018. PROMALS: A Multiple Sequence and Structure Alignment Server, Innexin6-Pannexin-1 PROMALS3D Alignment; [cited 2019 Oct 1]; [1 screen]. Available from: <http://prodata.swmed.edu/promals3d/promals3d.php>
116. UniProt [Internet]. [Oxford, UK: University of Oxford]; 2018. UnitProt Consortium: A Knowledge Resource for Proteins (SIB), Innexin-6 Topology; [cited 2018 April 12]; [1 screen]. Available from: <http://www.uniprot.org/uniprot/Q9U3N4>
117. PROMALS Multiple Sequence and Structure Alignment Server [Internet]. [Place Unknown: Publisher Unknown]. 2007. PROMALS3D Multiple Sequence and Structure Alignment Server; [cited 2018 Mar 15]; [1 screen]. Available from: http://prodata.swmed.edu/promals3d/info/promals3d_help.html
118. Zaki Al Ajlan, Hui Z. James, Higbee Elizabeth, Tsourkas Andrew. Biodistribution, Clearance, and Toxicology of Polymeric Micelles Loaded with 0.9 or 5 nm Gold Nanoparticles. J Biomed Nanotechnol. 2105-[cited 2017 Nov 24]. Available from: <https://www.ncbi.nlm.nih.gov/pmc/articles/PMC4942304/>
119. NCBI [Internet]. [Bethesda, MD: National Library of Medicine]; 2017. NCBI: A Knowledge Resource for Biotechnology Information (NCBI), FASTA Chain A, Long-tail Fiber Proximal Subunit, 5NXH_A; [cited 2019 Sep 23]; [1 screen]. Available from: https://www.ncbi.nlm.nih.gov/protein/1NZP_A?report=fasta
120. Clustal Omega [Internet]. [Cambridgeshire, UK: EMBL-EBI]; 2018. Clustal Omega: A Knowledge Resource for Biomedical Sciences, CLUSTAL Panx1-Inx6 Single Template Alignment; [cited 2019 Oct 1]; [1 screen]. Available from: <https://www.ebi.ac.uk/Tools/psa/>

121. Leman Koehler Julia, Ulmschneider B. Martin, Gray J. Jeffrey. Computational Modeling of Membrane Proteins. Proteins. 2105-[cited 2018 March 15]. Available from: <https://www.ncbi.nlm.nih.gov/pmc/articles/PMC4270820/>
122. Dror Ron. Protein Structure Prediction [slides]. [place unknown: publisher unknown]; 2017. 53 slides: color with black & white.
123. Bioinformatics Tools: Sequence Alignment. Bates [Internet]. [place unknown]: BATES; c2017 [cited 2018 Mar 15]. Available from: <http://libguides.bates.edu/?b=s>
124. Freitas A., Robert, Nanomedicine, Volume I: Basic Capabilities [Internet]. Landes Bioscience, Austin, TX, c1999. Chapter 5.2.1 Free-Floating Solitary Nanodevices; [cited 2017 Dec 31]; [1 screen]. Available from: <http://kriorus.ru/sites/kriorus/files/nanomed/NANOMEDI.PDF>
125. NCBI [Internet]. [Bethesda, MD: National Library of Medicine]; 2017. NCBI: A Knowledge Resource for Biotechnology Information (NCBI), blastp Result; [cited 2019 Oct 1]; [1 screens]. Available from: <https://blast.ncbi.nlm.nih.gov/Blast.cgi>
126. PyMOL [Internet]. [Mannheim, Germany: Schrodinger]; 2018: PyMOL: A Molecular Visualization Program Towards Bio-Molecular Systems, Mimetic ¹⁰Panx1 bound to the Pannexin-1 Pore Region [cited 2019 Jan 21]; [1 screen]. Available from: <https://pymol.org/2/>
127. NCBI [Internet]. [Bethesda, MD: National Library of Medicine]; 2017. NCBI: A Knowledge Resource for Biotechnology Information (NCBI), FASTA Chain A, Large Tail Fiber Protein P34, 4UXF_A; [cited 2019 Sep 23]; [1 screen]. Available from: https://www.ncbi.nlm.nih.gov/protein/4UXF_A?report=fasta
128. NCBI [Internet]. [Bethesda, MD: National Library of Medicine]; 2017. NCBI: A Knowledge Resource for Biotechnology Information (NCBI), FASTA Chain A, 3d Polymerase, 4Y3C_A; [cited 2019 Sep 23]; [1 screen]. Available from: https://www.ncbi.nlm.nih.gov/protein/4Y3C_A?report=fasta

129. UniProt [Internet]. [Oxford, UK: University of Oxford]; 2018. UniProt Consortium: A Knowledge Resource for Proteins (SIB), Connexin26 Topology; [cited 2018 March 20]; [1 screen]. Available from: <https://www.uniprot.org/uniprot/P29033>
130. Baek Minkyung, Park Taeyong, Heo Lim, Park Chiwook, Seok Chaok. GalaxyHomomer: a web server for protein homo-oligomer structure prediction from a monomer sequence or structure. *Nucleic Acids Res.* 2017-[cited 2018 April 20]. Available from: <https://www.ncbi.nlm.nih.gov/pmc/articles/PMC5570155/>
131. Pierce Brian, Tong Weiwei, Weng Zhiping. M-ZDOCK: a grid-based approach for Cn symmetric multimer docking, *Bioinformatics*. 2005-[cited 2018 April 28]. Available from: <https://academic.oup.com/bioinformatics/article/21/8/1472/250889><https://academic.oup.com/bioinformatics/article/21/8/1472/250889>
132. Phyre² [Internet]. [London, UK: Imperial College]; 2018. PROMALS: web portal for protein modeling, prediction analysis, View PSI-Blast Multiple Sequence Alignment; [cited 2019 Sep 23]; [1 screens]. Available from: <http://www.sbg.bio.ic.ac.uk/phyre2/html/page.cgi?id=index>
133. NCBI [Internet]. [Bethesda, MD: National Library of Medicine]; 2017. NCBI: A Knowledge Resource for Biotechnology Information (NCBI), Non-Redundant Result; [cited 2019 Sep 23]; [1 screen]. Available from: <https://blast.ncbi.nlm.nih.gov/Blast.cgi>
134. Phyre² [Internet]. [London, UK: Imperial College]; 2018. PROMALS: web portal for protein modeling, prediction analysis, Phyre² Parameters; [cited 2018 Mar 17]; [2 screens]. Available from: <http://www.sbg.bio.ic.ac.uk/phyre2/html/page.cgi?id=index>
135. Worth L. Catherine, Gong Sungsam, Blundell L. Tom. Structural and functional constraints in the evolution of protein families. *Nature Reviews Molecular Cell Biology*. 2009-[cited 2019 Sep 23]. Available from: <https://www.researchgate.net/publication/26813852> Structural and functional constraints in the evolution of protein families

136. Kelley A. Lawrence, Mezulis Stefans, Yates MM. Christopher, Wass N. Mark, Sternberg J.E. Michael. The Phyre2 web portal for protein modeling prediction and analysis. Nature protocols. 2015-[cited 2019 Sep 23]. Available from: <https://www.nature.com/articles/nprot.2015.053>
137. Subach, Joel. Multiple Template Alignment [Internet]. Message to Venkat Reddy. 2019 Sep 5 [cited 2019 Sep 23]. [1 paragraphs].
138. Sali Andrej, Modeller, Program for Comparative Protein Structure Modeling by Satisfaction of Spatial Restraints [Internet]. San Francisco: UCSF; 2014. selection.assess_dope() -- assess a model selection with the DOPE method; 2009 June 12 [cited 2018 Feb 10]; [1 screen]. Available from: <https://salilab.org/modeller/9v7/manual/node242.html>
139. Sali Andrej, Modeller, Program for Comparative Protein Structure Modeling by Satisfaction of Spatial Restraints [Internet]. San Francisco: UCSF; 2014. Tutorial, 4. Model Building and 5. Model Evaluation; 2014 March 7 [cited 2018 Feb 10]; [about 2 screens]. Available from: <https://salilab.org/modeller/tutorial/basic.html>
140. Sali Andrej, Modeller, Program for Comparative Protein Structure Modeling by Satisfaction of Spatial Restraints [Internet]. San Francisco: UCSF; 2014. Documentation, Modeling with cryo-EM, Step 5: Assess the quality of the models; 2010 Sep 27 [cited 2018 Feb 10]; [1 screen]. Available from: <https://salilab.org/modeller/tutorial/cryoem/assess.html>
141. Sali Andrej, Modeller, Program for Comparative Protein Structure Modeling by Satisfaction of Spatial Restraints [Internet]. San Francisco: UCSF; 2014. model.assess_ga341() -- assess a model with the GA341 method; 2010 Sep 27 [cited 2012 Aug 29]; [1 screen]. Available from: <https://salilab.org/modeller/9.11/manual/node197.html>
142. Sali Andrej, Modeller, Program for Comparative Protein Structure Modeling by Satisfaction of Spatial Restraints [Internet]. San Francisco: UCSF; 2014. Model building, “model-single.log” file; 2018 Feb 13 [cited 2018 Feb 15]; [1 screen].

143. The Audiopedia. What is Loop Modeling [video]. Youtube; 2017. 1 video: 6:19 sec., sound, color. <https://www.youtube.com/watch?v=OI6hmcg4yt8>
144. NCBI [Internet]. [Bethesda, MD: National Library of Medicine]; 2017. NCBI: A Knowledge Resource for Biotechnology Information (NCBI), PSI-BLAST Result; [cited 2019 Sep 23]; [1 screens]. Available from: <https://blast.ncbi.nlm.nih.gov/Blast.cgi>
145. PDB [Internet]. [Piscataway, NJ; La Jolla, Ca: Rutgers, SDSC]; 2018. PDB: A Knowledge Resource to Understand Biological Macromolecular Structures (PDB), Connexin26 FASTA; [cited 2018 Mar 15]; [5 screens]. Available from: <https://www.rcsb.org/structure/2ZW3>
146. Sali Andrej, Modeller, Program for Comparative Protein Structure Modeling by Satisfaction of Spatial Restraints [Internet]. San Francisco: UCSF; 2019. Alignment file format; 2006 Feb 28 [cited 2019 July 27]; [1 screen]. Available from: <https://salilab.org/modeller/8v2/manual/node176.html>
147. Linqing Li, Weiwei Xu, Qiang Lu. Improving protein-ligand docking with flexible interfacial water molecules using SWRosetta Ligand. Journal of Molecular Modeling. 2005- [cited 2019 June 19]. Available from: <https://link.springer.com/article/10.1007%2Fs00894-015-2834-7>
148. Sali Andrej, Modeller, Program for Comparative Protein Structure Modeling by Satisfaction of Spatial Restraints [Internet]. San Francisco: UCSF; 2014. Tutorial, 4. Model Building, Input; 2019 March 15 [cited 2019 June 23]; [about 1 screen]. Available from: <https://salilab.org/modeller/tutorial/basic.html>
149. Modeller [Internet]. San Fransisco: UCSF; 2019- .Comparative Modeling, Multiple Template Modeling; [cited 2019 June 24]; [about 1 screen].
150. Modeller [Internet]. San Fransisco: UCSF; 2019- .Input Alignment File, Multiple Template Modeling; [cited 2019 June 24]; [about 1 screen].

151. Sali Andrej, Modeller, Program for Comparative Protein Structure Modeling by Satisfaction of Spatial Restraints [Internet]. San Francisco: UCSF; 2014. Tutorial, 4. Multiple Template Modeling, Input; 2019 March 15 [cited 2019 June 25]; [about 1 screen]. Available from: <https://salilab.org/modeller/tutorial/advanced.html>
151. Subach, Joel. Multiple Sequence Alignment [Illustration]. USA, Joel Subach; 2019. 1 illustration; color.
152. [Transmembrane Topology, 'Out and In Orientations'] [Illustration]. [AAAI]: [ISMB-96 Proceedings]; 1996. 1 illustration: black and white.
153. [Transmembrane Positioning, Inclination and Compressibility] [Illustration]. [Oxford University Press]: [PEDS]; 2016. 1 illustration: color.
154. Subach, Joel. Modeller Modeling Question [Internet]. Message to: Venkat Reddy. 2019 June [cited 2019 June 26]. [1 paragraph].
155. CourseHero [Internet]. [place unknown: publisher unknown]; 2019-[cited 2019 Sep 8]. Available from: <https://www.coursehero.com/file/22698941/Gen-Lab-Questions/>
156. Heijine von Gunnar. Membrane-protein topology. Nature Reviews Molecular Cell Biology. 2006-[cited 2019 June 30]. Available from: <http://people.umass.edu/bioch623/623/Second.Section/11.%20vonheijne.pdf>
157. Yamaguchi Hiroshi, Muth N. James, Varadi Maria, Schwartz Arnold, Varadi Gyula. Critical role of conserved proline residues in the transmembrane segment 4 voltage sensor function and in the gating of L-type calcium channels. PNAS. 1999-[cited 2019 June 30]. Available from: <https://www.pnas.org/content/96/4/1357>
158. Structural Bioinformatics: Practical Guide [Internet]. [Lund, Sweden: Lund University]; 2019. Department of Biochemistry and Structural Biology, Salam Al-Karadaghi; [cited 2019 June 30]; [3 webpages]. Available from: <https://proteinstrutures.com/Structure/Structure/amino-acids.html>

159. [Three Pannexin Family Members][illustration]. [Amsterdam, Netherlands]: [Elsevier]; 2013. 1 illustration: color.
160. Webb Benjamin, Sali Andrej. Comparative Structure Modeling Using MODELLER. *Curr Protoc Bioinformatics*. 2016 June-[cited 2019 July 20]. Available from: <https://www.ncbi.nlm.nih.gov/pmc/articles/PMC5031415/>
161. Marti-Renom A. Marc, Stuaart C. Ashley, Fiser Andras, Sanchez Roberto, Melo Francisco, Sali Andrej. Comparative Protein Structure Modeling Of Genes And Genomes. *Annu. Rev. Biophys. Biomol. Struct.*. 2000-[cited 2019 July 21]. Available from: https://salilab.org/pdf/Marti-Renom_AnnuRevBiophysBiomolStruct_2000.pdf
162. Andras Fiser, Gian Do Kinh Richard, Sali Andrej. Modeling of loops in protein structures. *Protein Science*. 2000-[cited 2019 July 22]. Available from: <https://www.ncbi.nlm.nih.gov/pmc/articles/PMC2144714/pdf/11045621.pdf>
163. Fushiki Daisuke, Hamada Yasuo, Yoshimura Ryoichi, Endo Yasuhisa. Phylogenetic and bioinformatics analysis of gap junction-related proteins, innexins, pannexins and connexins. *Biomedical Research*. 2010-[cited 2019 July 25]. Available from: https://www.jstage.jst.go.jp/article/biomedres/31/2/31_2_133/pdf/-char/en
164. InterPro [Internet]. [Cambridgeshire, Uk; EMBL-EBI]; 2019. InterPro: Protein sequence analysis & classification, Innexin; [cited 2019 July 25]; [1 webpage]. Available from: <https://www.ebi.ac.uk/interpro/entry/IPR000990>
165. Bhalla-Gehi Ruchi, Penuela Silvia, Churko M. Jared, Shao Qing, Laird W. Dale. Pannexin1 and Pannexin3 Delivery, Cell Surface Dynamics, and Cytoskeletal Interactions. *JBC*. 2010-[cited 2019 Aug 4]. Available from: <https://www.ncbi.nlm.nih.gov/pmc/articles/PMC2838334/>
166. Ambrosi Cinzia, Gassmann Oliver, Pranskevich N. Jennifer, Boassa Daniela, Smock Amy, Wang Junjie, Dahl Gerhard, Steinem Claudia, Sosinsky E. Gina. Pannexin1 and Pannexin2

Channels Show Quaternary Similarities to Connexons and Different Oligomerization Numbers from Each Other. *J Biol Chem*. 2010-[cited 2019 Aug 4]. Available from:

<https://www.ncbi.nlm.nih.gov/pmc/articles/PMC2915678/>

167. Locovei Silviu, Bao Li, Dahl Gerhard. Pannexin 1 in erythrocytes: Function without a gap. *PNAS*. 2006-[cited 2019 Aug 4]. Available from:

<https://www.pnas.org/content/103/20/7655>

168. Penuela Silvia, Bhalla Ruchi, Kakon Nag, Laird W. Dale. Glycosylation Regulates Pannexin Intermixing and Cellular Localization. *MBoC*. 2009-[cited 2019 Aug 4]. Available from: <https://www.molbiolcell.org/doi/10.1091/mbc.e09-01-0067>

169. Penuela Silvia, Harland Luke, Simek Jamie, Laird W. Dale. Pannexin channels and their links to human disease. *Biochemical Journal*. 2014-[cited 2019 Aug 4]. Available from: <https://www.ncbi.nlm.nih.gov/pubmed/25008946>

170. Penuela Silvia, Gehi Ruchi, Laird W. Dale. The biochemistry and function of Pannexin channels. *Biochimica et Biophysica Acta (BBA)-Biomembranes*. 2013-[cited 2019 Aug 4]. Available from: <https://www.sciencedirect.com/science/article/pii/S0005273612000211?via%3Dihub>

171. Wang Junjie, Dahl Gerhard. SCAM analysis of Panx1 suggests a peculiar pore structure. *J Gen Physiol*.. 2010-[cited 2019 Aug 5]. available from: <https://www.ncbi.nlm.nih.gov/pmc/articles/PMC2964519/>

172. Boasssa Daniela, Ambrosi Cinzia, Qiu Feng, Dahl Gerhard, Gaietta Guido, Sosinsky Gina. Pannexin1 Channels Contain a Glycosylation Site That Targets the Hexamer to the Plasma Membrane. *JBC*. 2007-[cited 2019 Aug 5]. Available from: <http://www.jbc.org/content/282/43/31733.long>

173. Bao Li, Locovei Silviu, Dahl Gerhard. Pannexin membrane channels are mechanosensitive conduits for ATP. *FEBS Letters*. 2004-[cited 2019 Aug 5]. Available from: <https://febs.onlinelibrary.wiley.com/doi/full/10.1016/j.febslet.2004.07.009>

174. Sandilos K. Joanna, Chiu Yu-Hsin, Chekeni B. Faraaz, Armstrong J. Allison, Walk F. Scott, Ravichandran S. Kodi, Bayliss A. Douglas. Pannexin 1, an ATP Release Channel, Is Activated by Caspase Cleavage of Its Pore-associated C-terminal Autoinhibitory Region. *JBC*. 2012-[cited 2019 Aug 5]. Available from: <https://www.ncbi.nlm.nih.gov/pmc/articles/PMC3322839/>
175. Murali S., Zhang M., Nurse C.A.. Evidence that 5-HT stimulates intracellular Ca^{2+} signaling and activates pannexin-1 currents in type II cells of the rat carotid body. *J Physiol*. 2017-[cited 2019 Aug 5]. Available from: <https://www.ncbi.nlm.nih.gov/pubmed/28332205>
176. Qiu Feng, Dahl Gerhard. A permeant regulating its permeation pore: inhibition of pannexin 1 channels by ATP. *APS*. 2009-[cited 2019 Aug 5]. Available from: <https://www.ncbi.nlm.nih.gov/pmc/articles/PMC2643853/>
177. Abeele Vanden Fabien, Bidaux Gabriel, Gordienko Dmitri, Beck Benjamin, Panchin V. Yuri, Baranova V. Ancha, Ivanov V. Dmitry, Skryma Roman, Prevarskaya Natalia. Functional implications of calcium permeability of the channel formed by pannexin 1. *J Cell Biol*. 2006-[cited 2019 Aug 6]. Available from: <https://www.ncbi.nlm.nih.gov/pmc/articles/PMC2064259/>
178. Segretain Dominique, Falk M. Matthias. Regulation of connexin biosynthesis, assembly, gap junction formation, and removal. *Biochimica et Biophysica Acta (BBA)- Biomembranes*. 2004-[cited 2019 Aug 10]. Available from: <https://www.sciencedirect.com/science/article/pii/S0005273604000355>
179. Atsunori Oshima, Kazutoshi Tani, Yoshinori Fujiyoshi. Atomic structure of the innexin-6 gap junction channel determined by cryo-EM. *Nature*. 2016-[cited 2019 Aug 10]. Available from: <https://www.nature.com/articles/ncomms13681>
180. UniProt [Internet]. [Oxford, UK: University of Oxford]; 2018. UniProt Consortium: A Knowledge Resource for Proteins (SIB), Connexin26 Amino Acids Modifications; [cited 2018 Aug 10]; [1 screen]. Available from: <https://www.uniprot.org/uniprot/P29033>
181. UniProt [Internet]. [Oxford, UK: University of Oxford]; 2018. UniProt Consortium: A Knowledge Resource for Proteins (SIB), Pannexin-1 Family and Domains; [cited 2019 Aug 10];

[1 screen]. Available from: https://www.uniprot.org/uniprot/Q96RD7#family_and_domains

182. Bunse Stefanie, Schmidt Matthias, Prochnow Nora, Dermietzel. Intracellular Cysteine 346 Is Essentially Involved in Regulating Panx1 Channel Activity. J Biol Chem. 2010-[cited 2019 Aug 10]. Available from: <https://www.ncbi.nlm.nih.gov/pmc/articles/PMC2992277/>

183. PDB [Internet]. [Piscataway, NJ; La Jolla, Ca: Rutgers, SDSC]; 2018. PDB: A Knowledge Resource to Understand Biological Macromolecular Structures (PDB), 5H1Q Structure Summary, Literature; [cited 2019 Aug 11]; [1 screens]. Available from: <https://www.rcsb.org/structure/5H1Q>

184. Mese Gulistan, Sellitto Caterina, Li Leping, Wang Hong-Zhan, Valiunas Virginijus, Richard Gabriele, Brink R. Peter, White W. Thomas. The Cx26-G45E mutation displays increased hemichannel activity in a mouse model of the lethal form of keratitis-ichthyosis-deafness syndrome. Mol Biol Cell. 2011-[cited 2019 Aug 11]. Available from: <https://www.ncbi.nlm.nih.gov/pmc/articles/PMC3237621/>

185. NCBI [Internet]. [Bethesda, MD: National Library of Medicine]; 2017. NCBI: A Knowledge Resource for Biotechnology Information (NCBI), Iterated profile searches with PSI-BLAST; [cited 2018 March 17]; [3 screens]. Available from: <https://www.ncbi.nlm.nih.gov/BLAST/tutorial/Altschul-2.html>

186. MedusaDock [Internet]. [place unknown: publisher unknown]; 2019. MedusaDock, New Task; [cited 2019 Aug 12]; [1 screen]. Available from: <https://dokhlab.med.psu.edu/medusadock/#/Home>

187. Bunse Stefanie, Schmidt Matthias, Hoffman Sarah, Engelhardt Kathrin, Zoidl Georg, Dermietzel Rolf. Single Cysteines in the Extracellular and Transmembrane Regions Modulate Pannexin 1 Channel Function. The Journal of Membrane Biology. 2011-[cited 2019 Aug 13]. Available from: <https://www.ncbi.nlm.nih.gov/pubmed/21938521>

188. Dahl Gerhard. ATP release through pannexon channels. PHILOSOPHICAL TRANSACTIONS B. 2015-[cited 2019 Aug 13]. Available from:

<https://www.ncbi.nlm.nih.gov/pmc/articles/PMC4455760/>

189. Li Shuo, Bjelobaba Ivana, Stojilkovic S. Stanko. Interactions of Pannexin1 channels with purinergic and NMDA receptor channels. *Biochimica et Biophysica Acta (BBA) Biomembranes*. 2018-[cited 2019 Aug 14]. Available from:

<https://www.sciencedirect.com/science/article/pii/S0005273617301098>

190. Poornima V., Madhupriya M., Kootar S., Sujatha G., Kumnar Arvind, Bera Kanti Amal. P2X₇ Receptor-Pannexin1 Hemichannel Association: Effect of Extracellular Calcium on Membrane Permeabilization. *Journal of Molecular Neuroscience*. 2012-[cited 2019 Aug 14]. Available from: <https://www.ncbi.nlm.nih.gov/pubmed/21932038>

191. Gehi Ruchi, Shao Qing, Laird W. Dale. Pathways Regulating the Trafficking and Turnover of Pannexin1 Protein and the Role of the C-terminal Domain. *JBC*. 2011-[cited 2019 Aug 14]. Available from: <http://www.jbc.org/content/286/31/27639.full>

192. Epp L. Anna, Ebert N. Sarah, Sanchez-Arias C. Juan, Wicki-Stordeur E. Leigh, Boyce K.J. Andrew, Swayne Anne Leigh. A novel motif in the proximal C-terminus of Pannexin 1 regulates cell surface localization. *Sci. Rep.*. 2019-[cited 2019 Aug 15]. Available from: <https://www.ncbi.nlm.nih.gov/pmc/articles/PMC6611761/>

193. Merriam-Webster [Internet]. Springfield, Mass.: Merriam-Webster Inc.. 2019-[cited 2019 Aug 16]. Available from: <https://www.merriam-webster.com/medical/caspase>

194. Subach, Joel. Cites of caspase 3 cleavage [Internet]. Message to Frederick Coffman. 2019 July 19 [cited 2019 Aug 16]. [1 paragraphs].

195. Lohman W. Alexander, Weiling L. Nicholas, Santos MF Silva, Bialecki Jennifer, Werner C. Allison, Anderson L. Connor, Thompson J. Roger. Regulation of pannexin channels in the central nervous system by Src family kinases. *Neuroscience Letters*. 2019-[cited 2019 Aug 16]. Available from: <https://www.sciencedirect.com/science/article/abs/pii/S030439401730753X?via%3Dihub>

196. Pogoda Kristin, Kameritsch Petra, Retamal Mauricio, Vega L. Jose. Regulation of gap junction channels and hemichannels by phosphorylation and redox changes: a revision. *BMC Molecular and Cell Biology*. 2016-[cited 2019 Aug 17]. Available from: <https://bmcmolcellbiol.biomedcentral.com/articles/10.1186/s12860-016-0099-3>
197. Bauer Reinhard, Loer Birgit, Ostrowski Katinka, Martini Julia, Weimbs Andy, Lechner Hildegard, Hoch Michael. Intercellular Communication: the *Drosophila* Innexin Multiprotein Family of Gap Junction Proteins. *Chemistry & Biology*. 2005-[cited 2019 Aug 17]. Available from: [https://www.cell.com/cell-chemical-biology/fulltext/S1074-5521\(05\)00072-4?_returnURL=https%3A%2F%2Flinkinghub.elsevier.com%2Fretrieve%2Fpii%2FS1074552105000724%3Fshowall%3Dtrue](https://www.cell.com/cell-chemical-biology/fulltext/S1074-5521(05)00072-4?_returnURL=https%3A%2F%2Flinkinghub.elsevier.com%2Fretrieve%2Fpii%2FS1074552105000724%3Fshowall%3Dtrue)
198. Michalski Kevin, Henze Erik, Nguyen Philip, Lynch Patrick, Kawate Toshimitsu. The weak voltage dependence of pannexin 1 channels can be tuned by N-terminal modifications. *JGP*. 2018-[cited 2019 Aug 17]. Available from: <https://www.ncbi.nlm.nih.gov/pmc/articles/PMC6279361/>
199. Oshima Atsunori, Tani Kazutoshi, Toloue M. Masoud, Hiroaki Yoko, Smock Amy, Inukai Sayaka, Cone Angela, Nicholson J. Bruce, Sosinsky E. Gina, Fujiyoshi Yoshinori. Asymmetric configurations and N-terminal rearrangements in connexin26 gap junction channels. *J Mol Biol*. 2012-[cited 2019 Aug 18]. Available from: <https://www.ncbi.nlm.nih.gov/pmc/articles/PMC3026138/>
200. UniProt [Internet]. [Oxford, UK: University of Oxford]; 2018. UniProt Consortium: A Knowledge Resource for Proteins (SIB), Connexin26; [cited 2018 Aug 10]; [22 screen]. Available from: <https://www.uniprot.org/uniprot/P29033>
201. UniProt [Internet]. [Oxford, UK: University of Oxford]; 2018. UniProt Consortium: A Knowledge Resource for Proteins (SIB), Innexin-6; [cited 2018 April 18]; [9 screen]. Available from: <https://www.uniprot.org/uniprot/Q9U3N4>
202. Foote C.I., Zhou L., Zhu X., Nicholson B.J.. The pattern of disulfide linkages in the extracellular loop regions of connexin 32 suggests a model for the docking interface of gap

junctions. J. Cell Biol.. 1998-[cited 2019 Aug 19]. Available from:
<http://jcb.rupress.org/content/140/5/1187.full>

203. UniProt [Internet]. [Oxford, UK: University of Oxford]; 2018. UniProt Consortium: A Knowledge Resource for Proteins (SIB), Pannexin-1; [cited 2018 Aug 20]; [11 screen]. Available from: <https://www.uniprot.org/uniprot/Q96RD7#Q96RD7-2>

204. Schubert Anne-Lane, Schubert William, Spray C. David, Lisanti P. Michael. Connexin Family Members Target to Lipid Raft Domains and Interact with Caveolin-1. Biochemistry. 2002-[cited 2019 Aug 20]. Available from: <https://www.ncbi.nlm.nih.gov/pubmed/11980479>

205. Weilinger L. Nicholas, Lohman W. Alexander, Rakai D. Brooke, Ma M.M. Evelyn, Bialecki Jennifer, Maslieieva Valentyna, Rilea Travis, Bandet V. Mischa, Ikuta T. Nathan, Colicos A. Michael, Tesket Campbell G., Winship R. Ian, Thompson J. Roger. Metabotropic NMDA receptor signaling couples Src family kinases to pannexin-1 during excitotoxicity. nature neuroscience. 2016-[cited 2019 Aug 21]. Available from:
<https://www.ncbi.nlm.nih.gov/pubmed/26854804>

206. Levit Alexander Noah. Inhibition of pathological connexin26 hemichannels implicated in keratitis-ichthyosis-deafness syndrome [dissertation]. [New York]: Stony Brook University; 2014. 115 p.

207. UniProt [Internet]. [Oxford, UK: University of Oxford]; 2018. UniProt Consortium: A Knowledge Resource for Proteins (SIB), Pannexin-1 Sequences; [cited 2018 Aug 20]; [11 screen]. Available from: <https://www.uniprot.org/uniprot/Q96RD7#Q96RD7-2>

208. UniProt [Internet]. [Oxford, UK: University of Oxford]; 2018. UniProt Consortium: A Knowledge Resource for Proteins (SIB), Innexin-6 Sequence; [cited 2018 April 18]; [9 screen]. Available from: <https://www.uniprot.org/uniprot/Q9U3N4>

209. UniProt [Internet]. [Oxford, UK: University of Oxford]; 2018. UniProt Consortium: A Knowledge Resource for Proteins (SIB), Connexin26 Sequence; [cited 2018 Aug 10]; [22 screen]. Available from: <https://www.uniprot.org/uniprot/P29033>

210. Mbaye Ndew Mame, Hou Qingzen, Basu Sankar, Teheux Fabian, Pucci Fabrizio, Rooman Marianne. A comprehensive computational study of amino acid interactions in membrane proteins. *Sci rep.* 2010-[cited 2019 Aug 25]. Available from: <https://www.ncbi.nlm.nih.gov/pmc/articles/PMC6700154/>
211. Dalbey E. Ross. Positively charged residues are important determinants of membrane protein topology. *Trends in Biochemical Sciences.* 1990-[cited 2019 Aug 25]. Available from: [https://www.cell.com/trends/biochemical-sciences/fulltext/0968-0004\(90\)90047-F](https://www.cell.com/trends/biochemical-sciences/fulltext/0968-0004(90)90047-F)
212. Ulmschneider B. Martin, Sansom S.P. Mark. Amino acid distributions in integral membrane protein structures. *Biochimica et Biophysica Acta (BBA) Biomembranes.* 2011-[cited 2019 Aug 25]. Available from: <https://www.sciencedirect.com/science/article/pii/S0005273601002991#BIB39>
213. Clustal Omega [Internet]. [Cambridgeshire, UK: EMBL-EBI]; 2018. Clustal Omega: A Knowledge Resource for Biomedical Sciences, CLUSTAL Panx1-Multiple Template Alignment; [cited 2018 Mar 15]; [1 screen]. Available from: <https://www.ebi.ac.uk/Tools/msa/clustalo/>
214. Betts M.J., Russell R.B.. *Bioinformatics for Geneticists* [Internet]. Heidelberg (Germany): Wiley; 2003-[cited 2019 Aug 27]. Available from: <http://www.russelllab.org/aas/aas.html>
215. Enngelhardt H. Kathrin. Molecular and functional characterization of communicating channels [dissertation]. [Dortmund, Germany]: Ruhr-University Bochum; 2011. 108p.
216. Pike J. Linda. Lipid rafts bringing order to chaos. *Journal of Lipid Research.* 2003-[cited 2019 Nov 20]. Available from: <http://www.jlr.org/content/44/4/655.full#:~:targetText=Lipid%20rafts%20are%20subdomains%20of,to%20extraction%20with%20nonionic%20detergents.>
217. Kurtenbach Sarah, Kurtenbach Stefan, Zoidl Georg. Emerging functions of Pannexin 1 in the eye. *Frontiers in Cellular Neuroscience.* 2014-[cited 2019 Nov 20]. Available from: <https://www.frontiersin.org/articles/10.3389/fncel.2014.00263/full>
218. Maeda Shoji, Nakagawa So, Suga Michihiro, Yamashita Eiki, Oshima Atsunori, Fujiyoshi

Yoshinori, Tsukihara Tomitake. Structure of the connexin 26 gap junction channel at 3.5 Å resolution. *Nature*. 2009-[cited 2019 Nov 21]. Available from:

<https://www.nature.com/articles/nature07869>

219. MOL PROBITY [Internet]. [Durham, NC; Dep. Biochemistry]; 2013. MOL PROBITY: structure validation, Main Page File Upload/Retrieval; [cited 2019 Nov 24]; [1 screen].

Available from: <http://molprobity.biochem.duke.edu>

220. Pail Rohan, Das Suranjana, Stanley Ashley, Yadav Lumbani, Sudhakar Akulapalli, Varma K. Ashok. Optimized Hydrophobic Interactions and Hydrogen Bonding at the Target-Ligand Interface Leads the Pathways of Drug-Designing. *PLoS One*. 2010-[cited 2019 Nov 27]. Available from:

<https://www.ncbi.nlm.nih.gov/pmc/articles/PMC2922327/>

221. Subach, Joel. Tertiary Structural Phylogeny [Internet]. Message to Frederick Coffman. 2019 July 19 [cited 2019 Oct 19]. [1 paragraph].

222. Wipf Peter, Mann Andre. Conformational Restriction and Steric Hindrance in Medicinal Chemistry. *The Practice of Medicinal Chemistry*. 2015-[cited 2019 Dec 1]. Available from:

<https://www.sciencedirect.com/topics/chemistry/steric-effect>

223. Ko Junso, Park Hahnbeom, Seok Chaok. GalaxyTBM: template-based modeling by building a reliable core and refining unreliable local regions. *BMC Bioinformatics*. 2012-[cited 2019 Dec 2]. Available from: <https://www.ncbi.nlm.nih.gov/pmc/articles/PMC3462707/>

224. Schaeffer Laurent. *The Practice of Medicinal Chemistry* [Internet]. 4th ed. Amsterdam, The Netherlands: Elsevier; 2008. Chapter 14-the Role of Functional Groups in Drug-Receptor Interactions; [cited 2019 Dec 2]; [about 1 screen]. Available from:

<https://books.google.com/books?id=dtScBAAQBAJ&pg=PA369&lpg=PA369&dq=Similarly,+the+overall+strength+of+the+hydrophobic+interaction+between+two+molecules+is+highly+dependent+on+the+quality+of+the+steric+match+between+the+two+molecules&source=bl&ots=DNQnOAHtiU&sig=ACfU3U3ib2kruRB9XX780IGyO4RhtyvzHA&hl=en&ppis=c&sa=X&ved=2ahUKEwiH1LDhzJPmAhXqY98KHaycA6QQ6AEwCXoECAoQAQ#v=onepage&q=Simila>

rly%2C%20the%20overall%20strength%20of%20the%20hydrophobic%20interaction%20between%20two%20molecules%20is%20highly%20dependent%20on%20the%20quality%20of%20the%20steric%20match%20between%20the%20two%20molecules&f=false

225. De Beer, B.A. Stephanie, Vermeulen P.E. Nico, Oostenbrink Chris. The role of water molecules in computational drug design. Chemistry. 2010-[cited 2019 Dec 2]. Available from: <https://research.vu.nl/ws/portalfiles/portal/42215616/hoofdstuk+6.pdf>

226. Subach, Joel. Electrostatic Interactions [Internet]. Message to Venkat Reddy. 2019 Dec 3 [cited 2019 Dec 4]. [1 paragraphs].

227. Stein C. Daniel, Briken Volker. Antigenic variation of microbial surface glycosylated molecules. Microbial Glycobiology. 2010-[cited 2019 Dec 5]. Available from: <https://www.sciencedirect.com/science/article/pii/B9780123745460000419>